NAL PROPOSAL No. 0026

Correspondent: K. Wendell Chen
Department of Physics
Princeton University
P. O. Box 708
Princeton, New Jersey 0

FTS/Off-net: 609-599-3511
452-4400

HIGH MOMENTUM TRANSFER INELASTIC MUON SCATTERING AND TEST OF SCALE INVARIANCE AT NAL

K. W. Chen
Princeton University

L. N. Hand
Cornell University

June, 1970

HIGH MOMENTUM TRANSFER INELASTIC MUON SCATTERING AND TEST OF SCALE INVARIANCE AT NAL

K. W. Chen

Princeton University

L. N. Hand

Cornell University

ABSTRACT

We propose a relatively simple first stage experiment with muons in the 50-150 GeV range. The experiment is designed to optimize conditions for testing scale invariance while providing some information about the final state, as a test of various theories of high energy interactions.

The proposed use of an iron spectrometer and of a high Z (> 1) target with a low intensity ($\sim 10^6$/sec) muon beam should greatly reduce the cost and complexity of the experiment and especially ease the construction of the beam. It may even be possible to make an adequate muon beam for this purpose from the planned 3.5 mrad high intensity pion beam. A higher intensity muon beam can be used to extend the range in q^2.

Information gained in this first experiment could greatly assist the planning of a more sophisticated experiment proposed for the high intensity μ beam.

I. Introduction

A. Physics

For a variety of reasons, inelastic muon scattering may be an even more interesting and effective way to probe nucleon structure at NAL energies (50-150 GeV and above) than in the past. Although the muon remains a mystery and should be studied in its own right for some clue as to the dynamics of the muon-electron difference, at NAL we encounter, for the first time, more muons than electrons. Previously the virtual photon has served us well as a useful way to insert a controllable amount of energy and momentum into a proton or neutron - the muon beams under discussion have adequate intensity to continue these studies. Although the level of sophistication in muon experiments has not in the past been perhaps as high as that encountered in the electron-scattering experiments, we feel that this situation is not intrinsic to the use of muons and will yield to a sustained effort to obtain high quality information. Muons will be useful because one observes directly an interaction "vertex" as a function of the dynamical variables. The usefulness of having such a probe, which is also the case for the inelastic neutrino experiments is immediately apparent when one considers the highly specific predictions for this process by parton models, for example, and the sum rules for integrals of W_2 and W_1. Although the form of the theories may change, we believe firmly that experiments with muons will present some of the strongest challenges to future dynamical theories due to the relative simplicity of a single interaction vertex. The comparison with the corresponding neutrino experiments will be necessary for separating vector and axial vector terms in the latter reactions.

Of course this simplification may be only apparent, since virtual photons, at least at small q^2, may behave in many respects like hadrons, through dif-

fraction dissociation. One immediate question to be answered concerns whether there exists a qualitative change in the nature of virtual photon interaction in the deep inelastic limit or whether some extension of the basic vector dominance idea can be maintained. Specifically, then, the following arguments can be presented for an early look at muon inelastic scattering:

The scale invariance predicted by Bjorken[1] and discovered by the SLAC inelastic electron scattering experiment[2] may or may not hold as one proceeds to even higher momentum transfers and energy losses. (See Figure 1) Of course if we have reached a truly asymptotic region without encountering "substructure", it will hold. In neutrino reactions, if the W meson exists, scale invariance is violated by the finite spatial extent of the interaction region caused by the W propagator. An analogous statement would appear in the muon scattering if the apparent (from the SLAC results) granularity of the proton charge distribution were not caused by fundamental entities like partons or quarks[3] but just by the "lumpiness" of the charge distribution predicted in the field theory from the cloud of virtual (non-exotic) hadrons around the proton. In more technical terms, one would like to know the limit of νW_2 as $X \to 0$ ($X = \frac{Q^2}{2M\nu}$) and whether scale invariance holds as q^2 becomes very large.

To go beyond the observations of the muon alone, one would like to know if scale invariance holds in the individual reaction channels, and what the multiplicity and transverse momentum distributions look like as functions of q^2 and ν. As a special case of this, the hypothesis of "limiting fragmentation" discussed by Yang, Benecke and others[4] predicts a separate fragmentation of the target nucleon and, by diffraction dissociation, the virtual photon. These fragments, in the high energy limit, approach a limiting probability distribution in the appropriate rest frame. It is predicted that the

average multiplicity associated with the target nucleon will be the same, regardless of whether the nucleon is excited by pp, πp, or μp collisions. Even crude measurements on the final state can test these theories and whether scale invariance holds for partial cross sections.

B. General Discussion of Experimental Approach

We believe that rather simple experimental apparatus will yield 10% answers quickly and cheaply, permitting efficient design of an "omnibus" detector at a later stage. We do not believe that it will be necessary to sacrifice the quality of the information of most immediate interest.

The specific ideas proposed here are:

1. The use of an iron spectrometer to achieve 7% resolution at 100 GeV very cheaply and simply. The experience of one of us (K. W. C.) in building a cosmic ray spectrometer has proved valuable and has given us confidence that such a spectrometer will meet specifications.
2. The choice of geometry and reaction kinematics to simplify and render more direct the test of scale invariance at these energies. As is discussed below, such a test can be related to observables in a way that minimizes systematic effects and permits increased precision.
3. The use of a low intensity muon beam (10^6/sec) eliminates the need for extensive collimation and momentum selection. An intense pion beam 1-2% of which decays into muons can easily produce such a beam and this experiment could possibly serve, for example, as the beam stop for the 3.5 muon high intensity beam. About 100 meters of drift space plus an 8-10 meter Be plug and an 18D72 bending magnet will be required to form the muon beam. (See Figure 2) This low

intensity can be used without achieving unacceptably low rates by using an interaction target of 100 gm/cm^2 spaced out over a distance which varies from 1-2 meters in the course of the experiment. Use of a high Z target requires some understanding of the A dependence of the cross section. An A dependence which differs from $A^{1.0}$, and experimentally equals $A^{0.91\pm.02}$ at 18 GeV and below, is predicted for $q^2 = 0$ by the "shadowing" model of Ross and Stodolsky(5). Agreement with Margolis' calculations using this model is seen in the total γA cross section measurements done at SLAC(6). The same model predicts a q^2 dependence shown in Figure 4, which reveals the region over which some shadowing might appear. Of course, by changing targets we can test the prediction of this model that $\sigma \sim A^1$ for the q^2 and ν values of interest here. An extension of this proposal to lower q^2 values would allow observation of the predicted shadowing but we prefer to concentrate first on the highest values of q^2 and ν available.

At even higher intensities ($10^7 \sim 10^8$ μ/sec), we give up the possibility of observation of the reaction products, but can obtain improved statistics on the region $q^2 > 100$ (GeV/c)^2. Availability of the intense beam at an early stage would dictate use of this apparatus to look at ultra high q^2 as soon as the beam becomes available.

4. The last new feature of this experiment will be the use of a reaction target distributed through the body of a 1-2 meter spark chamber with 40 5-cm gaps. If lead is used as the target material then we have about 16 radiation lengths available and over most of the chamber have a very high conversion probability for gamma rays. The combina-

tion of wide gaps and poorly conducting plates will support a large number of tracks and we hope to make significant observations on the multiplicities of charged and neutral tracks, and obtain information about π^0 transverse momentum distributions from the angular distribution of the observed gamma rays. If the average multiplicity is ~ 6 with 60 GeV energy loss, the average momentum is 10 GeV/c and the particles tend to emerge within a 40 mrad cone. Typically at 1 meter from the vertex, 6 tracks or developing showers are contained inside about a 3" diameter circle.

Ten X and Y Charpak chambers with 100% efficiency for multiple tracks will be inserted in the body of the production chamber. By combining this with the wide-gap optical chamber information we will obtain the multiplicity of fast charged particles, the angular distribution of these about the momentum transfer direction and from the observed gamma ray showers data concerning the π^0's.

We now turn to a more detailed discussion of these points.

II. Concept of Experimental Test of Scaling

Consider the effect on $\frac{d^2\sigma}{d\Omega dE}$ for inelastic muon (or electron) scattering of the transformation

$$E \to \lambda E$$

$$E' \to \lambda E'$$

$$\sin\frac{\theta'}{2} = \frac{1}{\sqrt{\lambda}}\sin\frac{\theta}{2}$$

$$q^{2'} = \lambda q^2$$

$$\nu' = \lambda\nu$$

$$X' = X = \frac{Q^2}{2M\nu}$$

If we ignore the very small change in $\cos^2\frac{\theta}{2}$ at small or even moderately large angles (essentially all angles of interest at these energies), then we find that $X = Q^2/_{2M\nu}$ (with W_1) remains invarient and, provided νW_2 is scale invarient, We have then

$$\frac{d^2\sigma}{d\Omega dE'} \to \frac{1}{\lambda}\frac{d^2\sigma}{d\Omega dE'} = \frac{1}{\lambda}\left(\frac{\alpha}{2E_o\sin^2\frac{\theta}{2}}\right)^2\left[W_2\cos^2\frac{\theta}{2} + 2W_1\sin^2\frac{\theta}{2}\right] \qquad (1)$$

Note that the proportionality to $1/\lambda$ is independent of the value of $R = \sigma_L/\sigma_T$.

Furthermore, $\Delta\Omega\Delta E'$ is invarient under this transformation so the counting rate decreases as $\frac{1}{\lambda}$, even if there is a spread in the incident beam energy, providing the relative distribution of energies remains the same.

Upon further investigation, we find that it is possible to extend this transformation so that most of the experimental effects such as finite resolution in determining the scattered muon momentum and angle do not affect the inter-comparison of different energies, i.e. different values of λ.

This means that we can compare experimental distributions directly and

ascertain immediately any violations of scale invariance.

Figure 3 shows this concept of testing scale invariance. The figure indicates the dependence on λ of the various experimental variables. If we scale the apparatus for each energy point (say 50, 100, 150 GeV) we remove the effects of:

1. Measurement error on the incident muon direction.
2. Beam divergence from multiple scattering in the Be filter.
3. A spread (from the pion decay spectrum) in the incident muon energies.
4. Multiple scattering in the target chamber and in the iron plate spectrometer.
5. Effects of dE/dx in the spectrometer.

Table I shows the actual statistics which might be obtained using an extrapolation of the SLAC results per 100 hours running time at 10^6 100 GeV muons per second. The number of events at 50 and 150 GeV is the same provided we make the appropriate transformation and scale invariance holds.

III. Experimental Arrangement

A. The Muon Beam

The boundary conditions imposed by the absence of a specially designed muon beam led us to consider the experimental factors in approaching the limit of zero cost--i.e. what can be done using a low intensity muon (10^6/sec) beam derived from the "existing" 3.5 mrad. pion beam in a minimal way. In order to achieve good rates for large Q^2 scattering we increase the target density by using a high Z target. The general experimental arrangement, intended to replace the 3.5 mrad beam stop, is shown in Figure 2 and Figure 3.

B. Use of a High Z Target.

Use of the lower beam intensity ($10^6 \mu$/sec) and high Z target has a number of advantages and some obvious disadvantages. We start with the advantages:

1. At these intensities we may determine the muon energy directly by observing the incident muon before and after a deflecting magnet.
2. The reaction itself may be observed by combining the target material and a beam spark chamber. Much useful information can be obtained even without magnetic analysis of the reaction products. This can be simultaneous with the single arm experiment.
3. Problems with beam halo and monitoring are substantially reduced.
4. The high probability of γ-ray conversion might allow part of the radiative corrections to be checked experimentally.

The chief disadvantages of the dense high Z target are:

-1. One does not a priori know the A dependence of the scattering cross section, although one believes it is A^1 at large q^2.

-2. A very dense target will have a background from energetic knockon electrons which might tend to obscure the event through secondary showers. We have assumed 100 gm/cm^2 for this limitation, based on simple calculations of the probability of obtaining an energetic knockon and observations at 12 GeV pion interactions in an iron plate spark chamber with several hundred gm/cm^2.

For point -1 above, extensive calculations have been performed using the Stodolsky optical model (which is in agreement with the measurement A dependence of the total photon cross section for k from 2-18 GeV as determined by DESY and (SLAC). To the extent one sees a deviation from $\sigma_{\gamma A} = A\sigma_{\gamma N}$, one is observing

shadowing of the incident (virtual) photon. This surprising effect was explained by Stodolsky[5] and has been extensively studied by many authors including Gottfried and Yennie[7] and Brodsky and Pumplin[7]. The results (Figure 4) of an explicit calculation (using a cylindrical nucleus for ease in calculation) shows

1. This (μ scattering) experiment should not observe shadowing for $q^2 > 2$ i.e. over almost the whole kinematic region accessible at NAL $\sigma_A \sim A\sigma$.
2. If a measurement of σ_{TOT} for the muons is possible then these shadowing effects might be observed. The maximum effect is

$$\frac{\sigma_{\gamma A}}{A\ \sigma_{\gamma N}} = .43 \text{ for } k > 20 \text{ GeV}$$

$$Q^2 = 0 \text{ in Pb.}$$

Actual observation of the shadowing requires measurement of very small scattering angles and elimination of μ-e events. In this proposal we consider:

$$10 \text{ mrad} < \theta_\mu < 160 \text{ mrad}$$

This confines us mostly (but not entirely) to the deep inelastic region where the shadowing effects are expected to be less than a few present. This can be experimentally checked by using different targets.

C. Rate Calculation and Radiative Corrections

1. Cross Sections

Cross sections for muon scattering at these large momentum transfers and energy losses are of course unknown and can only be guessed. In order to provide some basis for planning the experiment we have taken an approximate fit to the SLAC electron scattering data, assuming that $R = \sigma_L/\sigma_T$ approaches a limiting value of 0.2 and that

$$\sigma_T\,(k,q^2) \cong \frac{\sigma_T(k,0)}{(1 + 2.6q^2 + q^4/k)} \qquad (2)$$

As was discussed in a recent Physical Review Letter by Nauenberg[8] the choice of this form guarantees the scale invariance of νW_2 in the limit $q^2 \gg \nu^2$. In fact any functions of the form $1 + q^2\, f(q^2/k)$ in the denominator, plus the constancy assumed for $\sigma_T(k,0)$ guarantees a scale invariant $\nu\, W_2$. The above form only applies at some distance from the elastic limit $q^2 \to 2M\nu$.

Radiative corrections were applied to the cross sections, since these will be important in any precise test of scale invariance. It is found that these are not negligible, due to the appearance of the muon mass in the logarithm of the leading order terms.

Most, but not all of the radiative correction comes from the case where the muon radiates a photon in the forward direction and then scatters elastically at the lower energy. Both this, and the case where the radiation takes place after the scattering should be visible in the chamber and the extra photon might be identifiable by its collinearity with either the incident on scattered muon. However observation of this depends on the angular distribution and multiplicity of the reaction products, thus we prefer not to rely on it. The formulas used involve the

peaking approximation and were taken from Mo and Tsai[9].

As a typical example, figures 5 and 6 shows the calculated values of $\frac{d^2\sigma}{d\Omega dE'}$, for a variety of secondary muon energies E' at a fixed incident muon energy for 100 GeV. The rapid dependence on scattering angle ($\sim\frac{1}{\theta^4}$) and the slower dependence on E' are evident. Cross sections without radiative corrections are indicated by dotted lines and with radiative corrections by solid lines. It can be seen that in some cases the radiative correction is ~ 20-30%.

By looking at figures 5 and 6 we see that a precise muon experiment requires very good scattering angle resolution and at the same time requires very little in the way of resolution in E'; the 7% we hope to achieve being more than adequate for the experiment. This is a major reason why the simplicity of the iron spectrometer is well matched to this measurement.

2. Effect of Angular Error

A 1 mrad systematic error in θ at 10 mrad will make a 40% error in $\frac{d^2\sigma}{d\Omega dE'}$. At 60 mrad the same error is a 7% error in the cross section. Multiple scattering in the target chamber gives an rms $\delta\theta \sim 45$ mrad/$_{E'}$ (Gev). This is a random, not a systematic effect. The beam can be used to monitor systematic errors in θ. The importance of physically scaling the apparatus to eliminate systematic errors while checking scale invariance is clear. Of course thinner targets can be used for measurements at smaller values of θ, because the cross section is larger, but the measurement error in θ will always remain a problem for experiments which vary only the incident energy and not the geometry as well.

3. Counting Rate

Typical counts obtained and assumptions about the target and the beam in 100 hours of running are given in Table I. It should be emphasized that these are only best guesses, but plausible ones.

IV. Iron Spectrometer

A. General Consideration

In this section we describe in some detail the iron spectrometer we propose to use to analyze the inelastically scattered muons. Our prime motivation in considering the use of a toroidal solid iron magnet is that or tremendous reduction in power cost while permitting us to achieve a momentum and angular resolution sufficient for our purposes. The limiting factor of conventional spectrometers was that economics impose a limit on the magnitude of the magnetic field as well as the volume over which it acts. Cosmic ray spectrographs have been built using the solid iron magnet reaching a meximum detectable momentum in the neighborhood of 1000 GeV[10]. Our own experience with this concept has been also favorable.[11]

B. Magnet Parameters

We list in Table II the parameters considered in the spectrometer and Figure 7 shows a schematic diagram of one section of the iron magnet. The magnet is consisted of 4 identical sections each 1.5 meters long in the beam direction. Each section is in turn constructed from 120 low carbon magnet grade steel plates. The magnetizing coils each consisting of 500 turns of 10 s. w. g. lumax covered copper wire of total resistance $\sim 12\Omega$. At a current of $\sim$ 20A a field of 18 Kg $\pm$ 0.7 Kg is expected.

C. Uniformity of Magnetic Field

It is important to know the variation of the uniformity of the magnetic field in both the wound and unwould areas. Fortunately previous experiences[10,11] give the actual search coil measurement of the field for both areas. Figure 8 shows the variation of field at locations 1, 2 and 3 for the wound area. The variation in field over a given plate is $\lesssim 1.6\%$ whereas the overall variation is of the order ± 2.5%. In addition a measurement of the leakage field from the iron surface reveals that it magnitude is of the order of 0.1% of the field within the iron. (Figure 9a).

With an expected uniformity of the order of 2.5% the momentum resolution of the muon spectrometer will not be limited by the uncertainty in the magnetic field but will be limited by the multiple scattering of muons in iron.

D. Momentum Resolution

If the magnetic field is sufficiently constant over the entire length, the accuracy to which the momentum of a muon can be determined is limited by the multiple scattering it suffers. Figure 10 shows the three alternatives available to determine the muon momentum:

1. Single measurement of incoming and exit angle. (Figure 10a). The fractional error of momentum determination varies as $L^{-1/2}$ since the magnetic deflection varies as L while the r.m.s. multiple scattering angle varies as $L^{1/2}$. Practical limitation in solid angle acceptance and minimum cut off energy optimizes the length L. In this case the momentum of the muon is given by

$$p = \frac{\chi K(1 + \epsilon^2/K^2)}{I(\theta_2) - I(\theta_1)} \qquad (3)$$

where θ_1 and θ_2 are incoming and exit angles,

ϵ = energy loss per unit length of iron,

K = 300 B

χ = the lateral displacement of the emergent track position from the incident position, and

$I(\theta) = \exp. \left[\frac{\epsilon}{K}(\theta_1 - \theta)\right] \left(\cos\theta - \frac{\epsilon}{K}\sin\theta\right).$

It is to be noted that at high energy (> 100 GeV) equation (3) reduces to the familiar form

$$p = \frac{KL}{\sin\theta_1 - \sin\theta_2} \tag{4}$$

The variation of the calculated incident momentum with the incident angle at 150 mrad is less than ± 2%. Figure 9b shows this variation. The resolution is limited by the ratio of the transverse momenta P_T^B (bending) and $P_T^{M.S.}$ (Multiple scattering)

$$\frac{\Delta p}{p} \sim \frac{P_T^{MS}}{P_T^B} \simeq \frac{0.286}{3.24}\,\frac{(GeV/c)}{(GeV/c)} \simeq 9\%$$

which is the greatest uncertainty. We show the photograph of the cosmic ray muon spectrometer now in operation at Princeton. (Figure 11).

2. Multiple measurements. (Figure 10b).

The previous analysis still applies. One would expect crudely the improvement on the momentum resolution goes as N where N is the independent number of measurements. The major disadvantage is that the solid angle factor decreases as L^2 and that no all measurements are wholly independent to exploit the $\sqrt{N}$ factor.

3. Multiple measurements of positions. (Figure 10c).

For a track of projected length L with transverse coordinates Y_n measured and longitudinal coordinates χ_n ($n = 0,1,2,--N$), the curvature and direction error are values of β and γ in the least square fit of

$$Y = \alpha + \beta\chi + \frac{1}{2}\gamma\chi^2 \tag{5}$$

Variational techniques have been used to calculate the optimum resolution for a given magnet configuration from general considerations. The expected resolution is better in general than case 1). For 100 GeV muons, we found a momentum resolution of 7% for a measurement at four points by fitting the track to a circle. This is the approach that we have finally adapted in this proposal.

References

1. J. D. Bjorken, Physical Review 179, 1547 (1969).
2. E. D. Bloom et. al., Phys. Rev. Lett. 23, 930 (1969).
3. R. Feymann, International Conference on High Energy Collisions, Stony Brook, N. Y. (1969);
   S. D. Drell, Phys. Review, 187, 2159 (1969);
   H. Harari, Phys. Rev. Lett. 24, 286 (1970);
   J. D. Bjorken, E. A. Paschos, Phys. Rev. 185, 1975 (1969).
4. C. N. Yang, International Conference on High Energy Collisions, Stony Brook, N. Y. (1969).
5. L. Stodolsky, Phys. Rev. Lett. 18, 135 (1967).
6. D. O. Caldwell et. al., Phys. Rev. Lett. 23, 1256 (1969).
7. K. Gottfried and D. Yennie, Phys. Rev. 182, 1595 (1969);
   S. Brodsky and J. Pumplin, Phys. Rev. 182, 1795 (1969).
8. M. Nauenberg, Phys. Rev. Lett 24, 625 (1970).
9. L. W. Mo and Y. S. Tsai, Review of Modern Physics 41, 205 (1969).
10. R. M. Bull, W. F. Nash and B. C. Rastin, Il Nuovo Cimento 15, 349 (1965).
11. K. W. Chen et. al., R.S.I. to be published.

TABLE I

Total Counts in 100 Hours of Running

θ	Counts	$Q^2 = 2(100\ \text{GeV})(50\ \text{GeV})(1-\cos\bar{\theta})$
10-20 mrad	110,000	2.3 $(\text{GeV}/c)^2$
20-40 mrad	20,000	9 $(\text{GeV}/c)^2$
40-80 mrad	4,000	36 $(\text{GeV}/c)^2$
80-150 mrad	200	$\approx$ 100 $(\text{GeV}/c)^2$
Total	$\approx$ 134,000	

Assumed: 100 gm/cm^2 target

10^6 muons/sec.

$E' = 20\text{-}80$ GeV

$E_o = 100$ GeV

TABLE II

Torodial Magnet Spectrometer Specifications

Cross Section	1.5 m x 2 m
Total Length	6 m
No. of Sections	4
Length/Section	1.5 m
Energy Cut Off	10.74 GeV *
Material	1020 Steel
Lower Energy Cutoff (Straggling Limit)	20 GeV
$\oint B \cdot d\ell$	2000 Kg - in
No. of Turns/Section	5000
Total Coil Resistance/Section	12Ω
Magnetic Field in Iron	17.5 Kgauss.
Total Power Consumption	20 KW

* We use value of muon energy loss in iron

Figure Caption

1. Kinematic region for Muon inelastic scattering (q^2, ν plane) at NAL and SLAC.
2. A possible muon beam layout for μ inelastic scattering.
3. Plan view of proposed apparatus for test of scale invariance.
4. Predicted shadow correction versus $A^{1/3}$ for ν = 20 GeV and for a cylindrical nucleus.
5. Variation of $\frac{d^2\sigma}{d\Omega dE'}$ with θ at a fixed E .
6. Variation of $\frac{d^2\sigma}{d\Omega dE'}$ with E' at a fixed θ.
7. Details of the iron magnet. Only one section is shown. Four sections are proposed for the spectrometer. a) Plan view. b) Schematic view.
8. Variation of magnetic field in the wound region as a function of the plate number. 3 positions shown in Figure 7a).
9. a) Leakage field versus distance away from the surface at position shown in (c).
10. Three alternatives for momentum determination with a iron spectrometer.
11. Photograph of a cosmic ray muon spectrometer at Princeton. Method of 10a) is used here.

KINEMATIC REGION
FOR MUON INELASTIC SCATTERING
(q^2, υ PLANE)

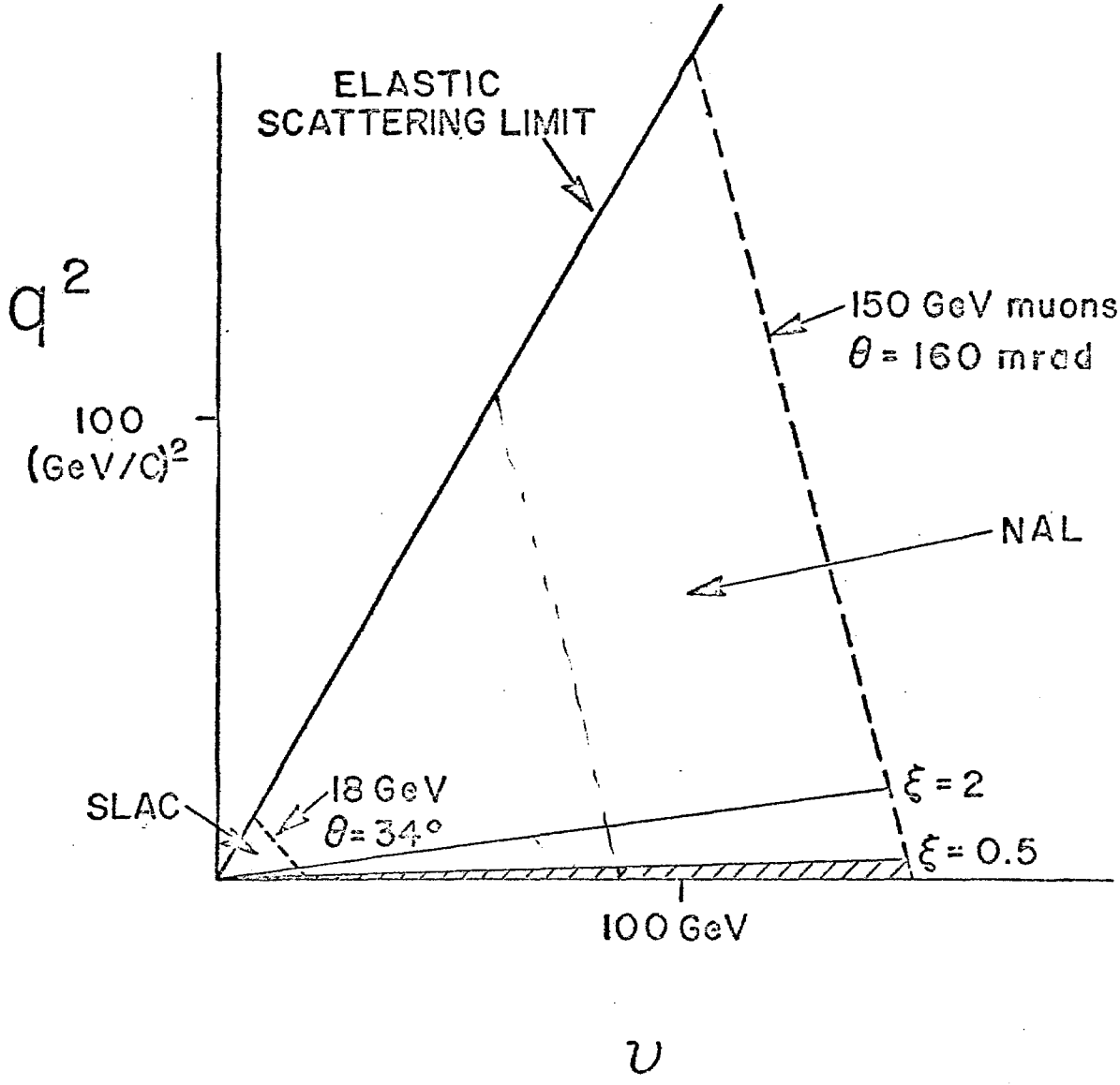

FIG. 1

A POSSIBLE MUON BEAM LAYOUT FOR μ INELASTIC SCATTERING

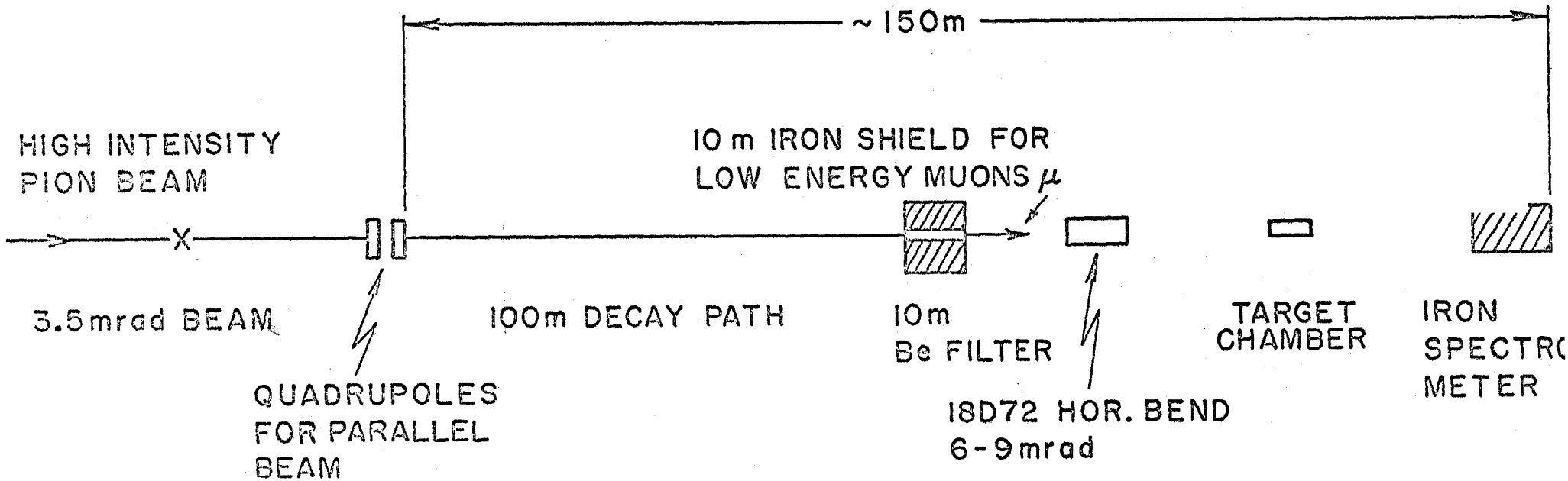

FIG. 2

PREDICTED SHADOW CORRECTION VS $A^{-1/3}$ FOR 20 GeV = ν
(CYLINDRICAL NUCLEUS)

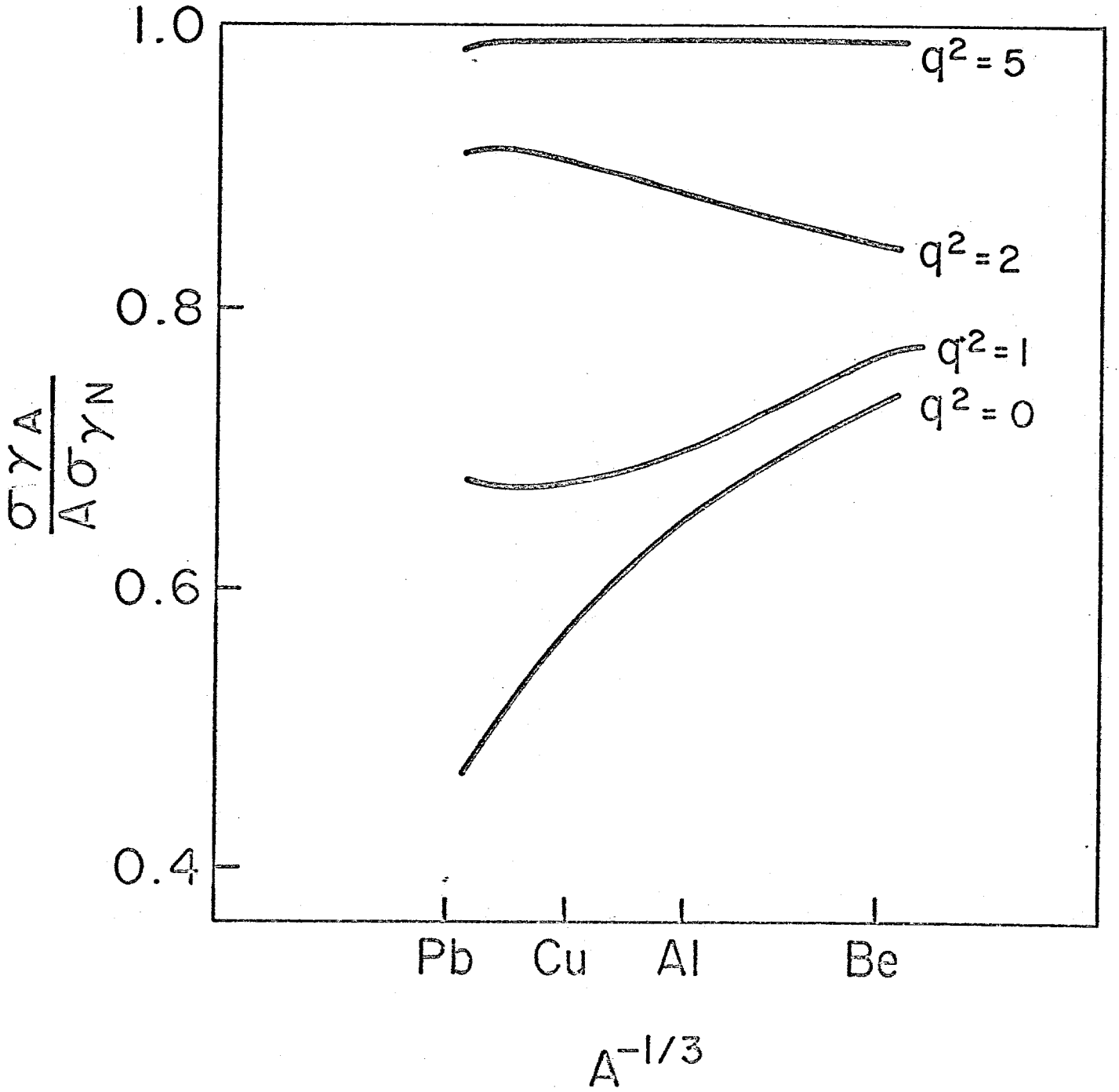

FIG. 4

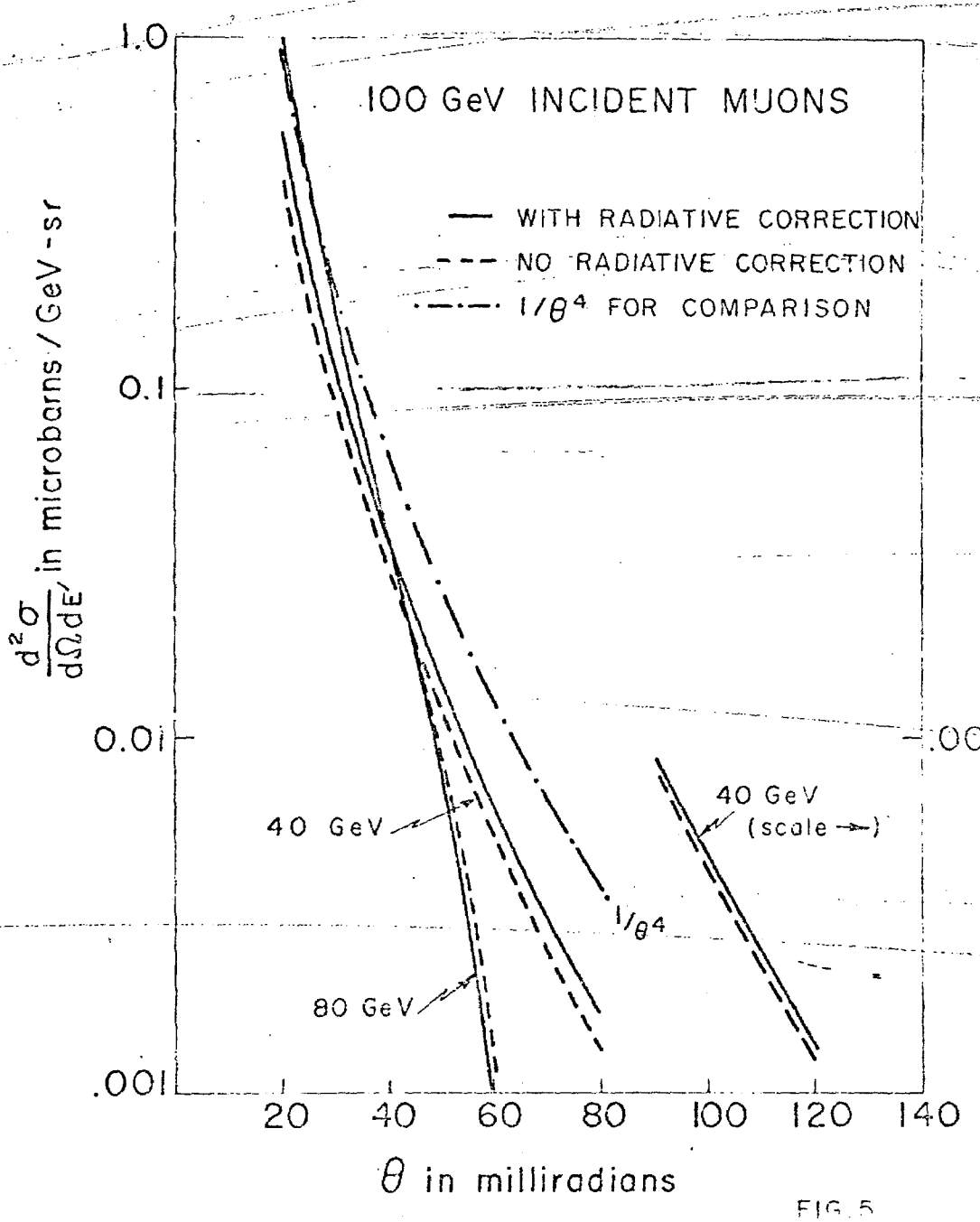
100 GeV INCIDENT MUONS
WITH RADIATIVE CORRECTION
NO RADIATIVE CORRECTION
1/θ⁴ FOR COMPARISON
1.0
0.1
0.01
.001
.001
40 GeV
80 GeV
1/θ⁴
40 GeV
(scale →)
20
40
60
80
100
120
140
θ in milliradians
d²σ/dΩdE′ in microbarns / GeV-sr

FIG. 5

VARIATION OF $\frac{d^2\sigma}{d\Omega\, dE'}$ WITH E' AT FIXED θ

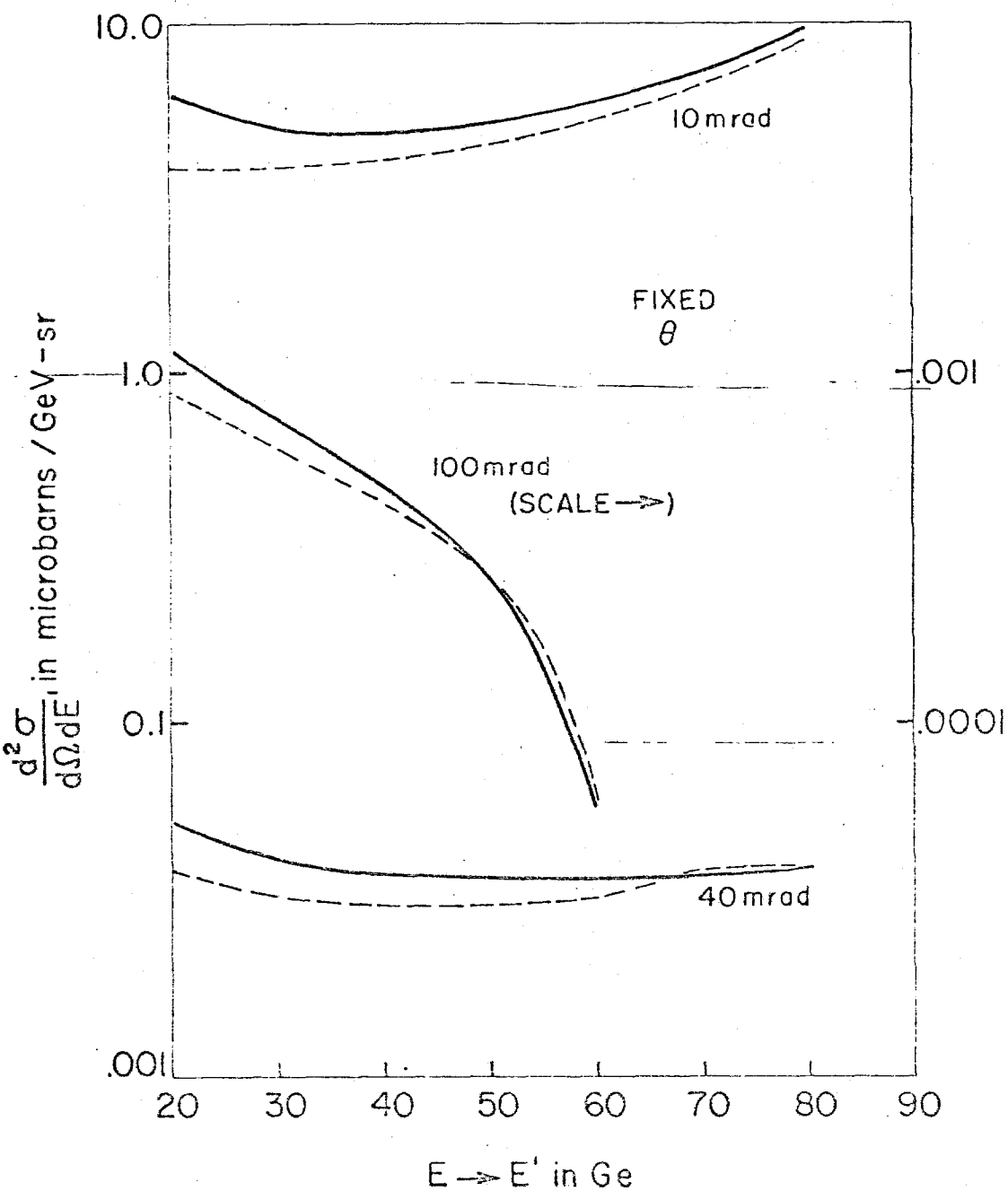

FIG. 6

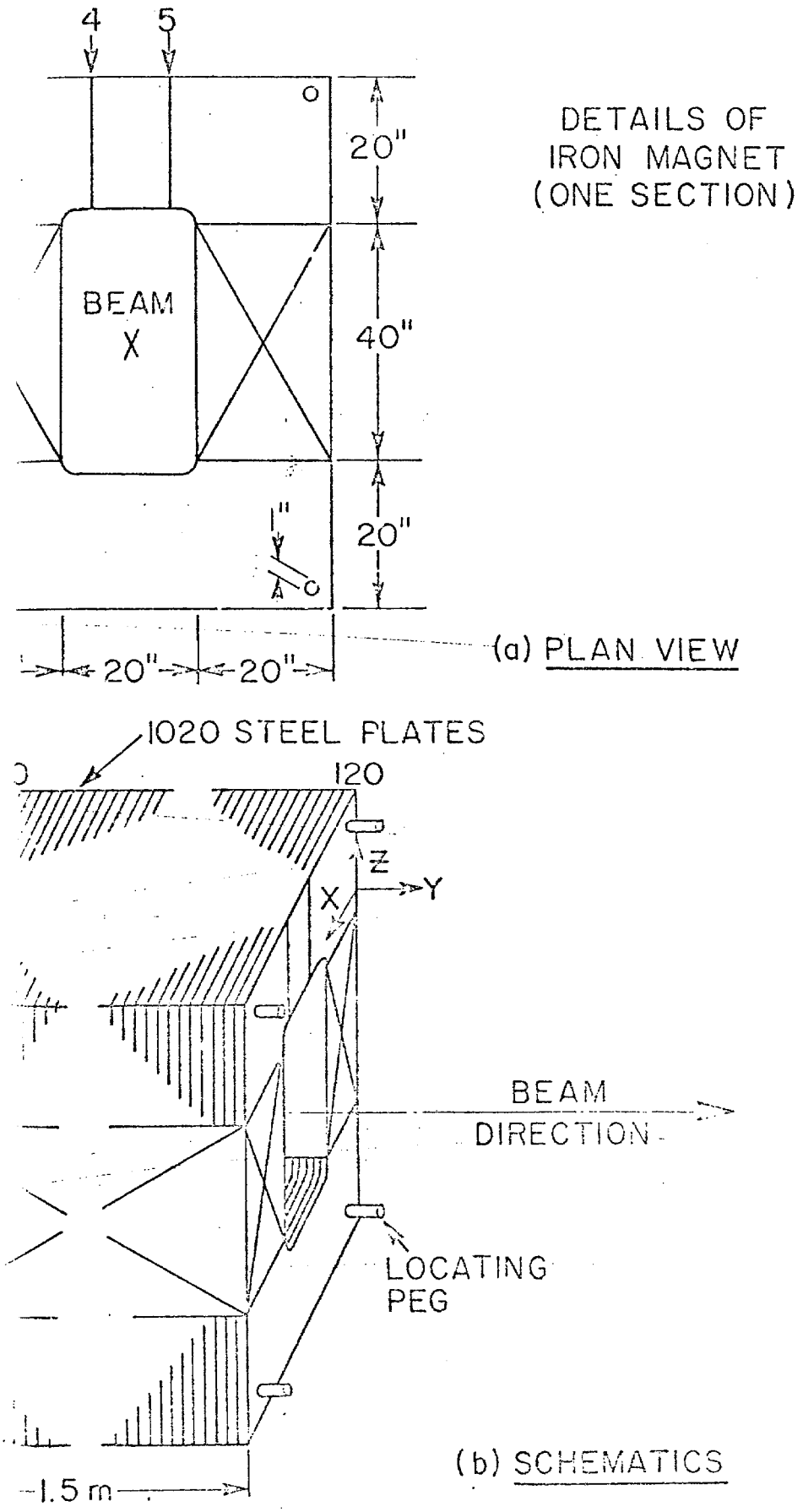
4
5
20"
40"
20"
BEAM
X
1"
20"
20"
DETAILS OF
IRON MAGNET
(ONE SECTION)
(a) PLAN VIEW
1020 STEEL PLATES
120
Z
Y
X
BEAM
DIRECTION
LOCATING
PEG
1.5 m
(b) SCHEMATICS

FIG. 7

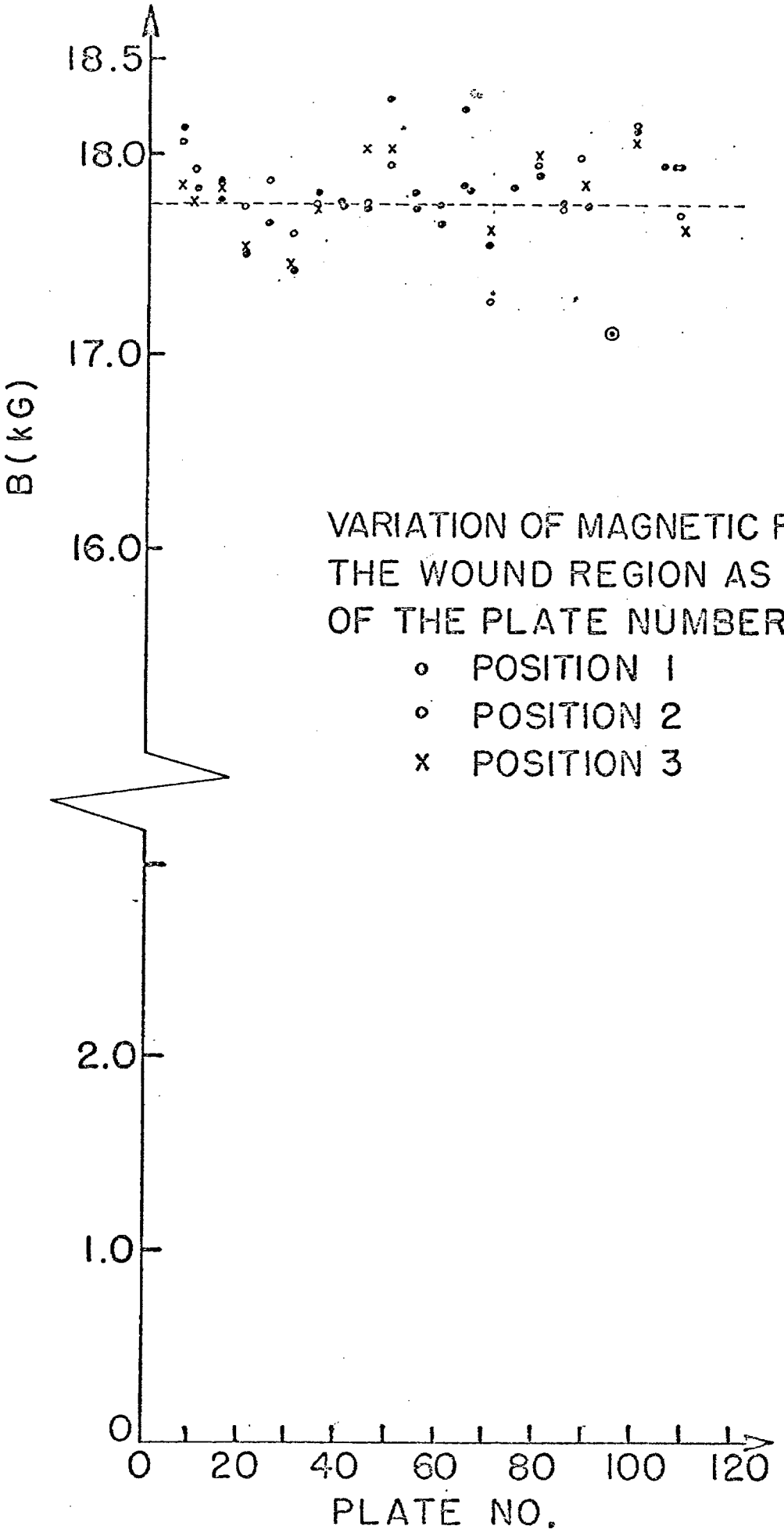

VARIATION OF MAGNETIC FIELD IN THE WOUND REGION AS A FUNCTION OF THE PLATE NUMBER.

- o POSITION 1
- o POSITION 2
- x POSITION 3

FIG.8

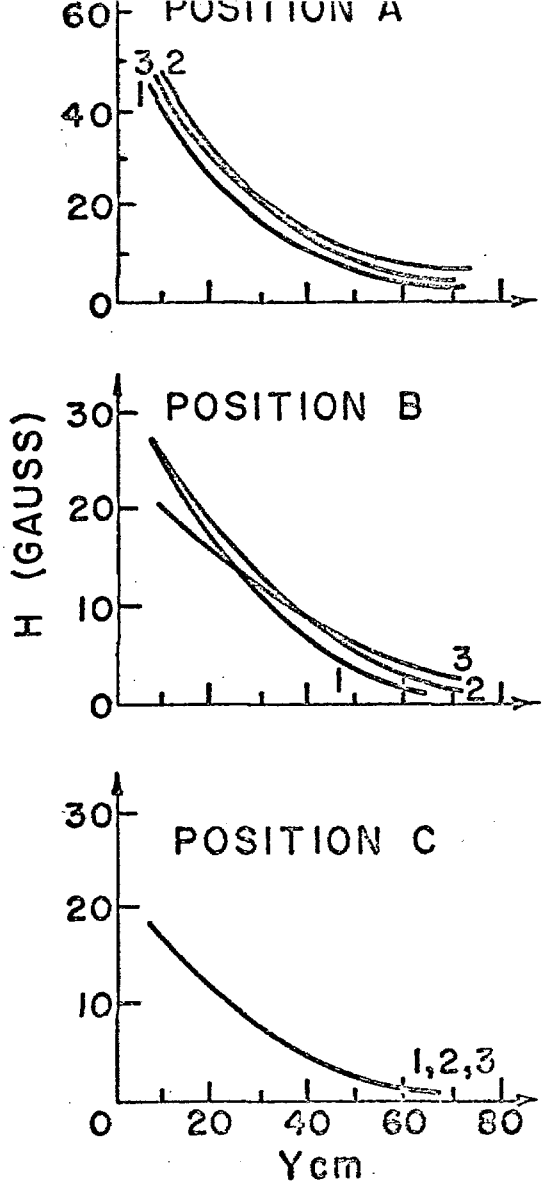

A) LEAKAGE FIELD AS FUNCTION OF DISTANCE FROM SURFACE AT POSITIONS SHOW IN (C)

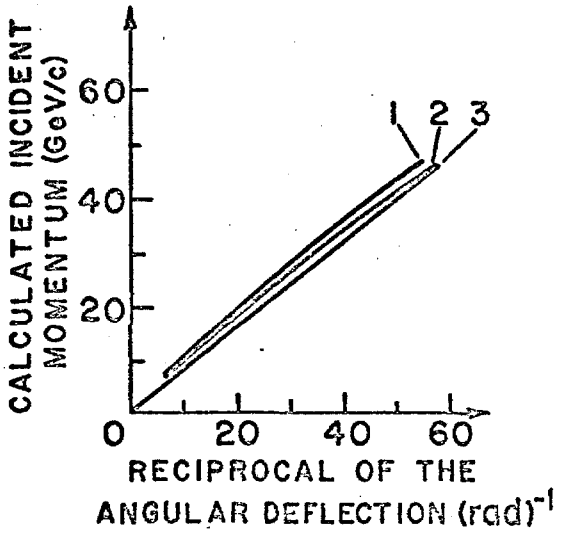

B) CALCULATED MOMENTUM vs $(\Delta \sin\theta)^{-1}$ AS FUNCTION OF INCIDENT AND EXIT ANGLES (θ_1 = 160 mrad)

1 - $\theta_1 < \theta_2$
2 - $\theta_2 > \theta_1$
3 - AIR GAP

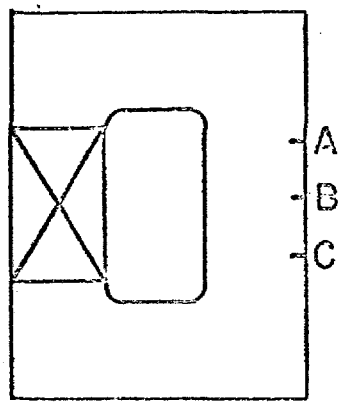

C) POSITION FOR MEASUREMENTS IN (C)

FIG. 9

3 ALTERNATIVE WAYS OF MEASURING MUON MOMENTUM

(a) SINGLE ANGLE MEASUREMENT

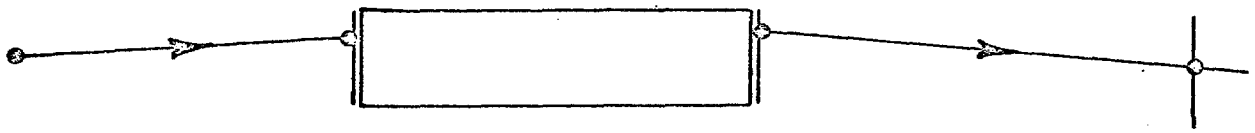

$$\frac{\Delta p}{p} \sim 10\%$$

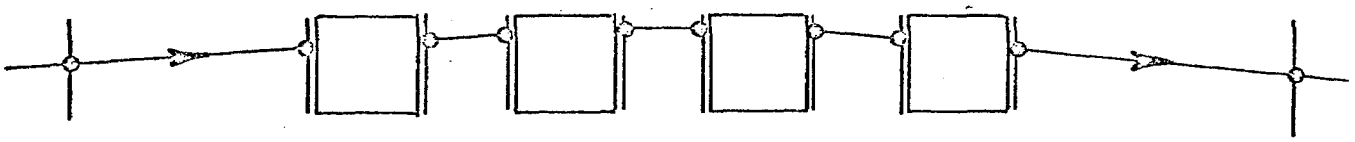

(b) MULTIPLE ANGLE MEASUREMENT

$$\frac{\Delta p}{p} \sim 8\%$$

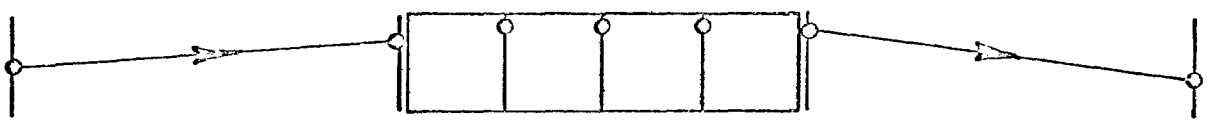

(c) MULTIPLE POSITION MEASUREMENT

$$\frac{\Delta p}{p} \sim 6.5\%$$

FIG. 10

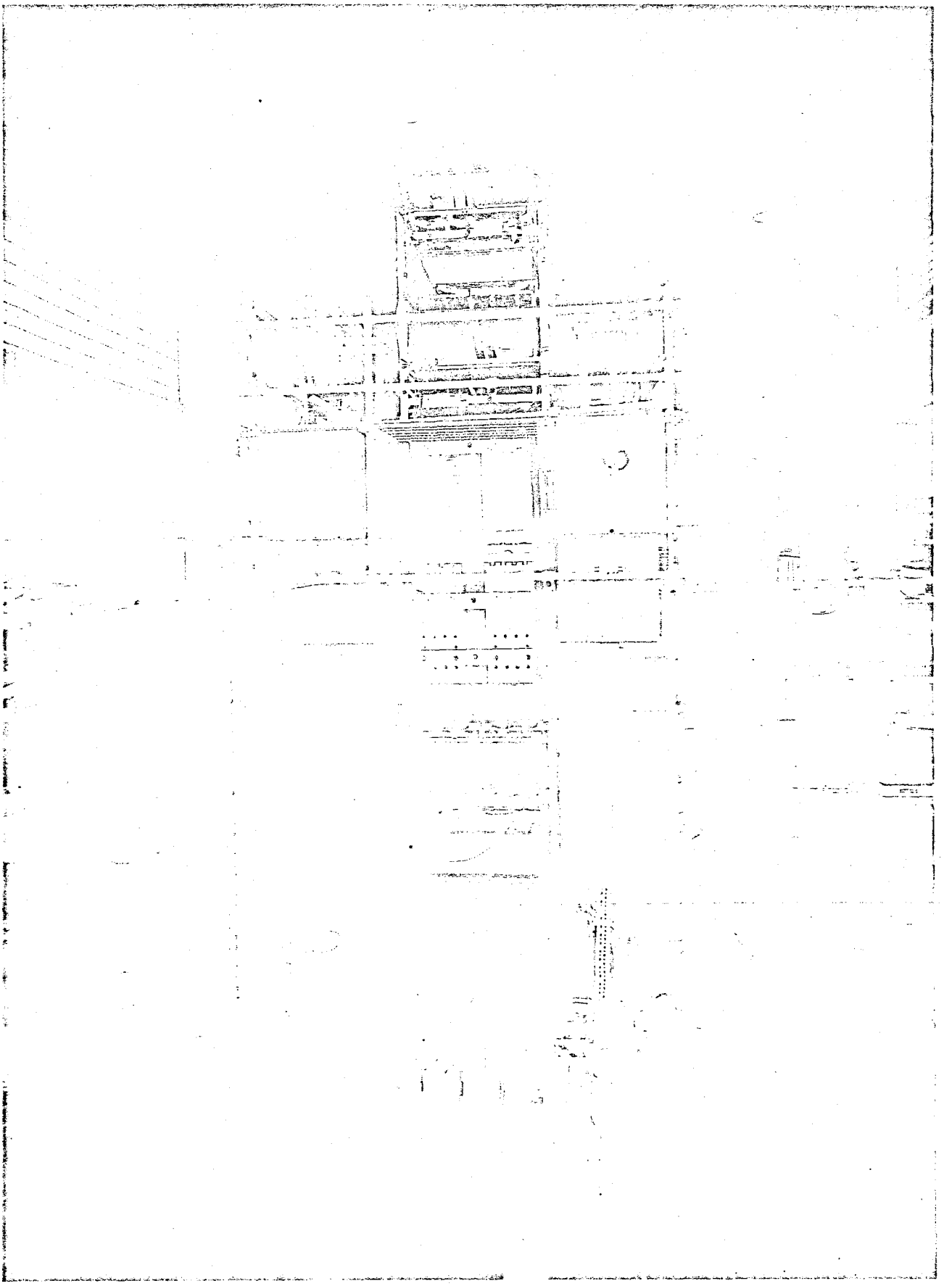

26-31

STATUS REPORT ON EXPERIMENT 26

E26 GROUP

JUNE 11,1974

TABLE OF CONTENTS

INTRODUCTION	PAGE	1
SCALING THE APPARATUS TO REDUCE DETECTOR BIASES IN THE RATIO COMPARISON		2
APPARATUS		10
DATA TAKEN TO DATE		16
STABILITY OF EVENT RATES		19
SENSITIVITY TO SCALING VIOLATIONS		21
PRESENT ANALYSIS SITUATION		23
APPENDICES:		
I. E26 SPECTROMETER MAGNETS (INTERNAL REPORT)		25
II. DEGAUSSING OF SPECTROMETER MAGNETS (INTERNAL REPORT)		41
III. INCIDENT ENERGY		48
IV. MOMENTUM FITTING AND SUBROUTINE FINAL		55
V. CALIBRATION OF FINAL (MOMENTUM FITTING) WITH MONTE CARLO		58
VI. CALIBRATION OF THE SPECTROMETER		61
VII. SURVEY OF INFORMATION FROM THE SPARK CHAMBERS UPSTREAM OF THE SPECTROMETER		65
VIII. RECON8 SPECTROMETER PART: TRACK HUNTING		77
IX. STUDIES OF TRACK RECONSTRUCTION..'BACKFIT' only		96

INTRODUCTION

This is intended as a status report on experiment 26. The emphasis here is on the technical features of the experiment, and the problems in analysis which would be general to all muon experiments at the high energies available at the FERMILAB.

We begin with a description of the scaling concept and the apparatus of the experiment, and review the data taken during the data runs in 1973 and 1974. We then consider the sensitivity of the experiment to systematic uncertainties. Many of these uncertainties are related to the analysis of the data and we describe the efforts underway at this time to better understand and improve the analysis.

The two most important aspects of the experiment which we consider in detail are the use of solid iron magnets and the use of a nuclear target with the resulting hadronic and electromagnetic showers in the target material. This material is quite technical and much of it is left to appendices. However, the information is important to the understanding of this experiment, and to the evaluation of other similar experiments at these energies.

I. "Scaling" the Apparatus to Reduce Detector Biases in the Ratio Comparison

The simplest and most direct form of scaling test would be to measure $d^2\sigma/d\Omega dE'$ at different E_o for the same q^2 and ω values to determine ($R \equiv \sigma_S/\sigma_T$, $F_2 \equiv \nu W_2$) and then plot F_2 vs. q^2 at fixed ω for different ω values. Such a method requires very high beam intensities and long running times to achieve sufficient statistical accuracy. In a muon scattering experiment one is faced with muon beam intensities considerably lower than comparable electron beam intensities available at SLAC (about 7-8 orders of magnitude less). Perhaps 2 or 3 orders of magnitude can be made up by the thicker targets possible with muons, but there is still a need to find a method which makes efficient use of the available data in the scaling comparison using only a relatively small number of muons.

For this reason a method was devised which attempts to compensate for acceptance changes by simultaneous variation of the apparatus geometry with the energy of the beam. Since the resolution of the magnetized iron spectrometer is determined primarily by multiple scattering in the iron, it is important in the comparison between muon energies to make the effect of multiple scattering nearly the same in both cases. Requiring

both the acceptance and the multiple scattering effects to be nearly the same in all parts of the spectrometer gives two conditions, the first one on the sum of certain distances, the latter on the sum of the squares of other distances (squares due to the random nature of multiple scattering). Since the density of iron is fixed and it is convenient to use the same magnets at both energies, it can be shown that these conditions plus the need to use integral numbers of magnets basically require a relation which can be expressed in a somewhat obscure fashion as the numerical accident

$$\frac{\sqrt{3}}{3} : \frac{\sqrt{5}}{4} : \frac{\sqrt{8}}{5}$$

These relations are not exact but hold to about the 2% level. Satisfying these constraints means that the incident energies for the comparison must be in the ratio 3:5:8 with the upper energy (150 GeV) being determined by the practical limit of the beam. The numbers 3,4,5 refer to the number of magnetized iron toroids used in these geometries. The actual amount of iron (doing the multiple scattering) is proportional to 3,5,8 which implies that the upper two energies require additional unmagnetized iron to equalize the multiple scattering and average energy loss effects.

To see how this works we consider two scattering geometries

corresponding to different incident beam energies.

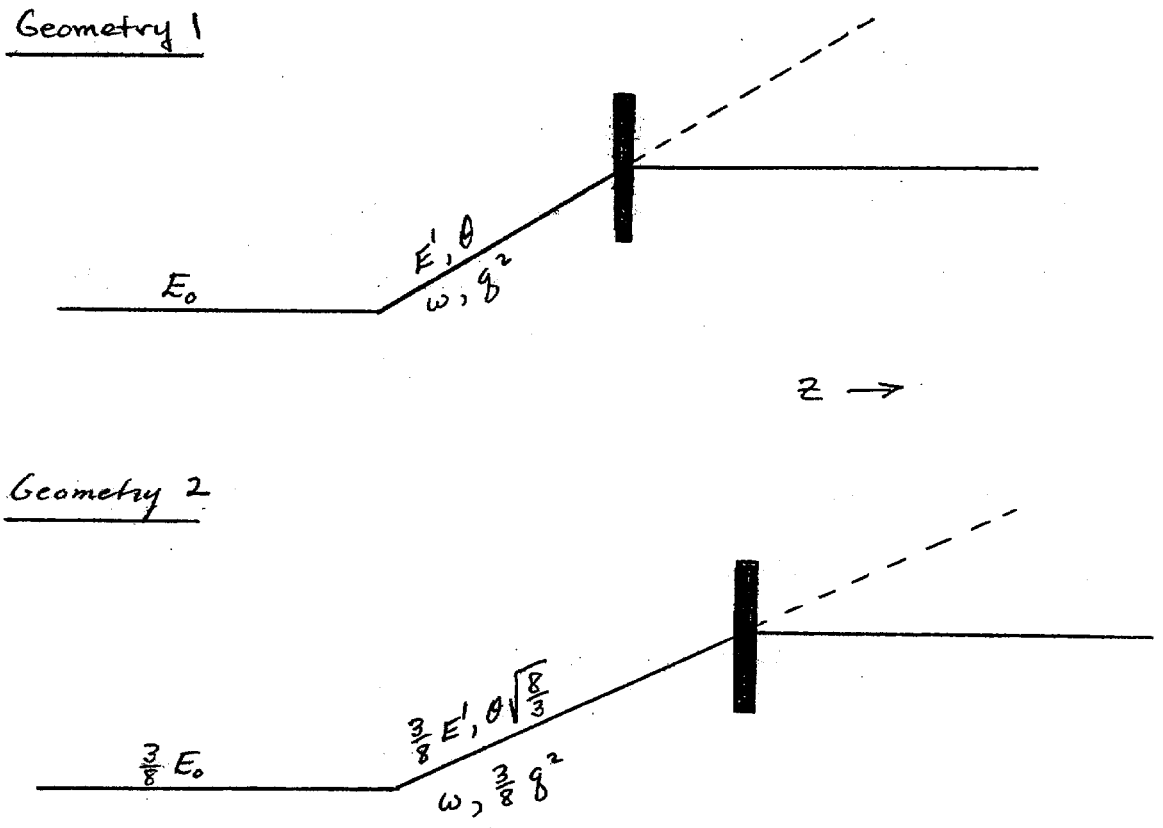

In each geometry E_0 is regarded as fixed and the incident muon energy in Geometry 2 is 3/8 that of Geometry 1. E', θ are to be considered as variable parameters with the relation between the scattered mesons in the two geometries given in the diagram. The box represents the bending imparted by the spectrometer used for momentum analysis of the scattered muon. In the special case shown, if C is the transverse momentum imparted by the spectrometer magnet (throughout this discussion we assume $\sin\theta \sim \theta$ and $\cos\theta \sim 1$) then for parallel rays

$$C_1 = E'\theta$$

We temporarily assume a uniform B field pointing into the paper (for μ^-). In real life this is a field with azimuthal symmetry about the beam and with some radial variation in magnitude. In order to achieve a corresponding ray in the second geometry $C_2 = \sqrt{\frac{3}{8}}\, E'\theta = \frac{3}{5}(1.02)\, E'\theta$. Since the magnetic field in saturated iron is not variable one needs to use 3/5 as many magnets in Geometry 2 as in Geometry 1. In general the total $\int B \cdot d\ell$ of the spectrometer must be proportional to the square root of the incident energy. If the "3/5 rule" were the only condition applied on comparing the two geometries, one would find that the ratio of multiple scattering r.m.s. transverse momentum in the direction of bending would be increased in the low energy geometry (Geometry 1) by a factor of $\sqrt{\frac{5}{3}} = 1.29$. Not only would the comparison of the two energies be sensitive to effects caused by differences in the spectrometer momentum resolution but the "edge" effects would be different--i.e. losses due to scattering out of (or into) the finite spectrometer aperture. In the experiment actually performed, this would have an effect on both the very high and the very low value of q^2 and would mean that the q^2 range of the experiment would have to be restricted, with a consequent loss of both dynamic range in the kinematic variables and statistical sensitivity to a scaling violation.

Thus we wish to find the condition which ideally maps the high energy distribution onto the low energy one provided the cross section is scale invariant. In the perfect apparatus one could observe the distribution in any measured quantity (i.e. a radial distribution) and no experimental bias in the comparison of the high and low energy geometries would be present. This of course by no means eliminates the need to treat systematic errors but should help to reduce the sensitivity of the final answer to these errors, acceptance questions, etc. as well as make more efficient use of the available data.

If we neglect (for simplicity) the scattered muon angular momentum with respect to the spectrometer symmetry axis and the average energy loss in the spectrometer, given a ray of initial transverse momentum $p_\perp$ and secondary energy E', the deflection of the ray from the $p = \infty$ line at any point Z within the spectrometer is:

$$d(z) = \sum_{z_i<z} (z - z_i) \frac{(p_\perp - C_i)}{E'} \qquad \text{impulse approximation}$$

The z_i are the centers of the toroidal magnets, C_i is the transverse momentum imparted by the ith magnet $C_i = C(r(z_i))$ since the field varies somewhat with radius. Although the above formula contains a number of approximations, mainly neglect of

the average energy loss by ionization in the spectrometer (about 10% of E_o), it is intended only to illustrate how the method works.

Now consider a number of tracks with the same initial $(p_\perp, E')$. Multiple scattering within the spectrometer produces a distribution of trajectories after some material has been traversed. If we ask for the mean square distribution $\sigma^2(z)$ of track deviations from d(z) (projected onto plane containing the average trajectory) it can be shown that (in the approximation that multiple scattering is Gaussian)

$$\sigma^2(z) = \int_{\substack{z'<z \\ \text{all material}}} dz' \, (z-z')^2 \, \frac{(.015)^2}{x_o} \, \frac{1}{E'^2}$$

where E' is in GeV and x_o is $x_o(z')$, the radiation length of the material at point z'. If we neglect all scattering except from the iron magnets and the thickness of a single magnet is Δ, we have

$$\sigma^2(z) = \left(\frac{.015}{E'}\right)^2 \frac{\Delta}{x_o \text{ (iron)}} \sum_{z_i + \frac{\Delta}{2} < z} \left[(z-z_i)^2 + \frac{\Delta^2}{12} \right]$$

Notice that, at a fixed point in the spectrometer the ratio σ/d is independent of E'. This means that, if we neglect the effect of measurement errors of various kinds, the resolution of the spectrometer will be independent of E'.

Now we are in a position to deduce the basic condition on the apparatus which allows us to maintain constant acceptance and resolution over a wide range of incident energies. As was shown in the original proposal, if we consider λ to be a scale factor applied to the incident muon energy and compare distributions in E', θ from energy E_o with distributions from energy λE_o in $(\lambda E', \frac{\theta}{\sqrt{\lambda}})$ we find that if $\cos^2 \frac{\theta}{2} \approx 1$ and $R = \sigma_S/\sigma_T$ scales as well as $F_2(x,q^2) = F_2(x)$ then the cross section is just multiplied by $1/\lambda$. If we, in changing from E_o to λE_o, change the geometry of our apparatus by moving magnets, counters and spark chambers along the beam according to $\sqrt{\lambda}$, increase the number of magnetized toroids by $\sqrt{\lambda}$ and the actual amount of material in both the scattering target and spectrometer by λ, we should obtain essentially the same $d(z)$ and $\sigma(z)$ at every point where these quantities are measured.

That this works out in practice has been checked with Monte Carlo calculations and ray tracing programs. The maximum possible deviation of two corresponding trajectories from each other is about 2.5 mm/f where $f \equiv \frac{E'_{min}}{E_o} < 1$ while deviations in track angle are less than 60 mrad + $\frac{4 \text{ mrad}}{f}$ inside the spectrometer (which is $\lesssim$ 1/4" offset between the two halves of a spark chamber module). In the rear of the spectrometer the correspondence of lines seen after all iron has been traversed

could be used as a scaling test by itself. Corrections to this apparatus scaling come from various sources. Among the most important are differences in the size of the beams at the two energies and the energy variation in dE/dx in the spectrometer which yields about a 2% shift of the upper edge in the E' distribution at one energy vs. the other energy. The effects of these and other small systematic corrections will be discussed in another section of this report.

We close this section by giving a table comparing the deflection d and the multiple scattering distribution width σ at 56 and 150 GeV for the actual geometries used. The values below are for $E' = E_o$.

Spark Chamber Module	σ (cm)		d (cm)	
Within Spectrometer:	56 GeV	150 GeV	56 GeV	150 GeV
11	0.14	0.14	0.54	0.51
12	0.54	0.52	2.70	2.51
Behind Spectrometer:				
13	1.02	1.02	6.20	6.22
14	1.18	1.17	7.45	7.50
15	1.41	1.34	8.70	8.81

II. APPARATUS:

The realization of the scaling geometry is shown in figure 1 for the two energies used in the experiment (150 GeV and 56.25 GeV). All longitudinal lengths have been scaled by the prescription of the previous section. In addition, to increase the kinematic range at each energy setting, we have taken data at a number of target positions with the rest of the apparatus unchanged. The next section summarizes the data taken at each energy.

MAGNETS:

The momentum analysing magnets (shown as blocks in the figure) are solid iron toroids 68 inches in diameter, with an inner diameter of 12 inches and a thickness of 31 inches. Each magnet runs at 35 amperes with an average B= 17.3 kilogauss.

A detailed study of the magnetic field is described in appendix I. These measurements leave an uncertainty of ±1.0% in the overall field normalization, and a ±0.5% uncertainty in the radial field dependence.

In the higher energy configuration three of the magnets (shown as unshaded blocks) are degaussed to achieve the desired scaling of multiple scattering. The degaussing procedure described in appendix II gives a residual field less than ±200 G, and could contribute 1.0% to the average field normalization and to the field shape.

TRIGGER COUNTERS

A scattered muon trigger is defined by three counter banks (labeled SA, SB, SC) which are slightly larger than a 70 inch diameter circle and have a 14" x 14" hole in the center to prevent beam triggers. A fourth identical bank of counters (HV_{II}) is placed upstream of the target to veto accidental beam-halo coincidences. A second veto counter HV_I overlaps HV_{II} and has a circular hole 7.5" in diameter to sharply define the beam size at the target.

Unscattered muons are vetoed by a coincidence of two veto counters BV

and BV'. To prevent an accidental veto by final state hadrons, the holes in each magnet are plugged with concrete. To test the effect of shower penetration the individual BV counters are latched for each trigger.

SPARK CHAMBERS:

Each spark chamber module, (labeled 7-15 in figure 1) consists of four planes 71" x 71" with magnetostrictive wands. Each module measures vertical and horizontal coordinates as well as two at ±45° to resolve multi-track ambiguities.

To improve spatial uniformity of the spectrometer efficiency the wands alternate in direction (eg. +x, -x etc.) in alternate spark chamber modules. The read out system permits a total of eight sparks or fiducials per wand with a overflow bit set for a ninth spark.

PROPORTIONAL CHAMBERS:

A multiwire proportional counter system is used to record the incident beam track and to locate the scattered track immediately down stream of the target. The beam chambers are approximately 20 x 20 cm, the down stream chambers are 40 x 40 cm.

The incident beam track is measured in three sets of chambers, (PC 2-4; only PC 4 is shown in figure 2) a total of 8 wire chambers, so that multiple beam tracks are resolved. The beam track is located at the target to ±1.5 mm, with the incident angle measured to ± .1 mr.

During energy calibration runs a fourth chamber PC 1 is used upstream of the last bend in the muonbeam line. This chamber allows a measurment of $\delta p/p$ and is used to reset the beam energy to its nominal value.

The chambers PC 5 and PC 6 have 2 mm wire spacing and read out four coordinates to resolve multi-track ambiguities.

TARGET COUNTERS:

For some events, typically having very high energy loss, ν, the track downstream of the target may be obscured by a hadronic or electromagnetic

shower. To provide information on these events the target is segmented into 4 inch blocks with scintillation counters between each block. These counters are pulse height analysed and the information used to provide a constraint on the vertex position for each event.

These questions of track reconstruction will be discussed in more detail in section IV.

BEAM COUNTERS:

The muon beam is defined by six counters shown as B 1 - 3 and C 1 - 3 in figure 3. The B counters (3 1/2" diameter) define the beam in the aperture of the bending magnets. The C counters restrict particles to a 7 1/2" diameter circle to stay within the active region of the proportional chambers PC 2 - 4.

Two counter hodoscopes are also installed in the beam, downstream of the last quadrupoles (enclosure 103) and downstream of the bend (enclosure 104). These counters, used with the proportional counters allow a measurement of the angle in and out of the last bend and give a momentum measurement ($\pm .5\%$) for each event.

TRIGGER LOGIC:

The trigger logic is shown schematically in figure 3. The data taken in this experiment comes from two types of triggers, labeled event and pulser. The event trigger defines a scattered muon event and provides about 70% of the data. The pulser trigger is designed to be a sample of the beam incident on the target without the bias of the event acceptance. Beam tracks from pulser triggers are reconstructed exactly as for event data and are used to monitor changes in the beam shape, and as input to Monte Carlo simulation programs.

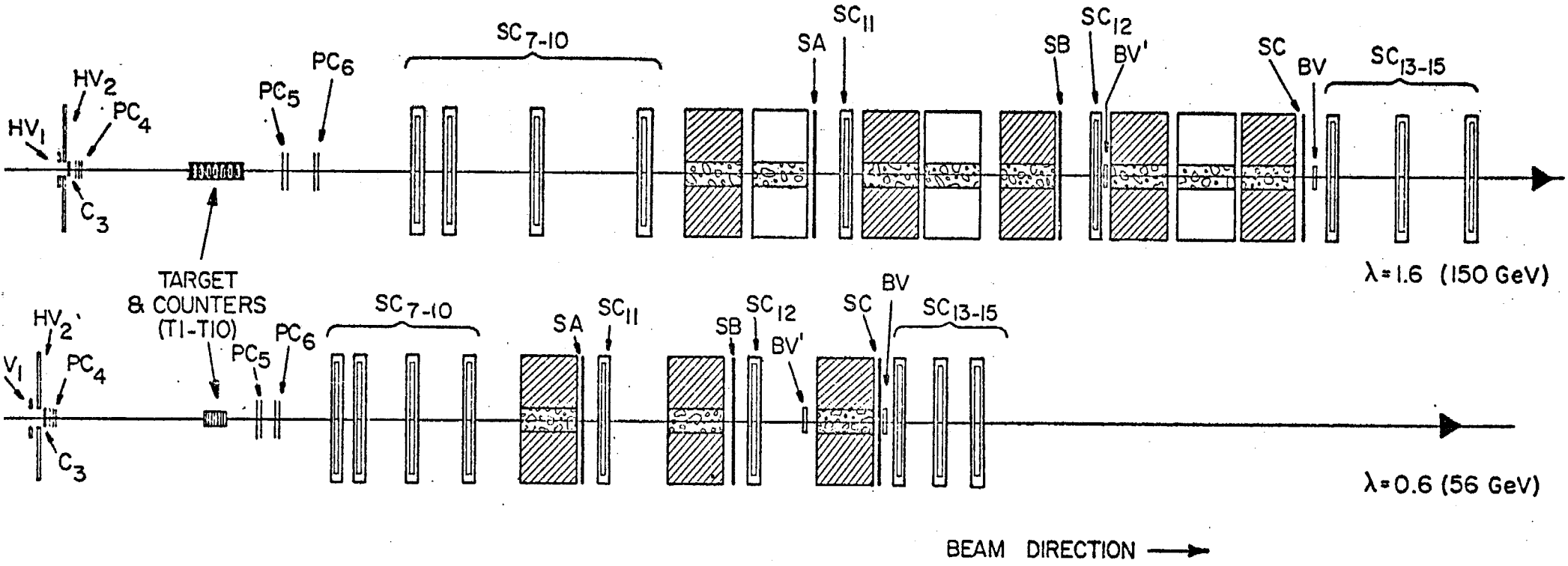

FIGURE 1. The Apparatus

26-40

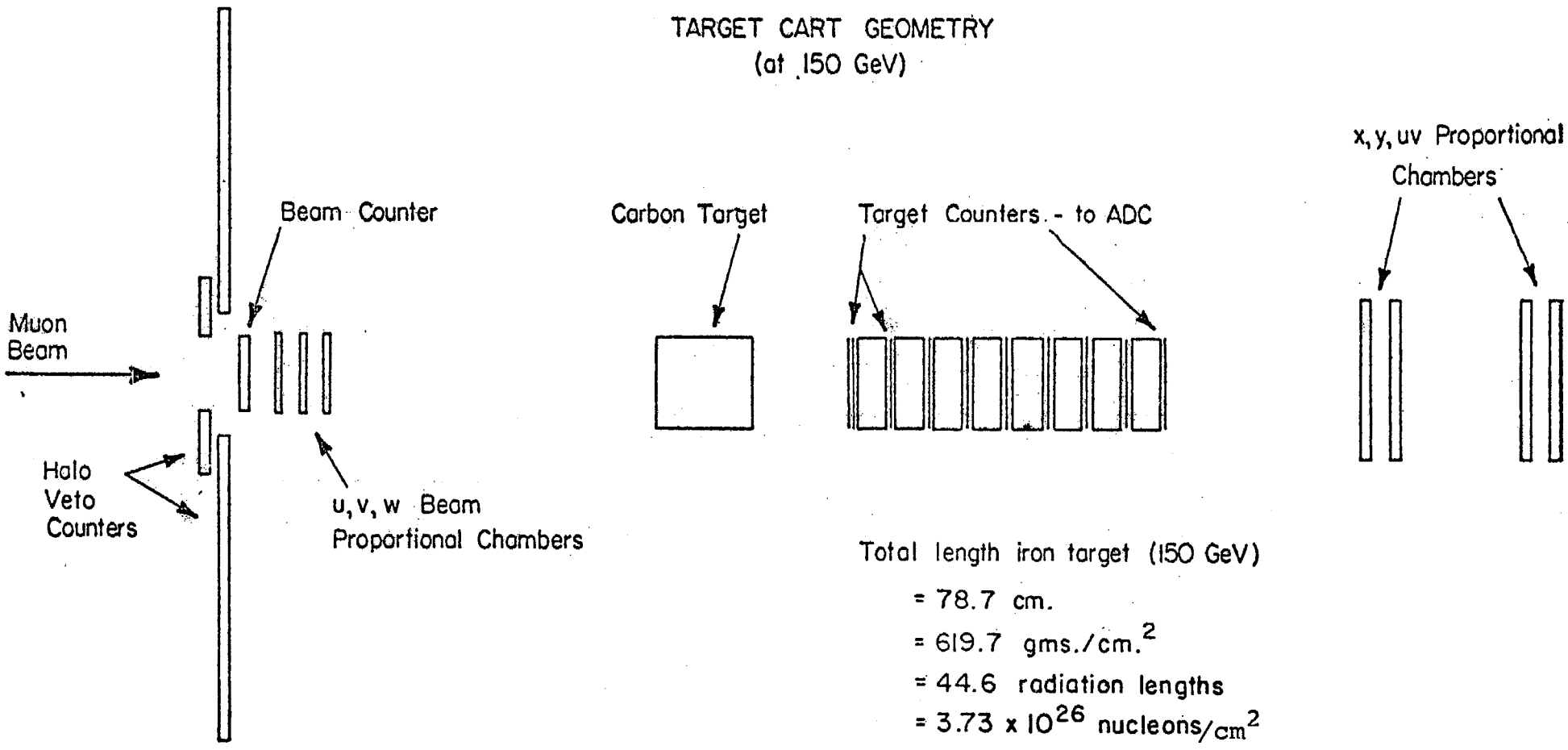
TARGET CART GEOMETRY
(at 150 GeV)
Muon Beam
Halo Veto Counters
Beam Counter
u, v, w Beam Proportional Chambers
Carbon Target
Target Counters - to ADC
x, y, uv Proportional Chambers
Total length iron target (150 GeV)
= 78.7 cm.
= 619.7 gms./cm.^{2}
= 44.6 radiation lengths
= 3.73 x 10^{26} nucleons/cm^2

FIGURE 2

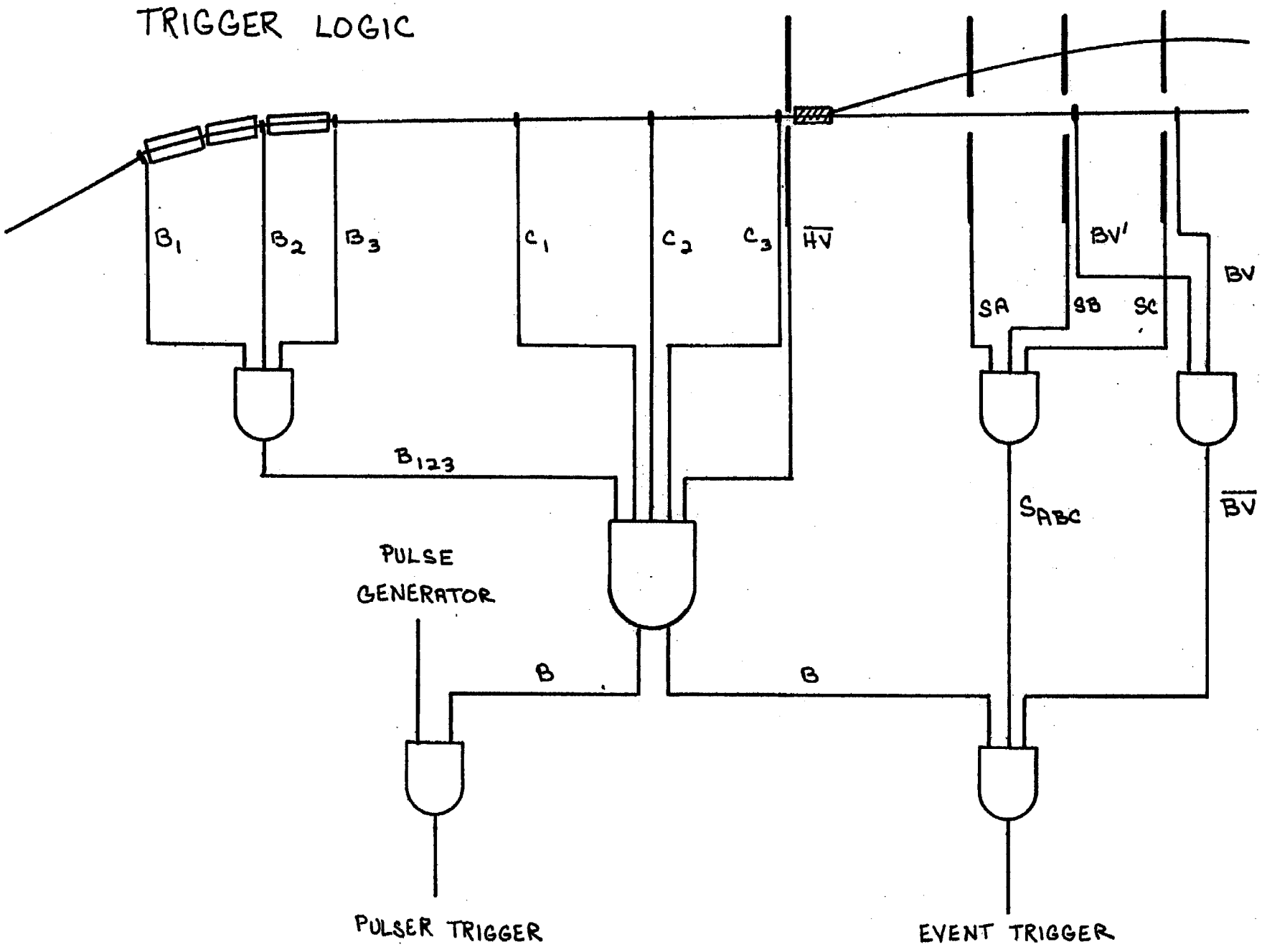

FIGURE 3. Trigger Logic and Counter Locations Along the Beam

III. DATA TAKEN:

The data taken is summarized in table 1. It is divided into three calendar periods, two incident energies, and four basic angular acceptance regions. The small angles of the 56 GeV data are the scaled values of 150 GeV small angles, using the prescriptions of section I.

The variation of the target position to change the angular acceptance is an important part of the data at each energy. The kinematic range of the data is increased significantly. In addition, the trajectory for a fixed momentum transfer will be detected at different radii in the spectrometer for each target position , providing information on the magnetic field shape and on efficiencies as a function of radius.

The qualitative effect of this variation is shown in figure 4 for the data taken in October 1973. For the very small angle configuration, data is accepted at momentum transfer down to 1.5 $(GeV/c)^2$. In the large angle configuration, data is obtained up to $Q^2 = 50\ (GeV/c)^2$.

E26 - Data Summary

Date	Nominal Setting	Angular Range	Incident Muons	Number of Triggers
Aug 73	150 GeV Small Angle	15 - 58 mr	$1.0 * 10^9$	47 k
	150 GeV Large Angle	24 - 88 mr	$1.5 * 10^9$	43 k
Oct 73	150 GeV Very Small Angle	13 - 50 mr	$0.7 * 10^9$	30 k
	150 GeV Small Angle	15 - 58 mr	$1.1 * 10^9$	50 k
	150 GeV Moderate Angle	19 - 70 mr	$0.8 * 10^9$	25 k
	150 GeV Large Angle	24 - 88 mr	$1.0 * 10^9$	50 k
	E = 150 GeV			
Apr 74	56 Small Angle	24.5 - 95.0	$2.6 * 10^9$	130 k
	56 Large Angle	39.2 - 144	$3.7 * 10^9$	80 k
	E = 56.25 GeV			

TABLE 1

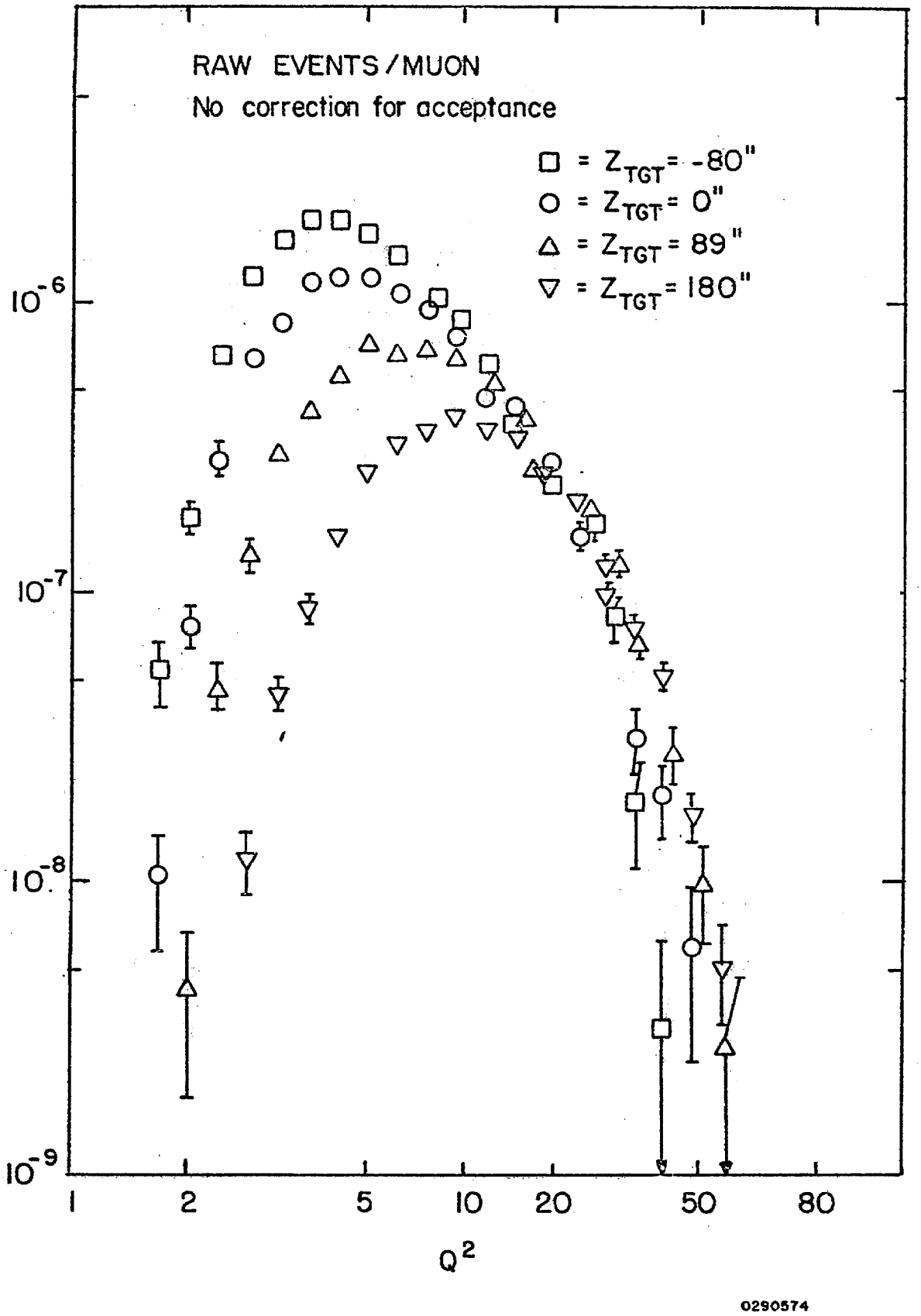

FIGURE 4. 150 GeV Data

STABILITY OF EVENT RATES

The data was taken at instantaneous beam intensities which vary over at least one decade. In addition the beam: halo ratio varied by more than a factor of two and the beam accidental rate varied from 0 to 3%.

We have studied the rate of reconstructed events, normalized to the incident flux, for each run to determine whether there exists any rate dependence. This study has particularly emphasized any bias in Q^2 which might result from such effects.

Figure 5 shows a representative distribution of events per incident muon, binned in Q^2 regions. In this and all other data samples we find no evidence of rate dependence in either the event yield or in the Q^2 distribution.

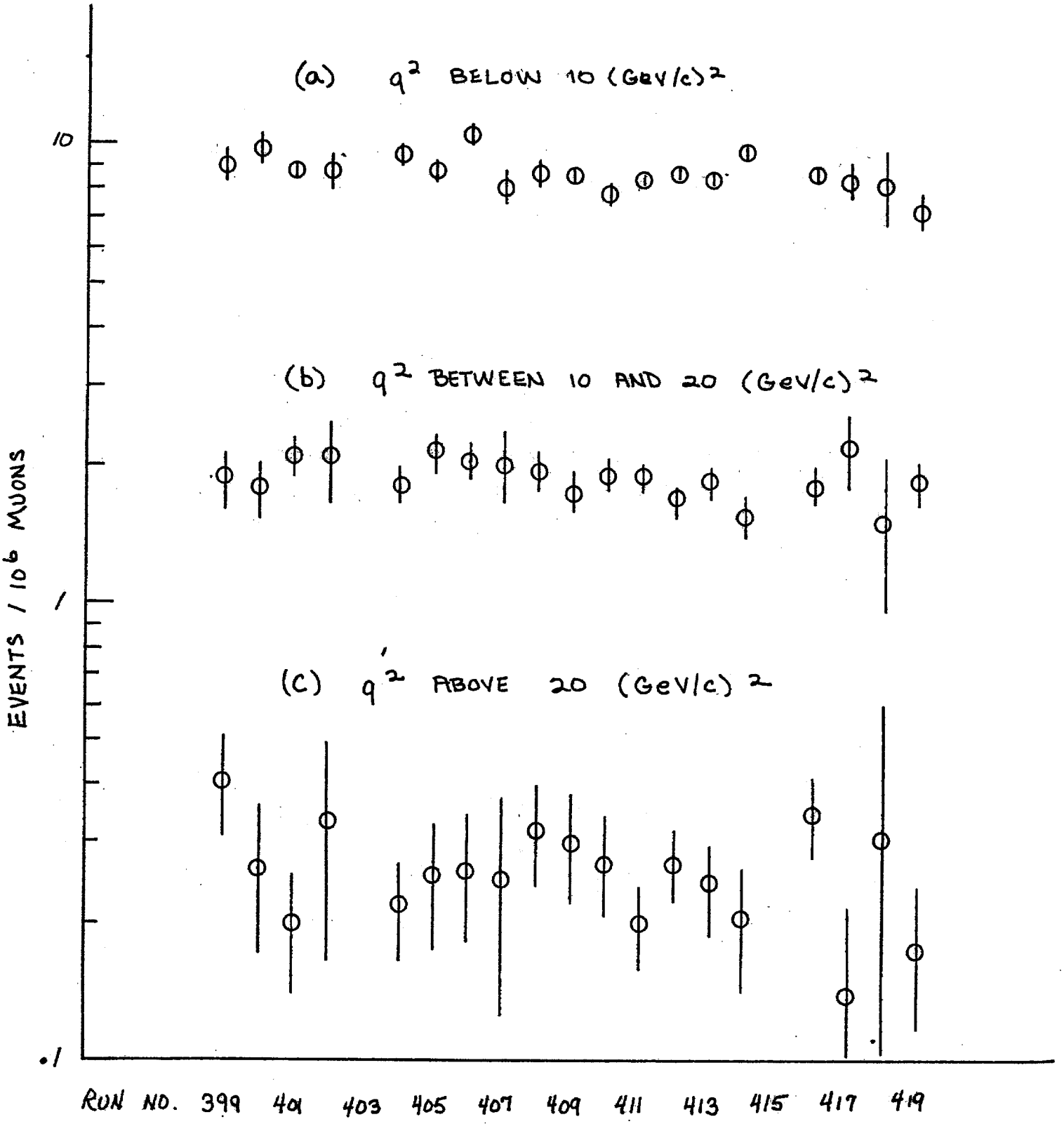

STABILITY OF 150 GeV DATA VS. RUN NO.

FIGURE 5

IV. SENSITIVITY TO SCALING VIOLATIONS

We discuss here the effect of our systematic uncertainties to a violation of scaling. We discuss in detail a violation which can be parametrized as a form factor as suggested by Drell and Chanowitz.

$$\nu W_2(x, Q^2) = F_2(x) \Big/ \left[1 + \frac{Q^2}{\Lambda^2}\right]^2$$

The "scale breaking mass", Λ, provides a simple measure of our sensitivity and is independent of specific theoretical models. Other ideas* of a scaling breakdown will require an analysis more dependent on the details of the specific model.

In the analysis of our data we compare data at different energies with our spectrometer and we compare data with the electron scattering data taken at SLAC, using a Monte Carlo simulation. The data to Monte Carlo comparison reduces our statistical uncertainty. The data to data comparison provides significantly smaller systematic errors.

SYSTEMATIC UNCERTAINTIES

We present here the more important systematic effects in the experiment. Most of these effects are less important for the internal scaling test than for the comparison of data to Monte Carlo. We will consider the most important effects in some detail.

ENERGY CALIBRATION

The energy of the incident beam must be scaled in the ratios 3:8 to achieve the scaling of the apparatus. In addition, we must know the absolute energy for comparison to Monte Carlo.

To test our sensitivity to this effect we have made a Monte Carlo simulation with slightly different incident energy. Comparison of these shows that a 1% change in incident energy would produce an apparent scaling violation of $(1/\Lambda^2) \cong 10 \times 10^{-4}$ $(\mathrm{GeV}/c)^2$ in our 150 GeV data.

* Such as modifications of the shape of $F_2(x, q^2)$ with q^2.

By steering the beam into the spectrometer we can measure the incident energy and can make any necessary corrections to the data. The relative setting of the beam energy can be done to ±.5% so that the remaining uncertainty is equivalent to $(1/\Lambda^2) = 5 \times 10^{-4}$ $(GeV/c)^{-2}$ in the data to data comparison. The absolute energy is known to ± 1% (see Appendix III).

SPECTROMETER CALIBRATION

The absolute calibration of the spectrometer magnetic field has been measured to ±1%. This uncertainty factors out of the ratio of data to data but can contribute $(1/\Lambda^2) = 10 \times 10^{-4}$ $(GeV/c)^{-2}$ in the ratio of data to Monte Carlo. See Appendix VI for further calibration details.

The radial dependence of the magnetic field can be measured better than the field normalization and the uncertainty is estimated to be less than ±.5%. At this level it has negligible effect on either scaling test.

In the high energy geometry some of the magnets are turned off so as to scale the magnetic field length relative to the length of mutiple scattering material. The degaussing procedure has been checked by magnetic measurements and the residual field is less than 200 Gauss, giving an uncertainty of 1% to the field integral in the eight magnets and in the radial field shape. This results in an uncertainty of $(1/\Lambda^2) = 10 \times 10^{-4}$ $(GeV/c)^{-2}$.

BEAM SHAPE

Since the radius of the muon beam at our target is approximately half the size of the first defining aperture in the apparatus, the acceptance for low Q^2 data varies significantly with changes in the beam shape. These changes are particularly important when changing incident energy in the scaling test since multiple scattering in the beam at low energy can change the effective beam spot size.

Computer simulations indicate that such changes can give an apparent Q^2 dependence and a fit gives $(1/\Lambda^2) = 10 - 20 \times 10^{-4}$ if not corrected in any way. This can be reduced by a factor of two if we ignore the lowest 10%

of the Q^2 spectrum. By cutting on beam radius, weighting events by their radial position, or by Monte Carlo simulation, we can reduce this effect significantly and the uncertainty in the final result is estimated to be less than $(1/\Lambda^2) = 5\times10^{-4}(\mathrm{GeV/c})^{-2}$.

V. PRESENT ANALYSIS SITUATION

We have worked on a number of different analysis programs, with different track finding procedures, point filtering, and overall event selection criteria. The two important programs mentioned in this report are RECON (versions 7 and 8) and VOREP. These two programs are independent in most respects, but in all cases the momentum fit is done by the program FINAL described in Appendix IV. FINAL has been checked in a number of ways using both data and Monte Carlo (see Appendix V). The exact value of the minimum scattered muon energy allowable has not yet been determined, but is $E_o/3$ at present.

The detailed study of the analysis and the comparison of the different approaches to track finding has been very useful in understanding event losses and biases in the event sample. Some of these studies are described in the last three appendices. We may summarize the present status of the analysis in the following:

1. In the most recent analysis, halo can be completely eliminated. Some contamination from halo may exist in the earlier preliminary results but was not a significant problem. It is now clear that halo can be separated using only the fitted track in and behind the spectrometer iron. This opens the possibility of fitting all events using only these spark chambers and thereby eliminating the problems associated with showers in the target.

2. Losses due to the presence of other particles in the chambers

in front of the spectrometer can be significant (~25-30%) at low secondary muon energy (large ν). This is discussed in detail in Appendix VII. This loss need not scale and can cause changes in the ω distribution. Again, an analysis using only information from chambers behind the first magnet is much better for these events and the approach is a very important part of our present analysis effort. Another approach is the use of pulse height information from counters distributed through the target to provide complimentary information to the front spark chambers. Preliminary studies indicate this will provide significant help in eliminating possible biases since the counter information is most helpful with large ν events.

3. Convergence of the analysis efforts has been slow but beneficial to the understanding of the special problems inherent in this type of apparatus at these energies when working with a rapidly falling Q^2 spectrum. It now appears that agreement has been reached on the level of uncertainty introduced by these problems. The "best" final analysis may be some combination of all tools developed so far, but will take some time. A more immediate and interim step would be results which still look very much like those presented at the Chicago APS Meeting. However, there will be uncertainties in absolute normalization caused by the hadron multiplicity problems. We expect to be able to agree on how to describe this normalization question in the near future. Non-scaling corrections to the ratio method data are being investigated diligently at this time and should converge shortly.

[redacted]

E26 SPECTROMETER MAGNETS

NATIONAL ACCELERATOR LABORATORY

GENERAL CHARACTERISTICS:

OD 68"
ID 12" good to about $\frac{1}{4}$", hasn't been accurately checked
Length ~ 31 1/8 ", see table I
Each magnet contains 4 $7\frac{1}{2}$-8" slabs

Low-Carbon Steel; very high permeability at low fields -
$\mu \sim 20{,}000$ at H= 1 oersted (see fig 1)
$\mu \sim 1500$ at operating current (H~40-200 oersted)

Time constant for changing field in the iron depends on σ (conductivity), μ (permeability), and thickness (~4" = $\frac{1}{2}$ of slab thickness).
($t^2 \sim \mu d/\sigma$). For μ given above, t=
The field has been observed to change for as long as 15 minutes after changing voltage, when working at low fields during degauss cycle.

It is easy to change the field more rapidly by supplying enough voltage to force the current to change rapidly (ie $V \gg IR$) , 'bucking out'* the eddy currents which attempt to shield the interior of the magnet. This undoubtedly results in complex patterns of magnetization at low fields (A Hall-probe test suggested a layer of reversed magnetism near the outside of a magnet which had been rapidly turned off). Fortunately at standard operating currents hysteresis effects are very small (fig 2), described later. Some 'forced' time constants are shown in fig 3.

B(H) was measured for a small toroid cut from the same steel as the large magnets (4 small toroids exist, 1 from each of the different 'heats' from which the steel plates came). Dimensions are nominally 8" ID, 11" OD, 1.5" high; the cross-section is 1.500x1.500 square, centered at a radius of 4.75". Measurements of these distances made before the toroids were wound havn't survived- if one wants a measurement of B (H) with absolute normalization better than ~1% this must be done.

Standard operating current for all magnets was to be 35 amps. During the October Runs, AC voltage was low and the magnets usually (but not always) ran at about 33 amps. The August running was also mixed. To avoid scaling problems the magnets were run steadily at 33 amps for the April run: as discussed later, this drop in current results in close to a 1% drop in the magnetic field at all radii, with no observable change in the shape of the field.

The magnetic field in the large magnets was checked in 3 ways:

A. B(R) was predicted for the large magnets by projecting the measured B(H) curve onto the $H \propto 1/R$ field expected for a toroid

B. B(R) was measured by integrating current from flux loops wound at different radial positions on the faces of several magnets

C. The total flux in each magnet was measured using a single coil wound around the entire magnet.

* A colorful term suggesting some ignorance of detail

NATIONAL ACCELERATOR LABORATORY

FLUX LOOP MEASUREMENTS

From apprpppriate fundamental laws change of magnetic flux through a coil results in a flow of current

$R\int I\,dt = \Delta\phi = NA\,\Delta\bar{B}$

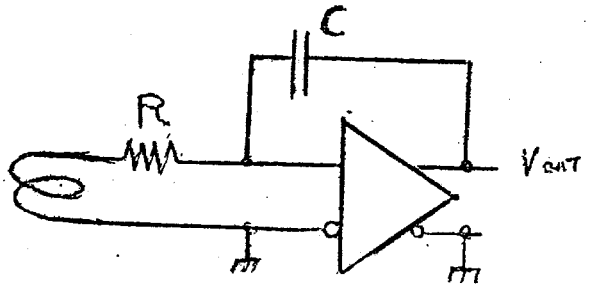

If this charge is integrated by a capacitor the voltage across the capacitor will be

$V_c = Q/C = \Delta\bar{B} * A/NRC$

An ideal integrator can be closely approximated by a high gain op amp connected as in figure. The op amp keeps the input voltage near 0 volts by raising the capacitor voltage to 'suck up' all charge injected at the input. Small non-ideal effects such as leakage currents from the input transistors are nulled out with potentiometer, and temperature stability of this null is the major limit on performance. The NAL integrators use an Analog Devices 234L , a chopper-stabilized module. Some of them use ferrite cores on the input lines to filter out SCR hash; this is desirable as I have irregularly noticed drift when running the magnets at low currents where the DC voltage waveform is extremely spiky.

In practice, integrating 1-10 volts with R=300k, C=1uf, drift was negligible ($\leq$.1%) over the 5-10 minute period used to take readings by reversing magnet polarity, and was unpredictable over the 4 hour period needed for a degaussing cycle. The integrator for my measurements in April was calibrated to the .1% level, as was the DVM, with a standard voltage source and other equipment used by the NAL mag measurements group. I have no reason to think that my measurements of $\Delta\phi$ are much worse than that (ie the 10 minute measurements). Relating $\Delta\phi$ to the B field in the magnets is a more substantial problem.

Most of the B measurements were made by running the magnet at +I, then switching to -I, and measuring $\Delta\phi$ for some region of the magnet. Measurements were also made in which the magnet was repeatedly turned on and off, ie +I,0,+I,0 , to demonstrate that the initial condition of the magnet did not affect the measured ϕ at +I . A sample set of measurements is shown:

Fig 2 shows a measurement of hysteresis at currents below the normal 35 amps. Coil #1, at outside of magnet 7 shows below 30 amps a larger field coming down from +35 amps than going up from -35 amps; close to a 'worst case' test. Coil #4, close to the inside of mag 7 shows a deviation opposite that exp ected, perhaps hysteresis in the current meter on the magnet power supply? In any case the effect at 33 amps is less than ½%, although it was noted in some other of the measurements at 33 amps and isn't understood.

MAGNET # 4 , Coil #3 ($\bar{R}$ = 19.5")

I	V_{int}
+35a	-.705v
0	
-35	1.288
0	
+35	-.705
0	
-35	1.290
0	
+35	-.704
0	
+35	-.704
0	
+35	-.704
+33	-.696
0	

ΔV_{35a} = 1.989v

(.004v DVM offset subtracted from result)

NATIONAL ACCELERATOR LABORATORY

Magnet #7

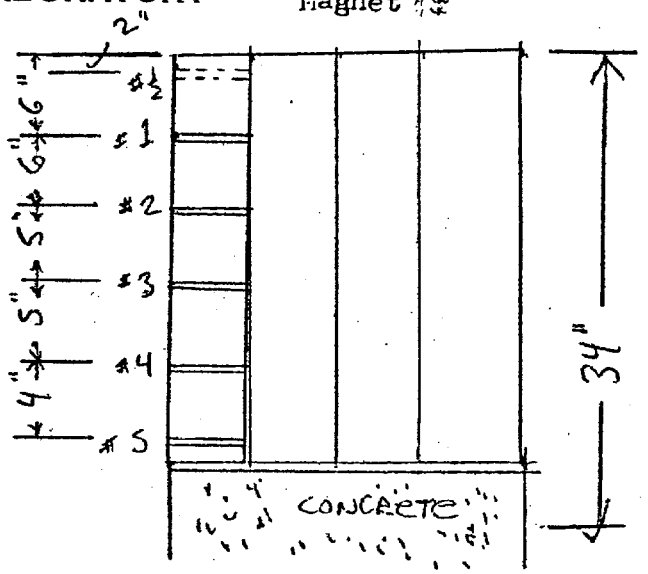

RADIAL FIELD MEASUREMENT

Because some of the magnets have up to 1/8" spaces between their plates it is possible to drill holes through a single 8" plate and with the aid of a thin snagging apparatus wind coils between the holes, thus sampling the field at different radii. Positions of holes, all $\frac{1}{4}$" diameter, for magnet #7 is shown. A coil wound between holes 2&3 would sample the field at an average distance of 15" from the outside of the magnet, for example. It is important that the holes not disturb the field in the magnet: The 6 holes shown occupy $1\frac{1}{2}$"/28", or about 5% of the area of the magnet-plate in transverse cross section. A simple analogy suggests that the total change in the rel uctance of the magnet will be much less than this 5%. In the ladder of resistors shown, removing a single resistor from the chain wil l shange the resistance of that link in the chain from R/5 to R/4, or 20%. The r esistance of the ladder changes by only 6% : the remaining resistors in the link carry more current. This doesn't work quite as nicely in the m agnet - because μ decreases as B increases, the 'resistance' of the iron remaining actually increases a bit when the hole is drilled.

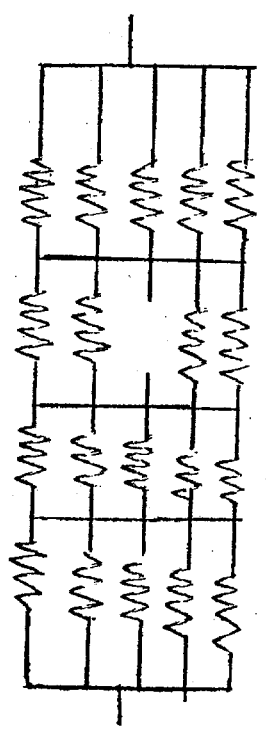

A direct test is to measure total flux before and after a hole is drilled. This was done in the region occupied by coil#1, extending from the outside of the magnet (34") to 6" in. A complete set of radial measurements was taken in September. Somewhat later hole#$\frac{1}{2}$ was drilled, at 32" radius, and a complete set of radial measurements was taken in April. Because the integrator measurements in Sept were not absolutely calibrated, I am comparing the ratios of the measurements at different positions;

Coil#	April	Sept	April/Sept
1	16.39kg	16.40	0.999
2	16.82	16.80	1.001
3	17.15	17.10	1.003
4	17.90	17.92	0.999
5	18.74	18.70	1.003

The average value is 1.001, so the additional hole in the space of coil #1 , occupying $\frac{1}{4}$"/6" = 4% of the area of the coil, has changed the field by 0.999/1.001, probably somewhere between 0 and .3%.

NATIONAL ACCELERATOR LABORATORY

MORE RADIAL FIELD MEASUREMENT

Another problem with the holes is that part of the magnetic field stays in the hole. A Hall Probe measurement at full field gave about 200 gauss in the holes, or about 1% of the field in the iron, which is entirely negligible for a measurement covering several inches of iron. This was tested directly by checking that the magnetic ~~fields~~ flux between the outside of the magnet and hole #½ , and between hole #½ and hole 1, added to the same result as coil #1. The result was agreement to .1% .

The largest error in the radial measurements is undoubtedly the measurement of the area of the coils. I have defined the area to extend to the center of each hole, because that is the area that the flu x lines would occupy if they had not been disturbed by the holes. This is wrong only to the extent that the flux divides unevenly between the two sides of the hole because of the difference in μ. The measurement of flux through coil #½ (outer 2" of magnet) may actually be affected by this - squeezing 1/8" of flux into the 2" area available results in a 6% increase in average field, so the flux may prefer the opposite side, where it can spread out. A 10% asymmetry in division of the flux would cause the ½% deviation of the measured flux for this coil shown in fig 4. The distance of the holes radially was measured on both the inside and outside faces of the plate, to an accuracy of between 1/16" and 1/32". The thick nes of the plate was measured only at the outside of the plate - because the plates (on the basis of rather poor statistics) are quite even in thickness about the outside diameter I have assumed that the thickness doesn't change much from inside diameter to Outside.

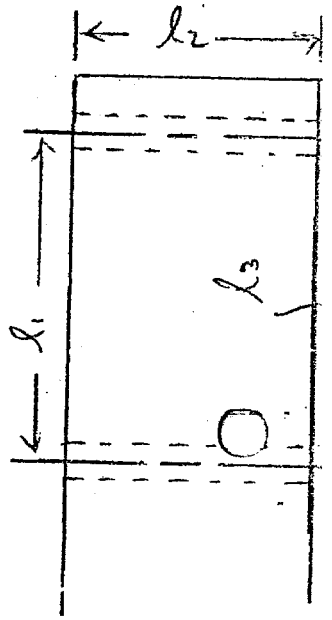

The effect of a 1/32" error in measure of distance is shown for coil #½ (assuming that one radial measurement is off by 1/32, changing the average by 1/64") which is 1/64"/2" =.8% . Because the other coils are 2-3 times as large the effect of a similar error on them will be less than ½%. The deviations of the measured points from the smooth line in fig 4 a re of this order.

Fig 4 shows complete sets of radial measurements for magnets 4&7. Agreement between the two is about 1/3%, suggesting that some of the deviations from the predicted field line are real: in particular I suspect that the higher field at the outside magnet radius is real, and the the measurement for coil½ at 32"' is low. Except for this point I have no reason to think that any of the measurements is wrong by more than ½%. Figure 5 shows the measured field for I=33 amps. The result is extremely close to a uniform shift of 1% across the face of the magnet. This shift was indep endently measured to be 1% by the integral field measurements discussed below.

NOTE: the close agreement (about .1%) between the Sept and April measurements is slightly fraudulent because it is the result of two compensating errors- the integrator u sed in Sept was apparently close to 1% low, and the thickness of the plate in mag 7 was measured high by 1/16/7.5" =1%. That both sets of data fall so close to the small toroid prediction is, of course, completely accidental .

NATIONAL ACCELERATOR LABORATORY

INTEGRAL FIELD MEASUREMENTS

Total flux through each magnet was measured with a single-turn coil. This may be converted to an average B by dividing by the area, which is not however well known - the ID's of the magnets cannot be measured with the coils in place. $\frac{1}{4}$" error in the OD or id results in 1% error in the area (which is about 31"x28"). The maximum measured deviation between magnets is about 1%, suggesting that the distances are good to +/- 1/8"; but this cannot be separated from differences in the fields at this level. Results are shown in Table I.

Because two different power supplies were used to run the magnets, and because connection of the magnets was different in the 56 gev and 150 gev configurations it is important to compare the field in the magnets as they were hooked up for the two configurations (fig below). I did this with the integral measurements.

56 GEV		150 GEV	
North Acme 35 amps ~120 v	South Acme 33 amps ~235 v	North Acme 35 amps ~120v	South Acme 66-70 amps ~235-250v
(Magnet 2)	(Mags 1&3,series)	(Magnet 5)	(Mags 1&3,series) in parallel with (Mags 6&8,series)

Standard measurements (eg radial) were always made with two magnets connnected in series to the South Acme supply. The following correction factors for different situations were discovered:

Magnet #2, powered by the North Acme at 35 amps, has the same flux as Magnet #2, powered by the South Acme supply at 33 amps.

The total flux in each magnet fell by close to 1% as the current was changed from 35 amps to 33 (here, as for coil #4, fig 2, values for the flux were about $\frac{1}{4}$-$\frac{1}{2}$% higher when the current was raised to 33 amps, than when the current was reduced to 33 amps. I have taken average values; presumably during the running both situations occurred.

For magnets 1 and 3, flux is $\frac{1}{4}$% low when they are run in parallel with 6&8, as at 150 gev.

For magnets 6&8, flux is $\frac{1}{2}$% low when they are run in papallel with 1&3, as at 150 gev.

In the absence of complete information I have adopted the following conventions for my best estimates of magnetic field in the spectrometer:

Assume B(R) same for all magnets when run at 35 amps by South Acme supply.

Use Integral field measurements to calculate correction factors depending on the way in which a magnet was hooked up, giving $B(R)_{150}$,etc.

Calcultate correction factors from measured magnet lengths,(and applying this factor also to B(R), compare B (R) * L for the different configurations. This is not to be confused with the integral field measurements ~~xxxxx~~ for which I trust the absolute result less because of the unmeasured radial distances.

Final correction factors are given in Table II

NATIONAL ACCELERATOR LABORATORY

SMALL TOROID MEASUREMENTS

Several years ago B(H) was measured by attempting to degauss small toroid #2 and then monitoring $\Delta\phi$ as it was turned on. Figure 6 shows the measured field, and figures 4&5 show the predicted B(R) in the large magnets. The 'neww' predicted value is a recent recalculation of B(R) from the old values of ΔV which benefits from use of a modern electronic calculator. The agreement with normalization of large magnet measurements is a bit worse than for the 'old' prediction but the shape looks better. I have not repeated the old small magnet measurement including the degaussing but have checked the high field points by measuring $\Delta\phi$ for reversing current in the small toroid. The results check well.

I	B(OLD)	B(NEW)*	NEW/OLD
60	20.18	20.22	1.002
40	19.31	19.28	1.002
30	18.81	18.73	0.996
20	17.91	18.08	1.009
10	16.53	17.15	1.038
5	15.50	-	

* these numbers come from Sept measurements and include a factor of 1.01 which was necessary to make the April and Sept measurements on Magnet #7 consistent

B(H) was also measured in Sept for the other 3 small toroids, with results shown in fig 7, without the 1% correction. Because the area of the coils may only be assumed, as well as the number of primary turns on the toroid, these measurements don't contribute much information at the level of precision at which I am operating. To improve the measurements, the toroids must be unwound and wound up again, probably a mere day of filthy work.

TABLE I (INTEGRAL FIELD MEASUREMENTS FROM APRIL)

MAGNET #	LENGTH	LENGTH/31.125"	$\overline{B*L}$,35amps ($\Delta\phi$/28")	$\overline{B}_{33}/\overline{B}_{35}$	ΔB (56 GEV)	ΔB (150 GEV) 66 amps	ΔB (150 GEV) 70 amps
1	31.125"	1.000	13.74 kg-m	.992	-.9%	-1.2%	-.3%
2	31.190	1.002	13.57 kg-m	.9935	-1.%	off	off
3	30.750	0.988	13.59	.992	-.9%	-1.2 %	-.3%
4	31.190	1.002	13.78	.991	off	off	off
5	31.125	1.000	13.70	.991	off	-1. %	-1. %
6	31.125	1.000	13.75	.992	off	-L.5 %	-.5%
7	30.560	0.982	13.61	.991	off	off	off
8	30.810	0.990	13.72	.992	off	-1.5 %	-.5 %

NOTES:

ΔB measures deviation from standard test measurement with 2 magnets in series connected to South Acme supply,35 amps

ΔB doesn't include magnet length correction, which must be included at some point to calculate bend of muons

B_{33}/B_{35} has been averaged to .9% for all magnets

26-48

31

TABLE II (COMPARE B\[illegible] for [illegible],150 gev com[illegible]ons)

56 GEV		150 GEV (66a)		150 GEV (70a)		$B*L_{56}/B*L_{150_{66}}$	$B*L_{56}/B*L_{150_{70}}$
MODULE 1		MODULE 1		MODULE 1			
Magnet 1	-.9%	Magnet 1	-1.2%	Magnet 1	-.3%		
		Magnet 2	off	Magnet 2	off	1.003	0.994
MODULE 2		MODULE 2		MODULE 2			
Magnet 2	-.8%	Magnet 3	-2.4%	Magnet 3	-1.5%		
		Magnet 4	off	Magnet 4	off	.504	.502
		Magnet 5	-1..%	Magnet 5	-1.0%	(x2=1.008)	(x2= 1.004)
MODULE 3		MODULE 3		MODULE 3			
Magnet 3	-2.1%	Magnet 6	-1.5%	Magnet 6	-.5%		
		Magnet 7	off	Magnet 7	off	.499	.492
		Magnet 8	-2.5%	Magnet 8	-.5%	(x2=0.998)	(x2=.984)
TOTAL B*L		TOTAL B*L		TOTAL B*L		TOTAL B*L	TOTAL B*L
2.962 (3.0 for no correction)		4.914 (5.0 for no correction)		4.962		.603 (ideally 3/5)	.597

NOTES:

A 'standard' magnet is defined to have B(R) as measured at 35 amps, with length 31.125"

FIG 1 26-4955

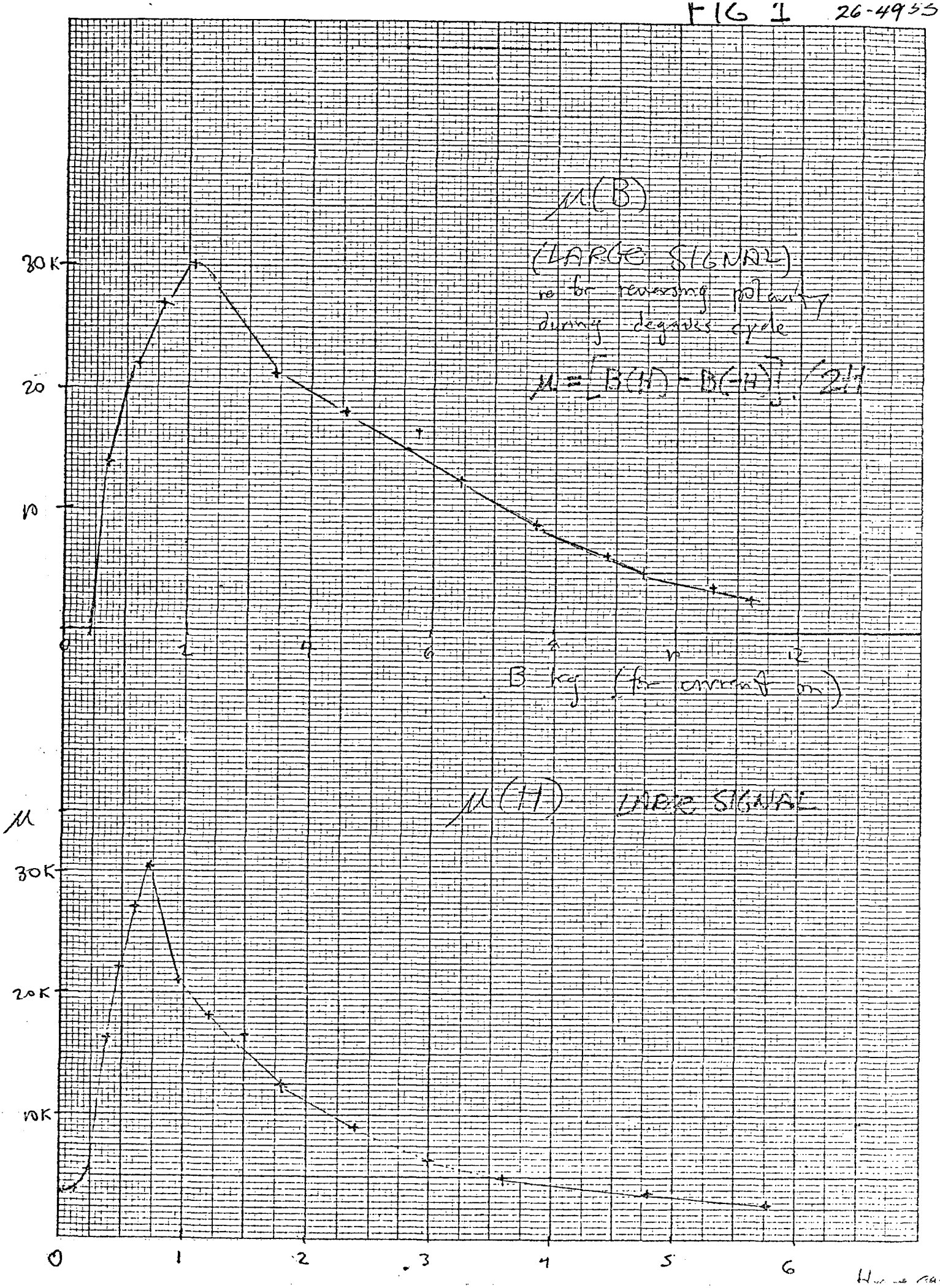
μ(B)
(LARGE SIGNAL)
no for reversing polarity during degauss cycle
μ = [B(H) - B(-H)] / 2H
30K
20
10
0
2
4
6
8
10
12
B kg (for current m)
μ(H) LARGE SIGNAL
μ
30K
20K
10K
0
1
2
3
4
5
6

HYSTERESIS IN E-26 MAGNETS

FIG 2

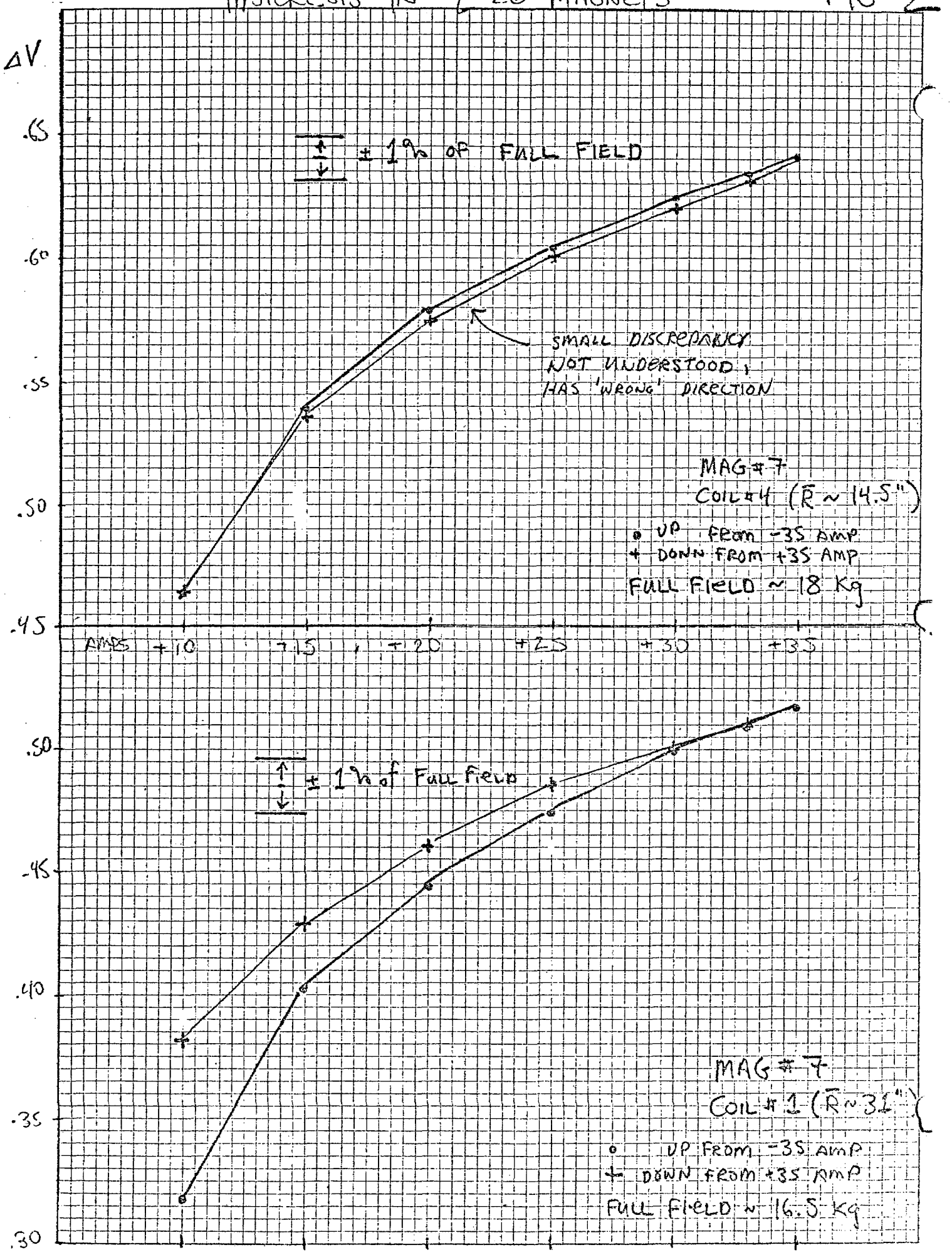

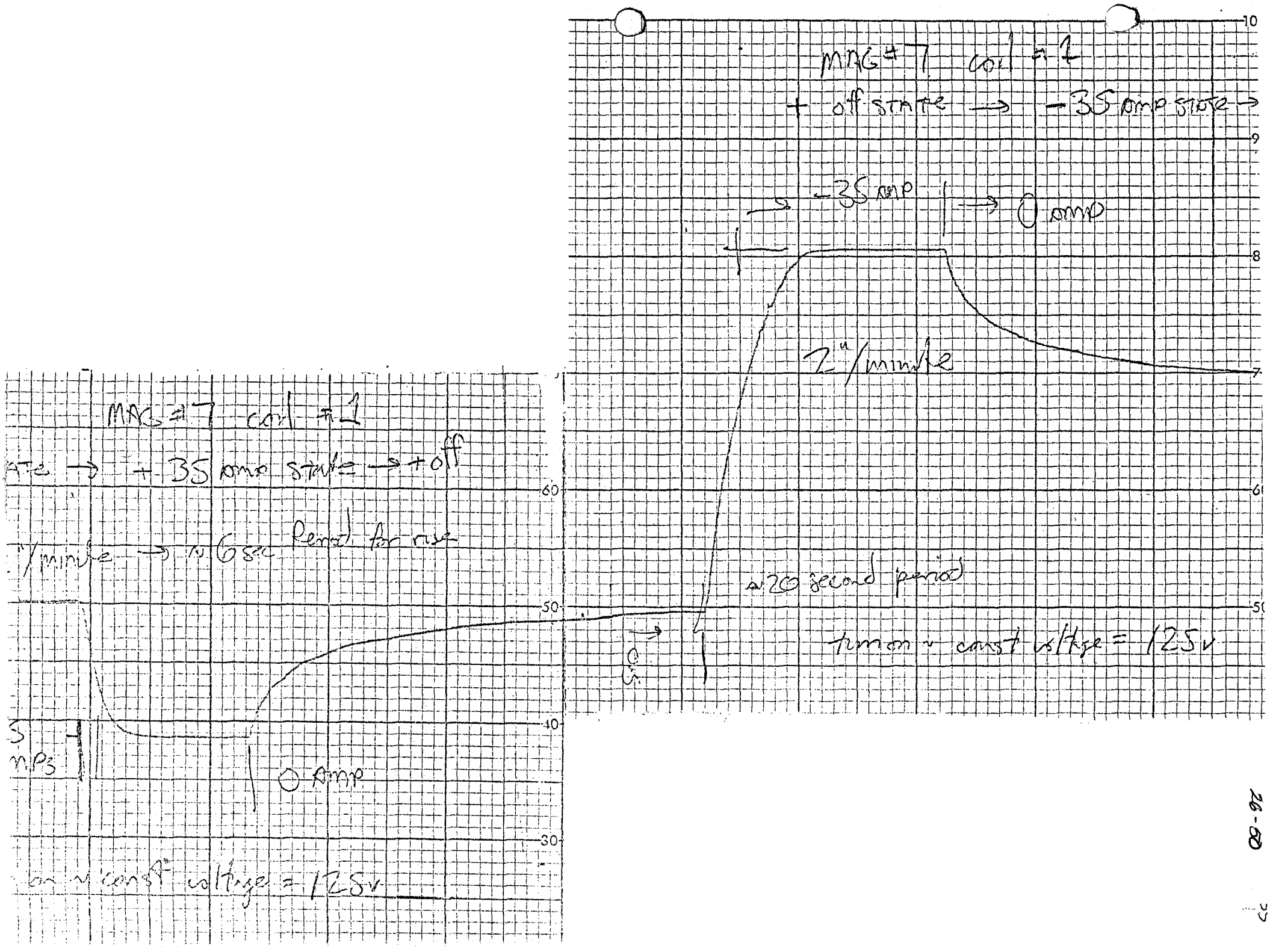
MAG #7 coil #1
+ off state → -35 amp state →
-35 amp
0 amp
2"/minute
~20 second period
timon ~ const voltage = 125v
MAG #7 coil #1
ate → + 35 amp state → + off
"/minute → ~6 sec Period for rise
0 Amp
on ~ const voltage = 125v

26-60

FIELD IN E-26 MAGNETS AT 35 AMPS FIG 9

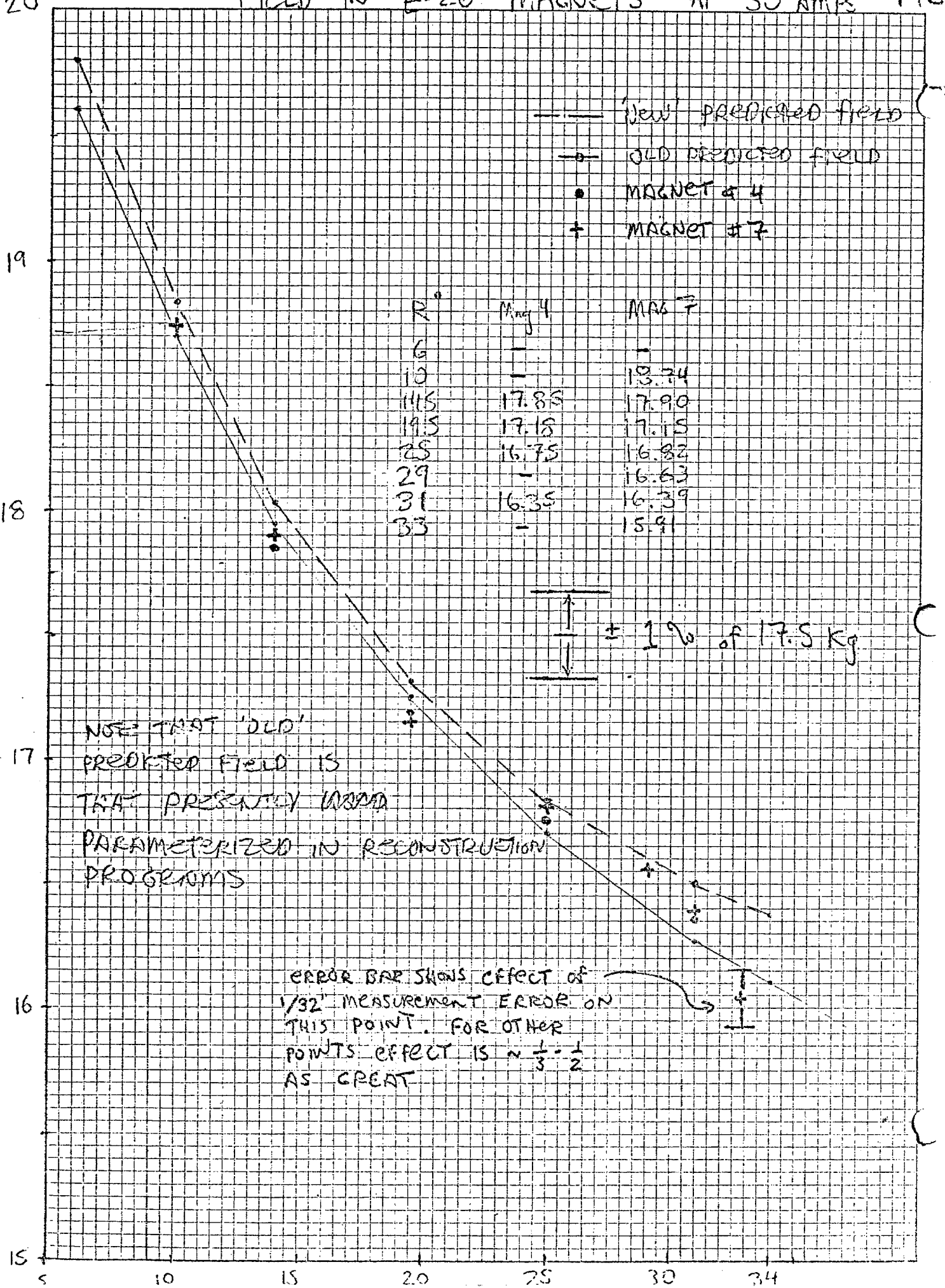

R°	Mag 4	MAG 7
6	–	–
10	–	19.74
14.5	17.85	17.90
19.5	17.18	17.15
25	16.75	16.82
29	–	16.63
31	16.35	16.39
33	–	15.91

FIELD IN E-26 MAGNETS AT 33 AMPS 26-51 FIG 5

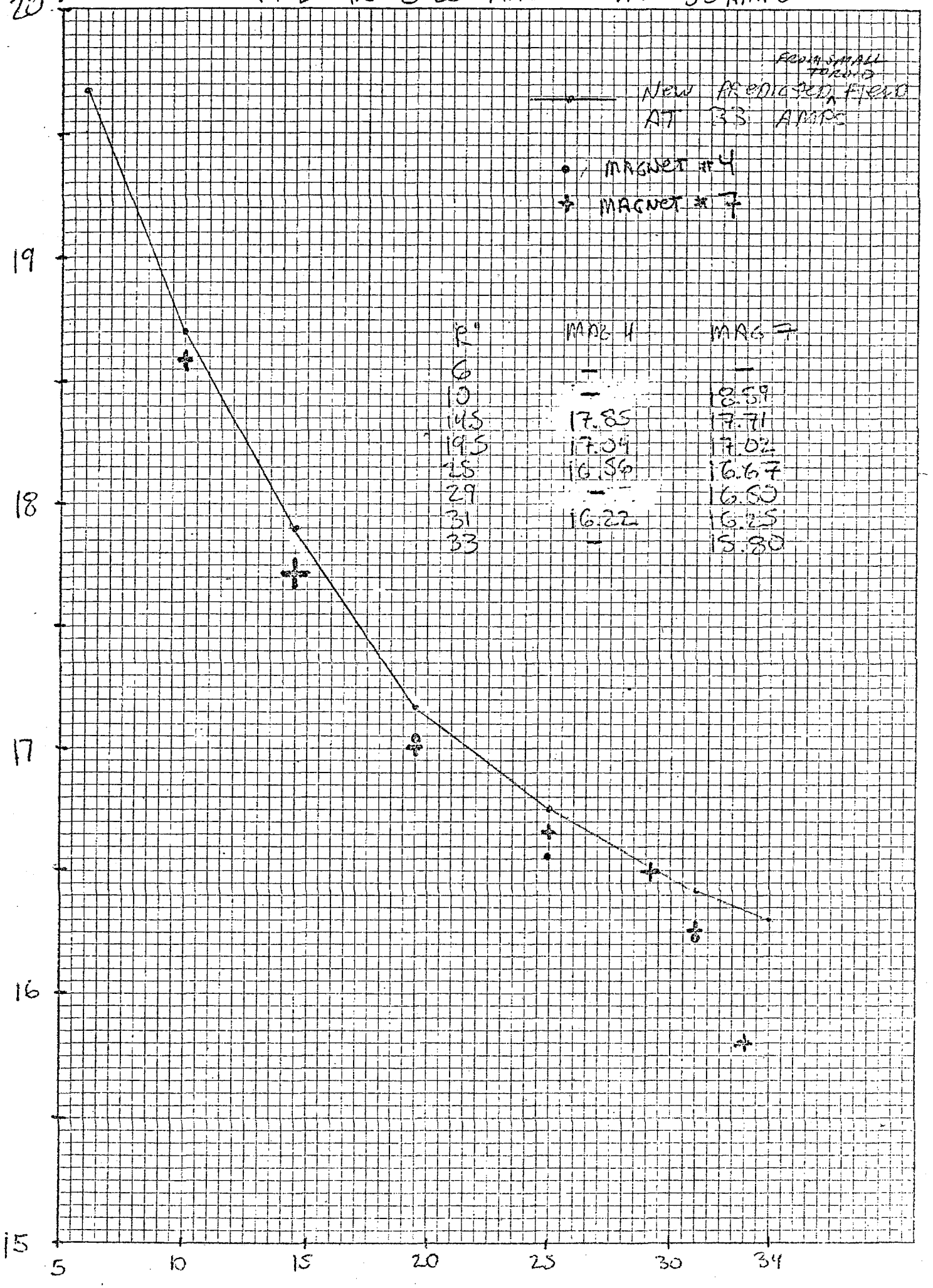

R"	MAG 4	MAG 7
6	—	—
10	—	18.59
14.5	17.85	17.71
19.5	17.09	17.02
25	16.56	16.67
29	—	16.50
31	16.22	16.25
33	—	15.80

37

B(H) from small Toroid

FIG 6

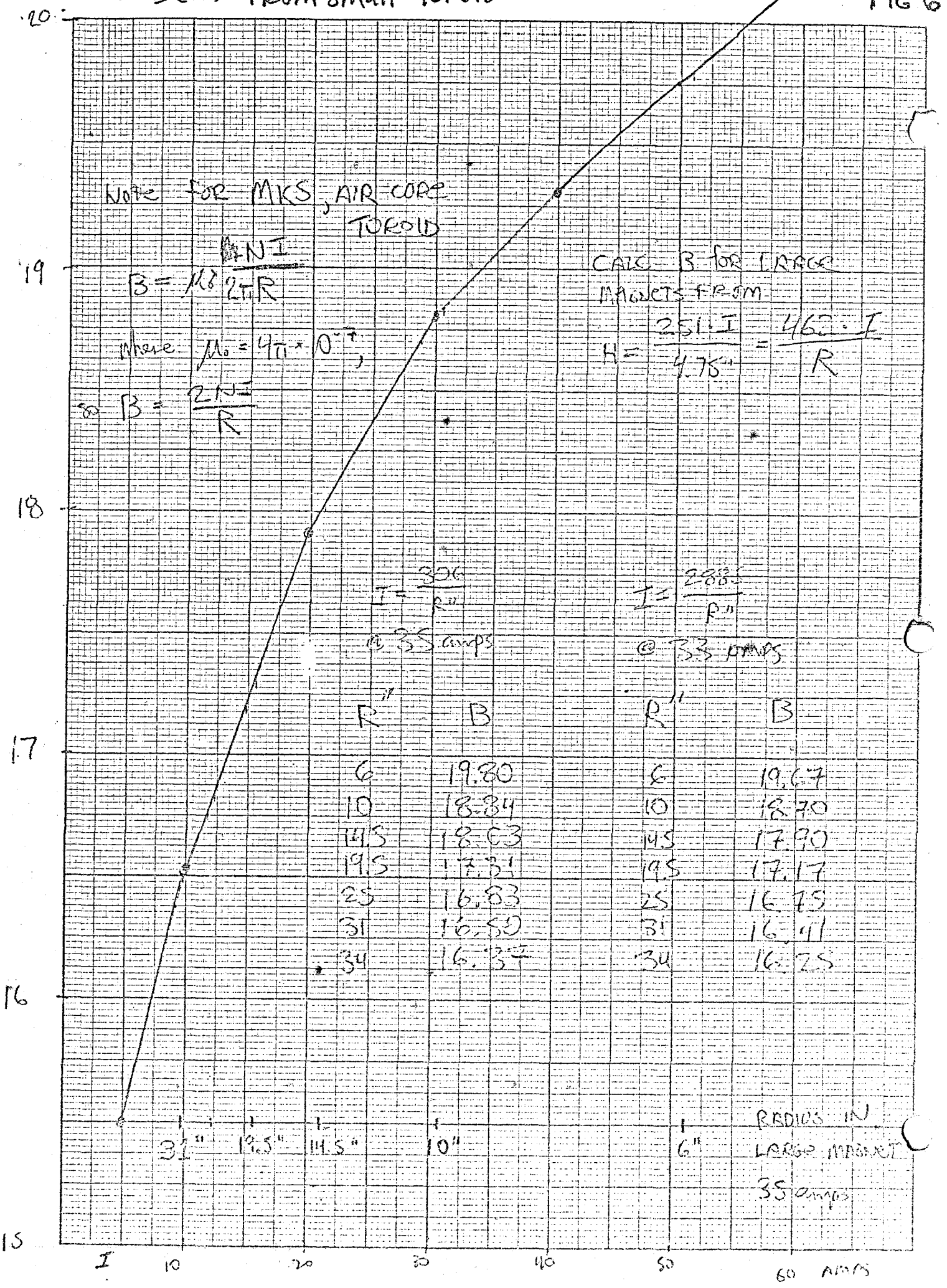

Note for MKS, AIR CORE TOROID

$$B = \mu_0 \frac{NI}{2\pi R}$$

where $\mu_0 = 4\pi \times 10^{-7}$,

$$\therefore B = \frac{2NI}{R}$$

CALC B for LARGE MAGNETS from

$$H = \frac{251 \cdot I}{4.75''} = \frac{46.7 \cdot I}{R}$$

$$I = \frac{396}{R''}$$

@ 35 amps

R"	B
6	19.80
10	18.84
14.5	18.03
19.5	17.31
25	16.83
31	16.50
34	16.37

$$I = \frac{280}{R''}$$

@ 35 amps

R"	B
6	19.67
10	18.70
14.5	17.90
19.5	17.17
25	16.75
31	16.41
34	16.25

DEGAUSSING OF SPECTROMETER MAGNETS
NATIONAL ACCELERATOR LABORATORY

Wristwatches are degaussed by placing them in a 60-cycle AC magnetic field whose amplitude is gradually reduced to 0. The skin depth of our magnets at 60 cycles is roughly 1mm, so a lower frequency must be used, about $(15 \text{ minutes})^{-1}$ at several kg where the permeability of the iron is as high as 20,000. Because the H field varies as 1/R in toroids, therefore by a factor of 6 from the inside to outside radius of our magnets, different regions of the magnet experience different degaussing cycles, and the voltage steps and time steps used must work for all regions.

Figures 1&2 show the excited and remnant fields in two different regions, $\bar{R}$= 31" and $\bar{R}$=10", decreasing as the magnet is cycled down. A crude description of the result is that not much happens until the excited field approaches the normal remnant field (about 6 kg). Time constants then become very large (10-15 minutes) and the excited and remnant fields move down together. Below perhaps 1kg the time constants become shorter again and the remnant field converges to some final value, which is 0 if the procedure has worked. Figure 3 shows a failure - I did not wait long enough for the magnet to reach full field at the 15v (~2 amp) setting and the cycle converged with B=700 gauss at 25" radius in the magnet. These measurements were taken by following the flux through coils at different radii with an integrator, and the voltage step sizes and time periods were chosen by requiring that the remnant field change gradually between steps for all regions of the magnets, and requiring that field in the magnet stop changing before each new change of the voltage across the magnet. Table I shows the 'standard' degauss procedure which was worked out during Sept and used to degauss the magnets for the Oct run. Figure 4 shows remnant fields which were measured at different radii during test runs of the procedure in Sept..

Because of integrator drift, the field in degaussed magnets could only be accurately measured by turning the magnets back on, to +/- 35 amps, and checking how far the degaussed was from the center, and because the magnets degaussed for the oct run were all turned on for the end of the running, the fields were not measured in this way and the results of figure 4 are the best available estimate for field in the magnets. Several small improvements in the integrators would probably reduce drift enough to follow the degauss cycle (about 4 hours) and measure the final field to better than 100 gauss in the off magnets.

I have also attempted to measure the field in degaussed magnets by sticking a hall probe into the ¼" holes which were drilled for the flux loops. When the exciting coils are off the field in the hole should be $B\mu^{-1}$, plus some multiplicative constant for the geometric 'hole form factor'. In figure 5 I have compared a calculated $B\mu^{-1}$ with Hall probe measurements as a function of B measured by a flux loop. The general agreement is implausibly good. As the field in the iron drops from about 5 to 1 kg, the permeability apparently decreases so that the field in the hole doesn't change- it is constant at about .2 gauss. Below 1 kg the hall probe field falls off about linearly with field, reaching .02 gauss with fields of several hundred gauss in the iron. Unfortunately .02 gauss is difficult to reliably measure; tiny pressures on the hall probe from the walls of the hole resulted in larger readings. I claim that this method can reliably demonstrate fields in the iron to be below 400-500 kg, corresponding to a measurement of B≤ .05 gauss. Magnet 4 passed this test after the October degaussing.

TABLE I (STANDARD DEGAUSS PROCEDURE)
(transcription of degauss for Oct run from pg 84, mag log)

I (Acme)	T(minutes)
+70	2
0	3
-70	2
0	3
+60	2
0	3
-50	2
0	3
+40	2
0	3
-30	3
0	3
+20	5
0	3
-10	5
0	5
+6	8
0	--

Switch to Sorenson Supply (Filtered DC), monitor voltage with simpson: voltage is across series pairs of magnets

V	T(minutes)
-46v	8
0	8
+40v	8
0	8
-30v	8
0	8
+25v	10
0	8
-20	10
0	8
+15	10
0	7
-12.5	12
0	11

Switch to small PD dc supply for better control of small voltages, still measure with simpson.

+10	15
0	8
-8	16
0	6
+6	15
0	8
-5	15
0	11

V	T
+4	15
0	8
-3	15
0	8
+2	15
0	8
-1	15
0	9
+½	15
0	7
-¼	14
0	--

NOTES:

The Acme supply was run with current regulation. It also differs from the other supplies because the voltage waveform from it is raw 3-phase SCR output, at low voltages a delta-spike. Therefore the lowest current from the Acme (3amps/magnet) was intentionally below the level at which the DC-filtered supply was started (23v/mag ~6 amps)

The supplies were turned on and off rather rapidly (about ½ minute to raise to full voltage and ½ minute to drop to 0, supposing that whatever perversities were created by eddy currents would be negated by the eddy currents of the next ½-cycle. So the time listed corresponds to a voltage flattop (current for Acme).

For the degaussing for the Oct running, the Acme cycle was done twice, first with magnets 1&4, and 2&3, then with magnets 5&7, and 6&8. Then all 8 magnets, still in the 4 series pairs, were run together through the rest of the cycle. All magnets were connected so that +V=focus μ^+, except for magnet 4 which was reversed to reduce the average remnant field in the spectrometer (magnets 2,4&7 were in degaussed state for most of the running).

The time periods shown were chosen during earlier test runs by waiting for flux measured with integrator in different regions of the magnet to stop changing.

26-62

VARIATION OF B WITH RADIUS

PROJECTION FROM B-H CURVE FOR SMALL TOROID

FIG 7

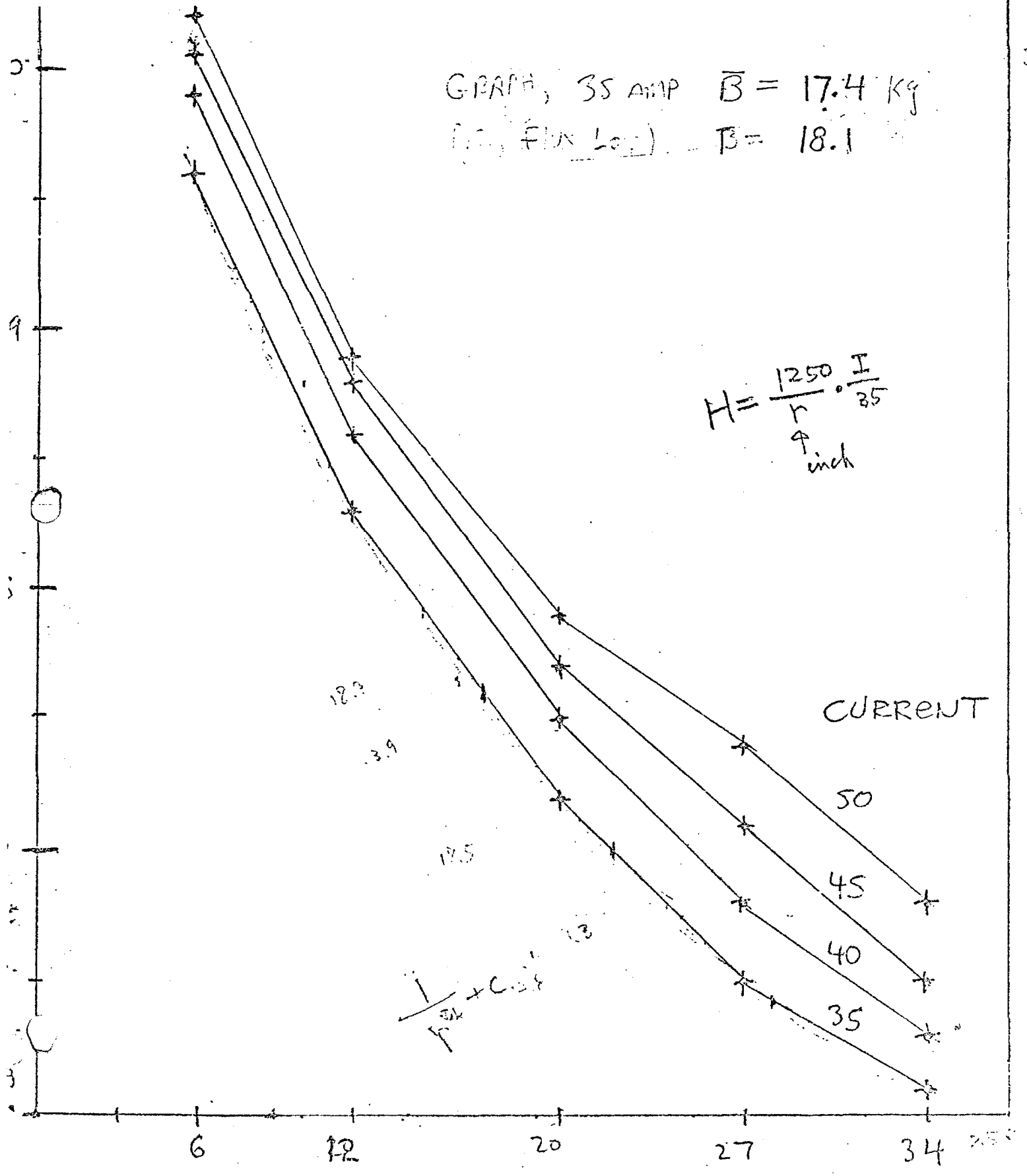

Fig 8

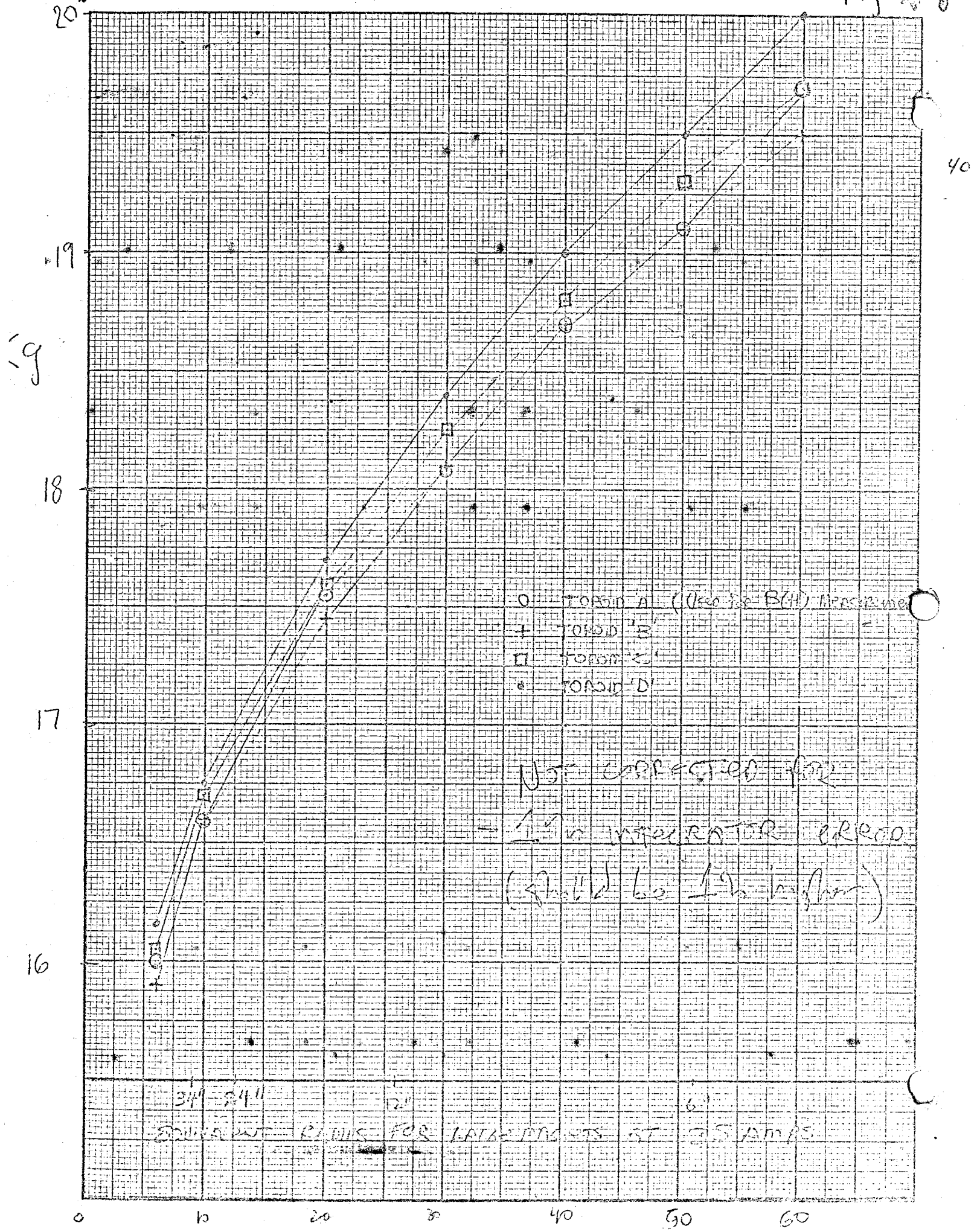

20
19
18
17
16
40
0
10
20
30
40
50
60
O TOROID 'A' (Used for B(H) Measurement)
+ TOROID 'B'
□ TOROID 'C'
• TOROID 'D'
NOT CORRECTED FOR
- 1% INTEGRATOR ERROR
(should be 1% higher)
34"
24"
12"
6"
EQUIVALENT RADIUS FOR LARGE PACKETS AT 25 AMPS

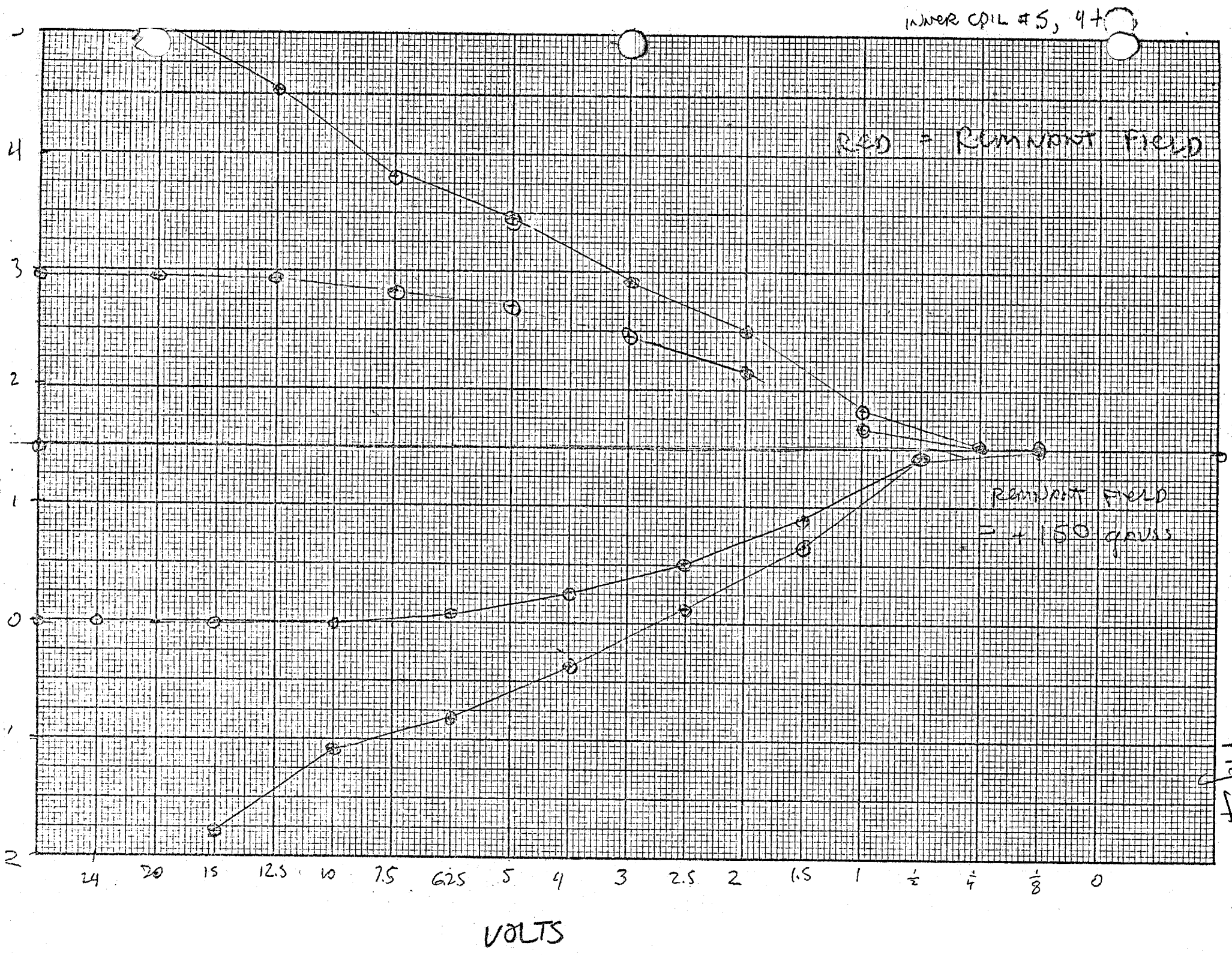
INNER COIL #5, 4+
RED = REMNANT FIELD
REMNANT FIELD
= +150 gauss
4
3
2
1
0
1
2
24
20
15
12.5
10
7.5
6.25
5
4
3
2.5
2
1.5
1
½
¼
⅛
0
VOLTS

Fig 4

26-5R 43

Pg 71 Acme + PD SUPPLIES Coil #1 (OUTSIDE), 14 turns MAGNET #4 B, 31"

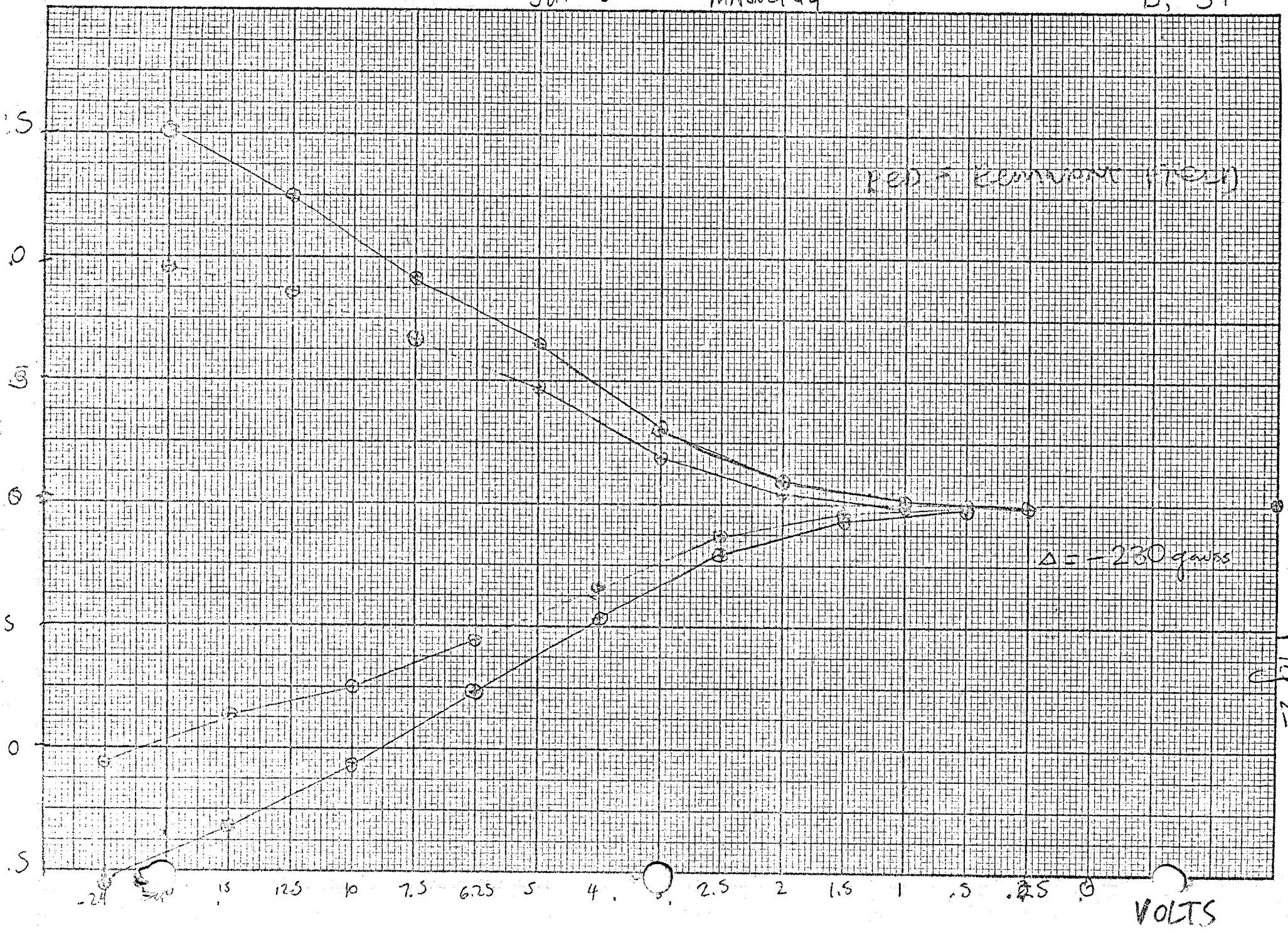

Fig 2

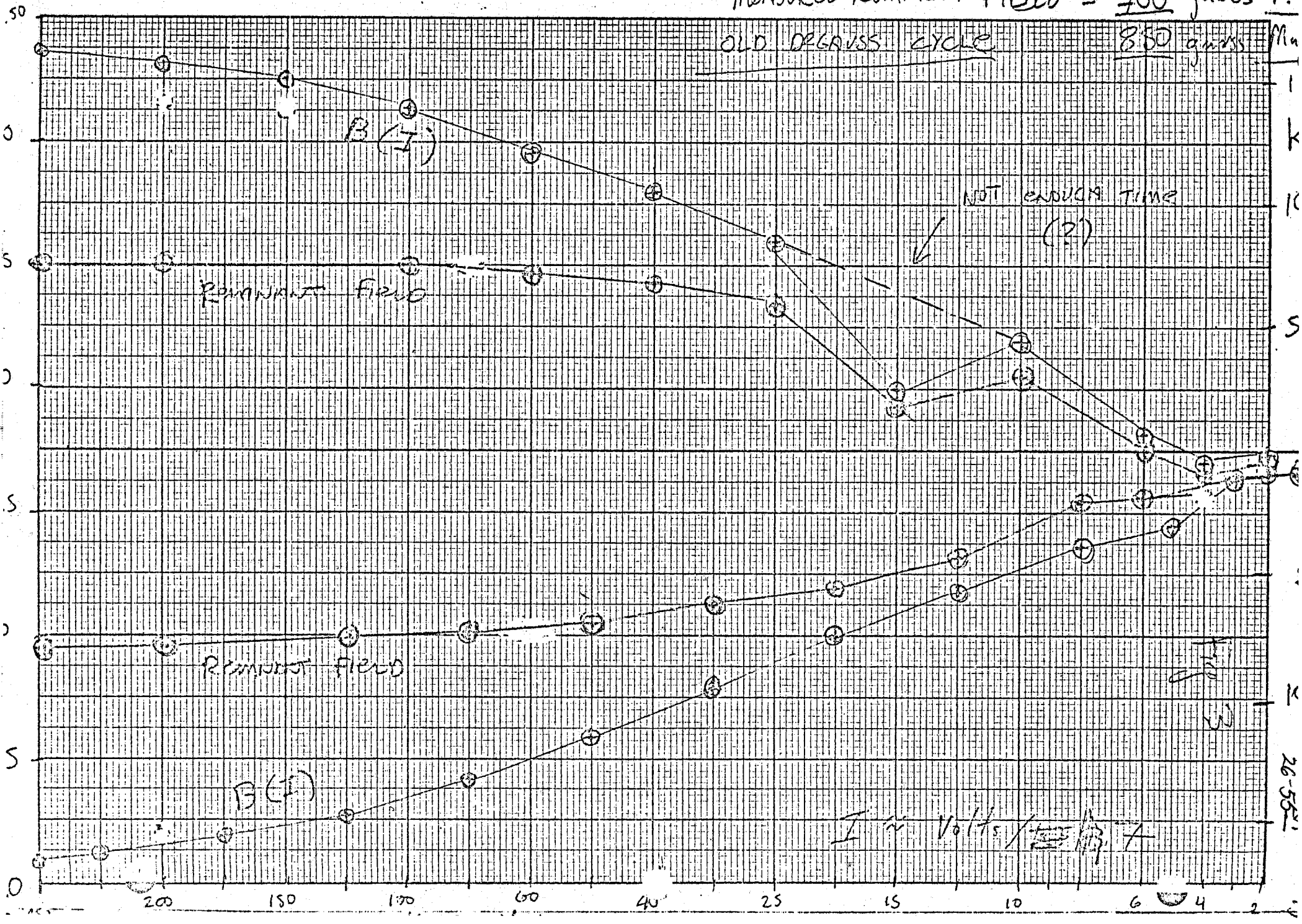
MEASURED REMNANT FIELD = 700 gauss
OLD DEGAUSS CYCLE
850 gauss
B(I)
NOT ENOUGH TIME (?)
REMNANT FIELD
REMNANT FIELD
B(I)
I ~ Volts/Amp
200
150
100
60
40
25
15
10
6
4
2

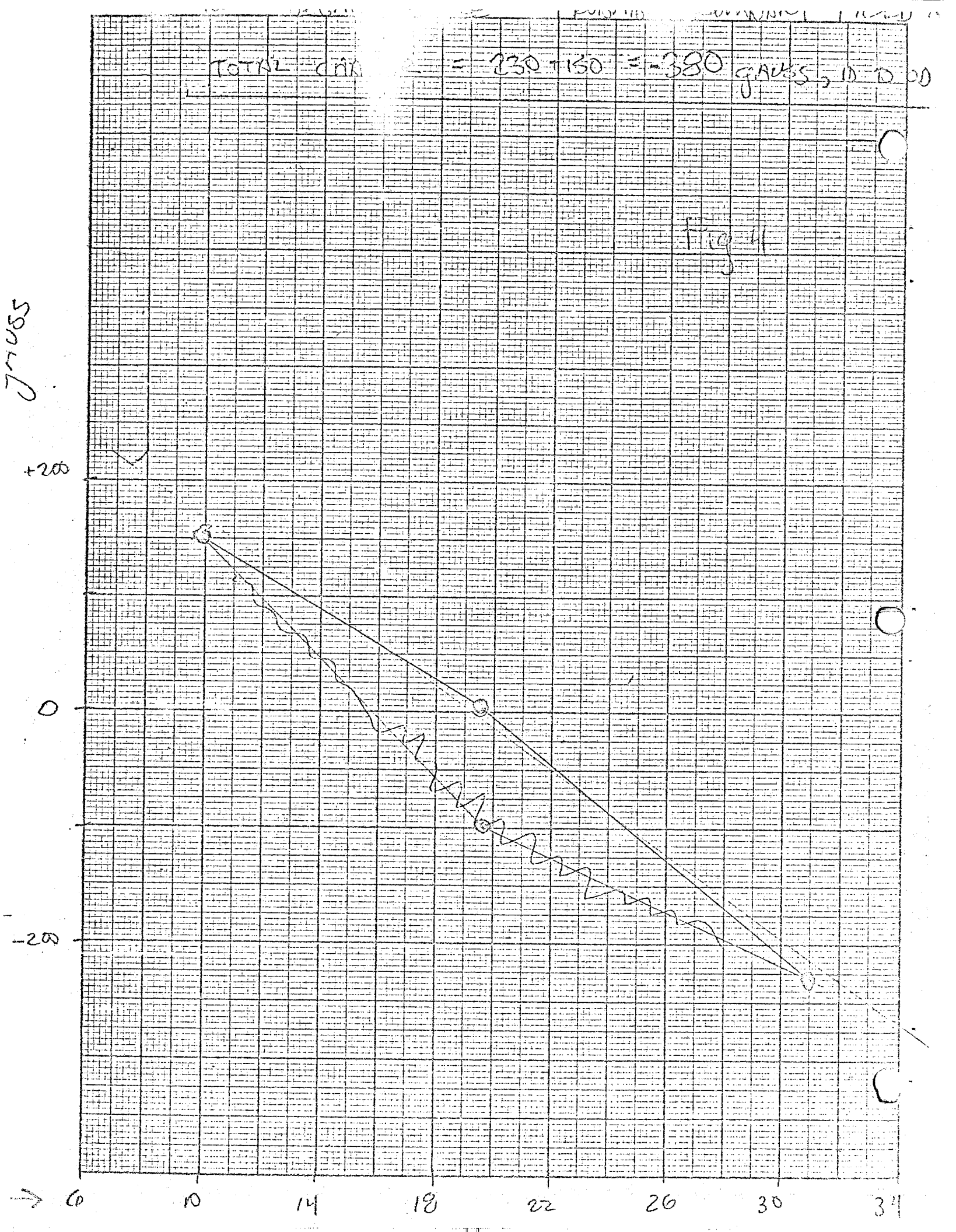
TOTAL CHA = 230 + 150 = -380 GAUSS, ID TO OD
Fig 4
GAUSS
+200
0
-200
6
10
14
18
22
26
30
34

B HALL PROBE in CYLINDRICAL HOLE 26-56 5

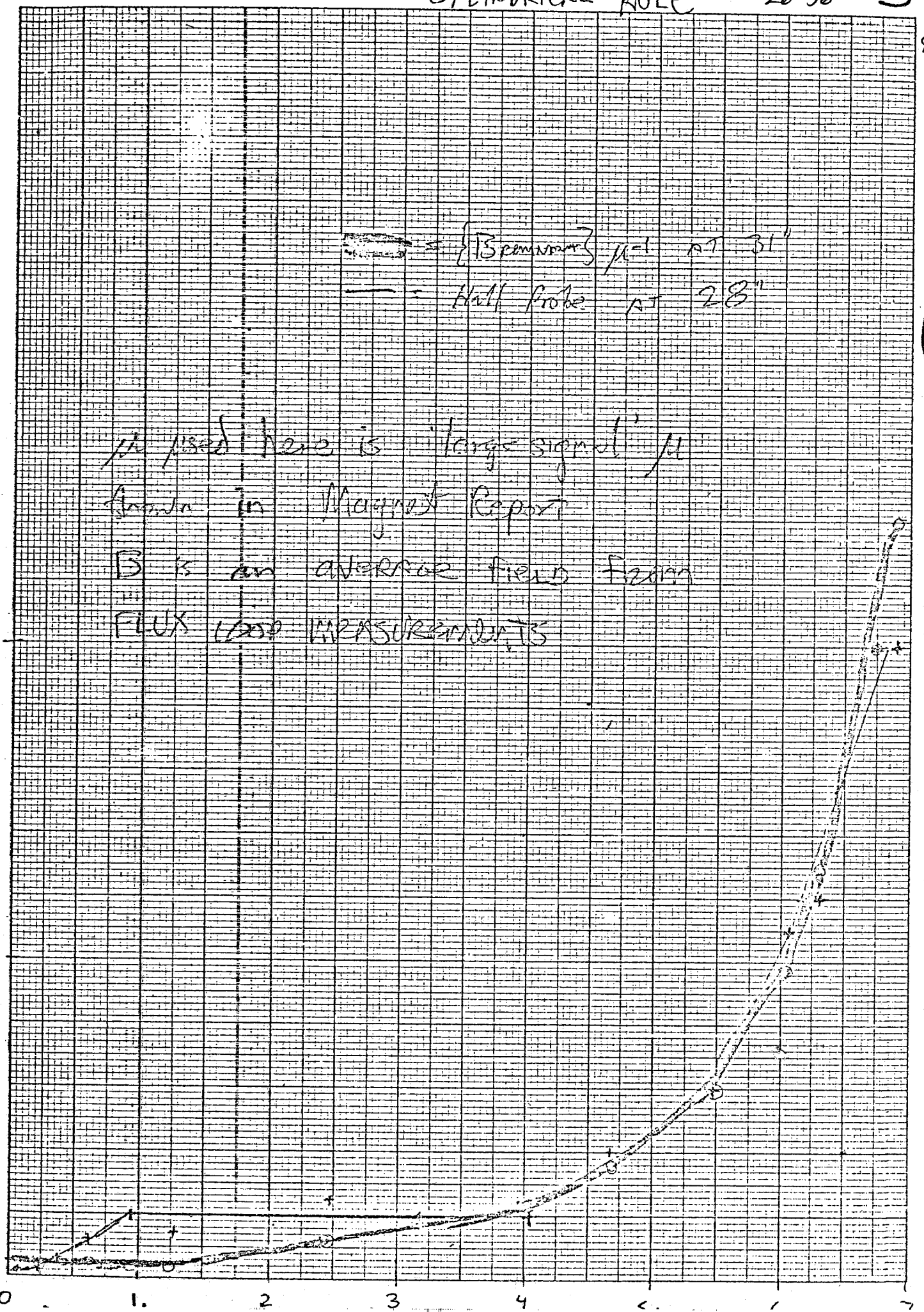

INCIDENT ENERGY FOR 150 GEV RUNS

The incident muon energy is only approximately determined by the first bending magnet (1W0). Some shift is possible from pions decaying after the momentum selection at 1W0. The flux could be maximized by setting the momentum slightly lower as shown in figure 1. This is consistent with the fact that the energy calculated from the 1E4 current is 147 GeV. There was in addition, a steering effect in the CEA quadrupoles for which we have good evidence. The purpose of this note is to summarize the existing knowledge and to estimate the actual incident energy.

I. Beam Line Magnets. Momentum vs. Current

1. 1W0

We have accurate measurements of the total field integral using a flip coil which is long enough to include the fringe field. The numbers given by P. Limon were corrected by 0.46% because of an error in the flip coil wire spacing. The values are given in Table I. Shorted coils can be detected by an inductance test and none were found during tests at the magnet factory.

2. 1E4

In principle the magnets are identical to 1W0 and we have, in addition, a measurement by WV and AR using an accurate Rawson probe. The result is 0.7% lower than 1W0, which is within the measurement error. We assume these magnets are identical to those in 1W0.

3. 1E1 and 1W2

There exist no special measurements of these magnets but they are standard main ring B2 magnets. The relation is

$$p(\mathrm{GeV}) = 0.073526 * I\ (\mathrm{A}$$

4. CEA Quadrupoles

The property of the CEA quadrupoles was checked by DJF in July '73, with no strange behavior found.

II. Typical Beam Line Settings

Magnet	August	October
1W0	6.495 V(DVM) p=154.1	6.493 V p=154.1
1Q0	756. A	831. A
1V01	25 A (P=1)	17 A (P=0)
1Q1	2000. A	2000. A
1E1	4.112 V (2056A) 151.2	2069.9 A p=152.2
1V1	24.6 A	off
1W2	4.237 V (2119A) 155.8	2082.4 A p=153.1
1F3	1022 A	950 A
1D3	1040 A	1000 A
1E4	6.210 V (3105A) 147.3	3113 A p=147.7

The momentum is calculated assuming the canonical 28.68 mr. bend angle.

III. Evidence for CEA quad steering

1. The 1W2 current was set higher than 1E1 by 3% in August and by 0.6% in October. With the quads off, a tune of 1W2 gave a peak value the same as the 1E1 current. There is no tune of 1E4 with quads off.

2. The fact that 1W2 was higher and 1E4 was lower suggests that the beam was shifted west at the CEA quads. On-line studies of counter hodoscopes seemed to confirm this but an accurate measurement requires more precise counter alignment.

3. There are two important differences between August and October.

The CEA quadrupoles were realigned (presumably only in the vertical) after the August runs.

In addition, according to P. Limon, 1Q1 was not reversed after the run on negative muons. 1Q1 was reversed later and caused a .9 cm. shift to the east, and a change in the CEA quad setting.

26-30

IV. An Estimate of the Incident Energy

The energy shift due to muons from pion decay after 1W0 cannot be greater than the half width of the momentum bite as long as the contribution is smaller than that of muons from the decay pipe. A maximum of 1% gives 149.5 GeV, which could be as much as 0.8GeV higher. Using 1E4 involves accurate alignment of the counter hodoscope, but assuming ideal trajectories we get a value of 149.6 GeV. (see figure 1)

A final check comes from Experiment 98 who have used a counter hodoscope. They observe a +13% shift from the value given by the 1E4 current. (ie. 147.7*1.013=149.6)

An incident energy of 149.5 corresponds to 152.6GeV at 1E1 which is consistent with the current setting. The energy for the August data is lower by 0.3 GeV because of the additional pion absorber in the beam.

TABLE I

Current-Momentum Relation for 1W0 and 1E4*

p(GeV/c) = k(I) * I(A)

I Amperes	1W0		1E4*	
	k	p	k	p
500	0.04755	23.78	0.04717	23.59
1000	0.04748	47.48	0.04715	47.15
1500	0.04746	71.19	0.04714	70.71
2000	0.04746	94.92	0.04714	94.28
2500	0.04746	118.65	0.04714	117.85
3000	0.04744	142.32	0.04717	141.50
3500	0.04739	165.90	0.04714	165.00
4000	0.04739	189.60		

* Rawson probe measurement with assumed magnetic field effective length as for 1W0

INCIDENT ENERGY FOR 56 GeV DATA

As described in the previous section, the muon beam energy is quite linear in the magnet currents and we can set the beam to approximately 1%. In the lower energy data of this experiment we wish to scale the energy by exactly 3/8. In order to check this setting, we have also used the proportional counters and beam hodoscope counters. Since the counters were not moved between the two runs, the relative energy setting is independent of the alignment and,in fact, depends only on the scaling of the current in the bending magnets 1E4.

Figure 2 shows the beam momentum distribution for the two sets of data, relative to the nominal settings. There is an apparent shift of 1.2%, presumably due to effects of quadrupole steering upstream in the beam and slight differences in the muon energy loss in the pion absorber. This shift can be corrected in the comparison of data to data and any uncertainty due to energy shifts will be extremely small.

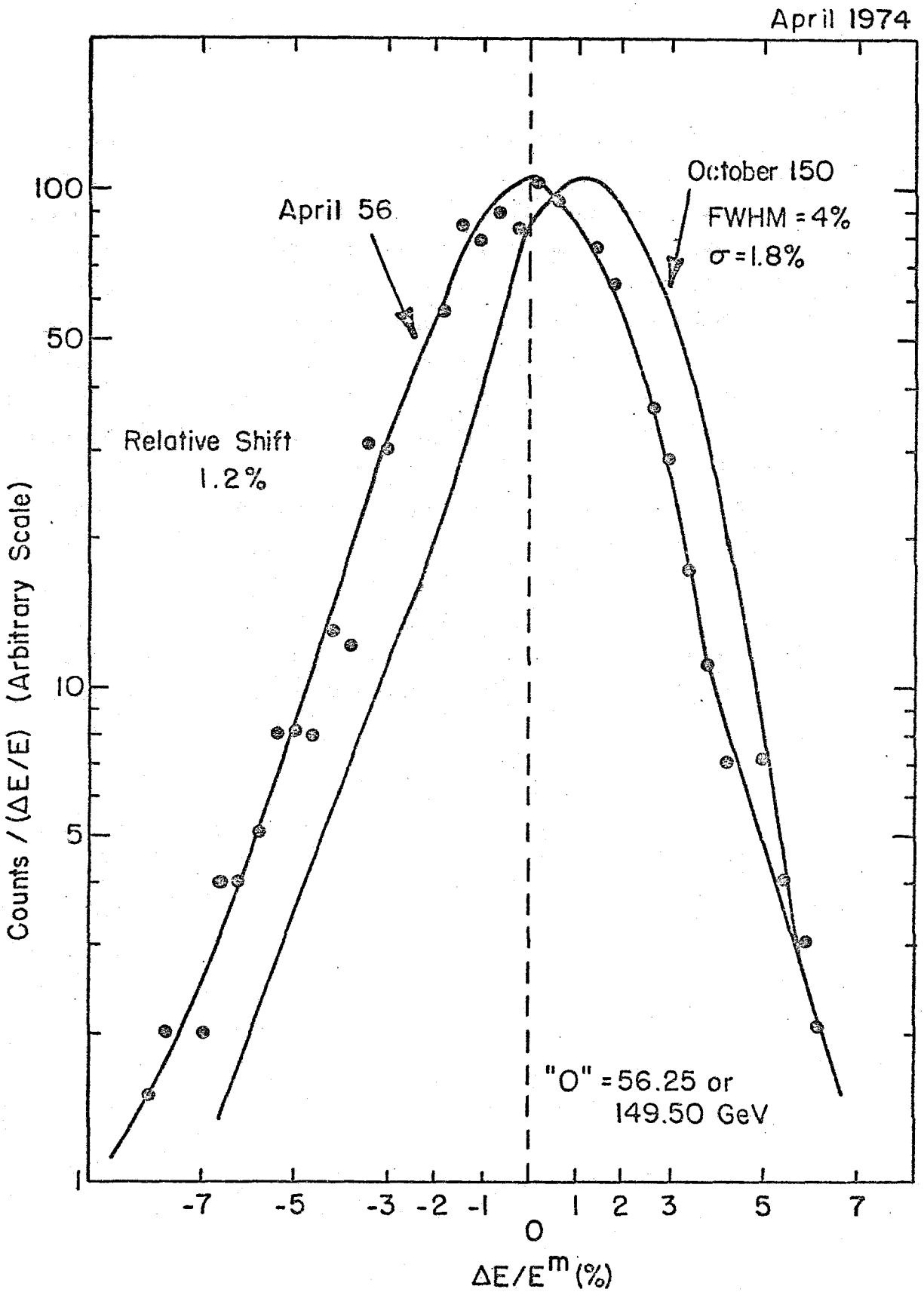

Beam $\Delta E/E_0$ from Proportional Chambers and Counter Hodoscope

0290574

Fig 1

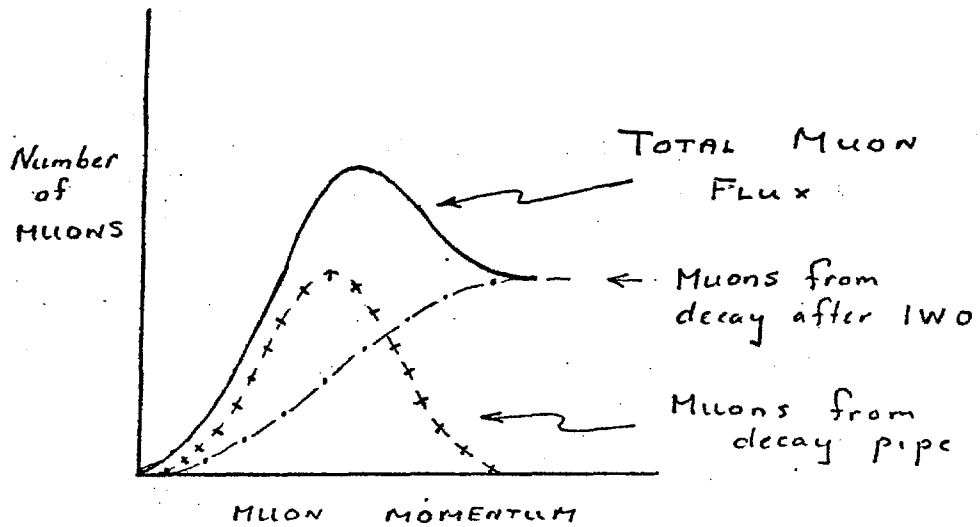

MOMENTUM SHIFT FROM DOWNSTREAM DECAY

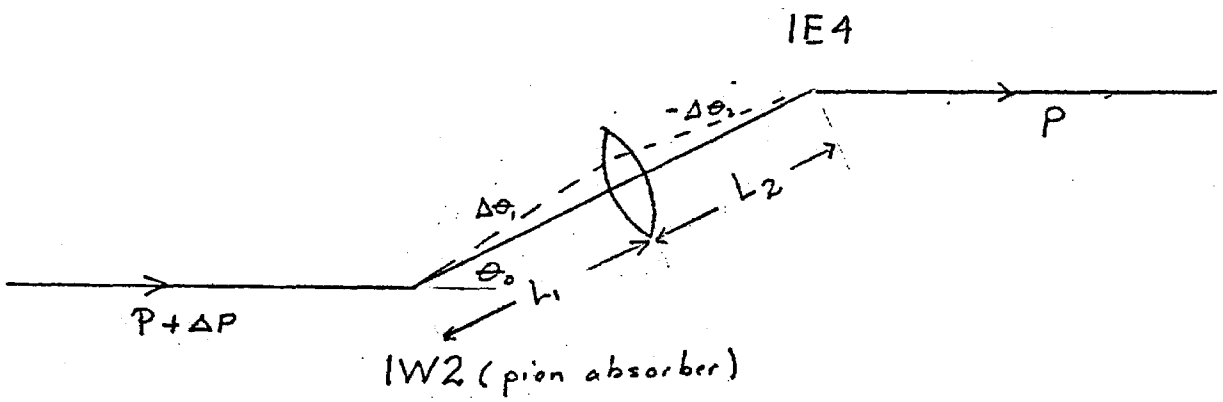

CALCULATION OF INCIDENT ENERGY
ASSUMING CEA QUAD STEERING

$$L_1 \Delta\theta_1 = L_2 \Delta\theta_2$$

$$\frac{P+\Delta P/2}{P_{IW2}} = \frac{\theta_0+\Delta\theta_1}{\theta_0}$$

$$\frac{P}{P_{IE4}} = \frac{\theta_0-\Delta\theta_2}{\theta_0}$$

$\theta_0 = 28.68$ mr.

$P_{IW2} = 153.1$

$P_{IE4} = 147.7$

$$P = \frac{1+\frac{L_2}{L_1}-\frac{\Delta P}{2P_{IW2}}}{\left(\frac{1}{P_{IW2}}+\frac{L_2}{L_1}\cdot\frac{1}{P_{IE4}}\right)} = 149.6$$

MOMENTUM FITTING AND SUBROUTINE FINAL

The problem of determining a momentum in an unbiased way with statistically optimum use of the available information is not completely trivial. Random deviations from a perfect trajectory are caused by both measurement error in the spark chambers and multiple scattering in the iron magnets. The number of points used in the fitting can vary and we need a statistically correct criterion for judging the goodness of fit for a given track. The normal criterion for $\chi^2 \propto \Sigma (dx_i^2 + dy_i)^2$ is quite useless here and if used will result in a resolution about 2.5 times the optimum possible, even at the highest energy used. It is clear that deviations in the most downstream spark chambers are a) larger than those in the upstream ones because of the multiple scattering , b) not statistically independent. If the correct treatment of errors is used, including all correlations, it can be shown that:

1. For monochromatic incident muons the distribution obtained from the fit is gaussian in 1/E. This leads to a high energy tail when plotted vs. E. It is easy to see that the curvature (1/E) is given by a properly weighted linear combination of measured points and hence is a gaussian variable. This feature of the iron spectrometer is also observed experimentally.

2. A χ^2 can be defined with an expectation value equal to the number of degrees of freedom and possessing the standard distribution. With some further effort, question of resolution etc. could be answered using the inverse matrix of second derivatives of χ^2 with respect to the varied parameters.

$$\chi^2 = \sum_{i,j} Y_{ij}^{-1} \left[\delta x_i \, \delta x_j + \delta y_i \, \delta y_j \right]$$

where $\delta x_i, \delta y_i$ are the residuals at the ith spark or proportional chamber and

$$Y_{ij} = \langle \delta x_i \, \delta x_j \rangle$$

The expectation value of $\delta x_i \delta x_j$ over an ensemble of tracks of identical momentum, measurement errors etc. With this definition of χ^2 it is obvious that

$$\langle \chi^2 \rangle = 1.0 * \text{\# degrees of freedom}$$

The Y_{ij} matrix depends on the particular sparks used in the fit and on the geometry of the apparatus. If our spark chambers were imbedded in a continuous medium with $\langle \theta^2 \rangle$/unit length equal to k then it can easily be shown that

$$Y_{ji} = Y_{ij} = K x_i (3x_j - x_i) + \sigma^2 \delta_{ij} \quad j \geq i$$

The x_i are the distances of the chambers from the starting point of the scattering medium. σ^2 is the square of the measurement error.

For the case of discrete scatterers, the solution is still quite simple:

$$Y_{ij} = \sigma_F^2 \delta_{ij} \qquad i \text{ or } j = \text{front chambers}$$

$$Y_{ij} = K d_{ij} + \sigma_R^2 \delta_{ij} \qquad \text{rear chambers}$$

$$K = \langle \theta^2 \rangle \text{ for one magnet} = 1.1 \times 10^{-2} / P^2 \text{Gev}$$

$$d_{ij} = \sum Z_{im} Z_{jm}$$

where Z_{im} is the distance between the center of a magnet and the spark chamber plane. $Z_m = 0.$ if the magnet is downstream of the spark chamber.

The matrix in the program is handled in double precision using standard routines. The dimensionality of Y_{ij} varies with the number of sparks detected, but the non-diagonal part has a maximum dimensionality of 5 * 5.

We wish to solve for that trajectory which minimizes χ^2 defined above. When considered from an exact rigorous viewpoint this is a problem in non-linear curve fitting using piecewise smooth curves and taking into account the radial variation of the magnetic field etc. Fortunately it is possible to achieve sufficient accuracy, even at the lowest momenta, by expanding the trajectory at any measurement point in powers of 1/E. This greatly simplifies the trajectory computation: at any point it is sufficient to write

$$X_i = X_{0i} + A_i\left(\frac{1}{E}\right) + B_i\left(\frac{1}{E^2}\right)$$
$$Y_i = Y_{0i} + C_i\left(\frac{1}{E}\right) + D_i\left(\frac{1}{E^2}\right)$$

X_0, Y_0, A, B, C, D are functions of the initial slope and positions of the trajectory.

We are attempting to minimize a function of 5 varibles:

the initial slopes in directions x and y
the initial positions x and y at z=0
the radius of curvature

To find this minimum we need the derivatives of the residuals with respect to these variables. By a straightforward but tedious exercise in linear algebra we can invert the proper matrices to obtain corrections to the 5 initial parameters. With the power series expansion in 1/E it is relatively easy to compute the proper derivatives above and solve for the new values of the parameters. This procedure is iterated until the momentum correction is less than 10% or the number of iterations would exceed 3. In practice this never happens and at most 2 iterations of this procedure suffice.

A further complication is that Y_{ij}' depends on the momentum which in turn depends on the Y_{ij}. In order to get the above procedure started on its radidly convergent path, we extend the original ray in front of the spectrometer and vary only the momentum to minimize $\sum \delta_x^2 + \delta_y^2$. The resultant momentum is used as the starting value in making the first estimate of the Y_{ij}''s etc.

Appendix V

Calibration of FINAL (Momentum Fitting) with Monte Carlo

Monte Carlo tracks were generated for the 56 GeV large angle, 150 GeV large angle, and long target configurations at fixed E', θ, with 1,000 tracks at each point.

Multiple scattering and energy loss in the target were turned off, and all tracks originated at a point. Multiple scattering and straggling were turned on in the spectrometer. The magnetic field and magnet lengths were taken from recent memo, and were put into FINAL as well as the Monte Carlo (Table I).

Histograms of $(1/E'_{fit} - 1/E'_{gen})E'_{gen}$ were fitted with a gaussian. The low E' tails were not included in the fit. The energy loss was at first taken to be $dE/dx = 0.01216/E'^2 - 0.01141/E' 0.016 + 0.5359\times10^{11}E' + 0.2975\times10^{-8}(E')^2$ which is a fit to the average energy loss given by Theriot. Various corrections to this energy loss were tried to make the mean of the $\Delta(1/E')$ distribution be zero for the entire range of energies tried: 25-145 GeV for the 150 GeV configuration, and 9.4-145 GeV for the 56 GeV configuration. An energy dependent correction was necessary, and a good choice seemed to be multiplying dE/dx by (1.26 - 0.00233E').

FINAL begins to break down between 40 and 50 GeV in the 150 GeV configuration, and between 12 and 15 GeV in the 56 GeV configuration. Above these energies the fitted energy is within 0.5% of the generated energy.

Because of this breakdown, the data should be cut at 50 GeV in the 150 GeV configuration, and at 18.75 GeV in the 56 GeV configuration. This can be cured by an improved algorithm.

26-33

Table I

B Field Parametrization: $B = a/R + b + cR + dR^2$
(B in kG, R in cm)

150 GeV Configuration

Magnet	a	b	c	d	Length
1	12.17	19.87	-0.08338	0.0004336	79.06 cm
2		Off			79.22 cm
3	12.17	19.87	-0.08338	0.0004336	78.11 cm
4		Off			79.22 cm
5	12.20	19.91	-0.08355	0.0004345	79.06 cm
6	12.14	19.81	-0.08313	0.0004323	79.06 cm
7		Off			77.62 cm
8	12.14	19.81	-0.08313	0.0004323	78.26 cm

56 GeV Configuration

Magnet	a	b	c	d	Length
1	12.21	19.93	-0.08363	0.0004349	79.06 cm
2	12.21	19.93	-0.08363	0.0004349	79.22 cm
3	12.21	19.93	-0.08363	0.0004349	78.11 cm

Configuration	Generated		Fitted				
	E'	Θ	$\left\langle\left(\frac{1}{E'_f} - \frac{1}{E'_q}\right)E'_q\right\rangle\%$	$\sigma\left(\frac{1}{E'}\right)\%$	χ^2/df	$\left\langle\left(\Theta_f - \Theta_q\right)/\Theta_q\right\rangle\%$	$\sigma(\Theta)\%$
150 LA	25.0	0.060	3.33±0.47	12.0	16.9/9	-0.03±0.01	0.42
150 LA	30.0	0.060	2.59±0.45	13.6	28.9/19	-0.04±0.01	0.44
150 LA	40.0	0.050	0.88±0.46	12.8	9.6/11	-0.03±0.02	0.52
150 LA	60.0	0.050	-0.12±0.42	12.8	23.5/20	-0.04±0.02	0.52
150 LA	85.0	0.040	0.36±0.43	13.2	28.5/17	-0.03±0.02	0.61
150 LA	85.0	0.050	0.01±0.45	13.8	13.7/17	-0.01±0.02	0.49
150 LA	145.0	0.040	0.35±0.45	13.5	25.3/17	0.00±0.02	0.54
150 LA	145.0	0.050	0.42±0.46	14.1	15.8/17	-0.01±0.01	0.44
56 LA	9.4	0.098	3.60±0.47	13.8	21.2/17	-0.06±0.01	0.36
56 LA	11.3	0.098	2.35±0.46	13.7	13.0/16	-0.03±0.01	0.34
56 LA	15.0	0.082	0.12±0.43	13.1	11.6/16	-0.04±0.01	0.43
56 LA	22.5	0.082	-0.61±0.46	14.0	19.1/17	-0.06±0.01	0.44
56 LA	31.9	0.065	-0.38±0.54	14.4	5.2/11	-0.04±0.02	0.55
56 LA	31.9	0.082	0.55±0.42	13.0	11.8/17	-0.02±0.01	0.43
56 LA	54.4	0.065	0.21±0.47	14.2	11.0/16	0.00±0.02	0.58
56 LA	54.4	0.082	0.61±0.49	14.6	32.2/17	-0.02±0.01	0.43
Long Target	25.0	0.065	-0.36±0.51	13.8	11.4/11	-0.08±0.02	0.62
Long Target	25.0	0.082	-0.59±0.44	13.4	15.9/16	-0.04±0.02	0.49
Long Target	85.0	0.065	-0.44±0.50	15.0	22.9/17	-0.02±0.02	0.63
Long Target	145.0	0.065	-0.45±0.55	16.2	13.8/17	0.01±0.02	0.63

CALIBRATION OF THE SPECTROMETER

In order to test the energy calibration and resolution of the spectrometer, the muon beam, at a number of energies, was steered directly into the spectrometer. This was achieved using a small toroidal magnet (2" ID, 12" OD, 73" long) set at approximately the position of the muon scattering target.

This permitted a test of the spectrometer for muon trajectories closely resembling a typical scattering event. In addition, the azimuthal symmetry of this test magnet allowed all parts of the spectrometer to be studied simultaneously.

The small toroid did not have sufficient bending power ($P_\perp$ = 1 GeV/c) to map the outer regions of the spectrometer at high energy. To accomplish this the Chicago cyclotron magnet of muon 98 was used. This magnet deflected the muon beam to approximately 30 inches radius at the rear of the spectrometer.

The absolute energy setting of the muon beam comes from the calibration of the beam line magnets measured by the personnal of the NAL magnet factory before installation in the beam line. This energy is corrected slightly to get the energy steered into the spectrometer. These corrections are:

a). additional pion decays downstream of magnets reduce the mean muon energy by approximately 1%.

b). Energy loss in the pion absorber reduces energy approximately 3.3 GeV.

c). energy loss in small toroid reduces energy approximately 3.6 GeV

The third of these does not apply to runs using the cyclotron magnet.

Figure 1 shows the result of these calibrations. The mean energy at each setting agrees with the calibration energy to ±2%. These measurements include both μ^+ and μ^- and for many of the energies the small toroid was moved closer to or farther from the spectrometer to map more of the spectrometer radius.

26-35 63

Fig 1

Feb. 1974

SPECTROMETER CALIBRATION

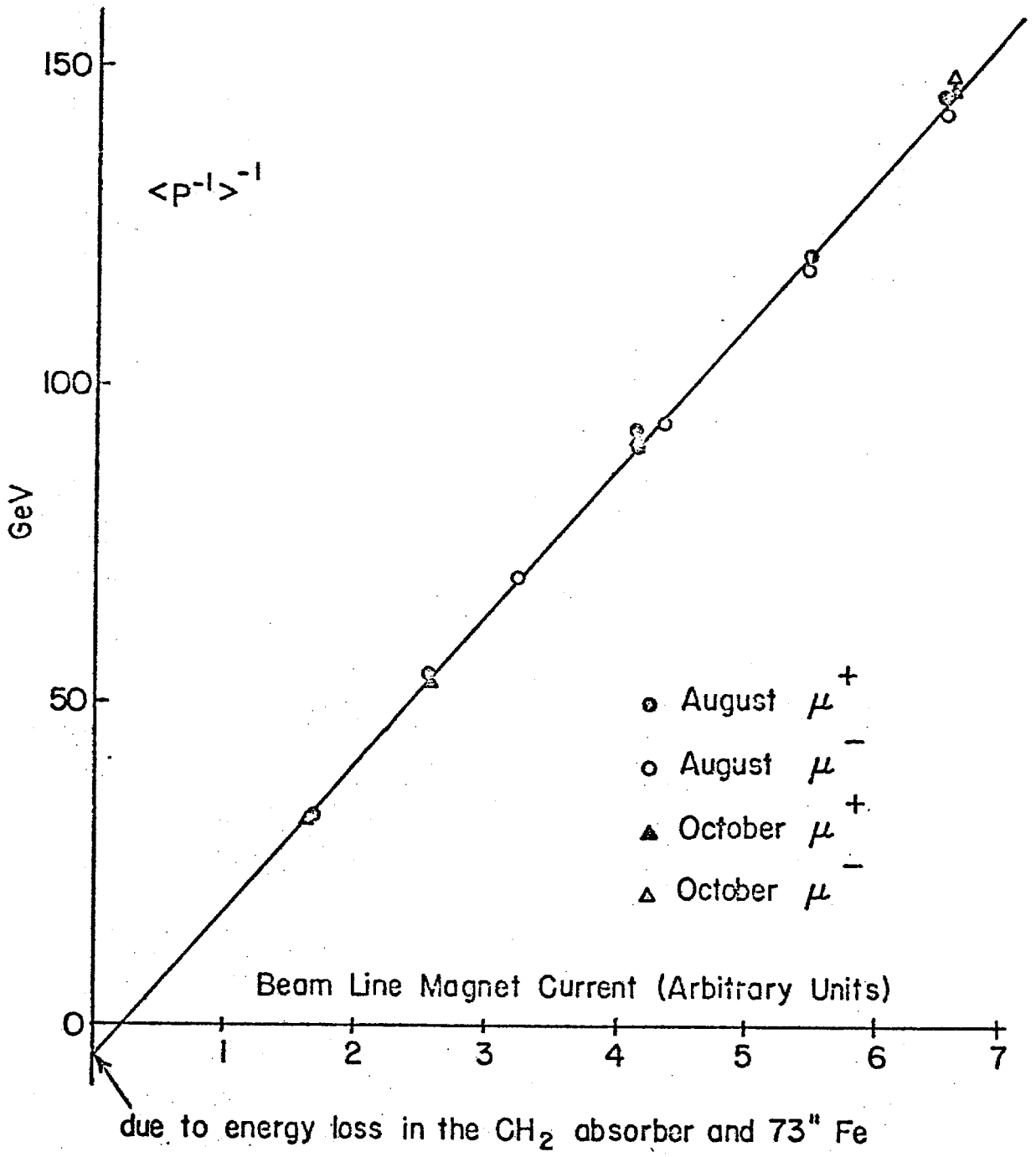

Fig 2

Feb. 1974

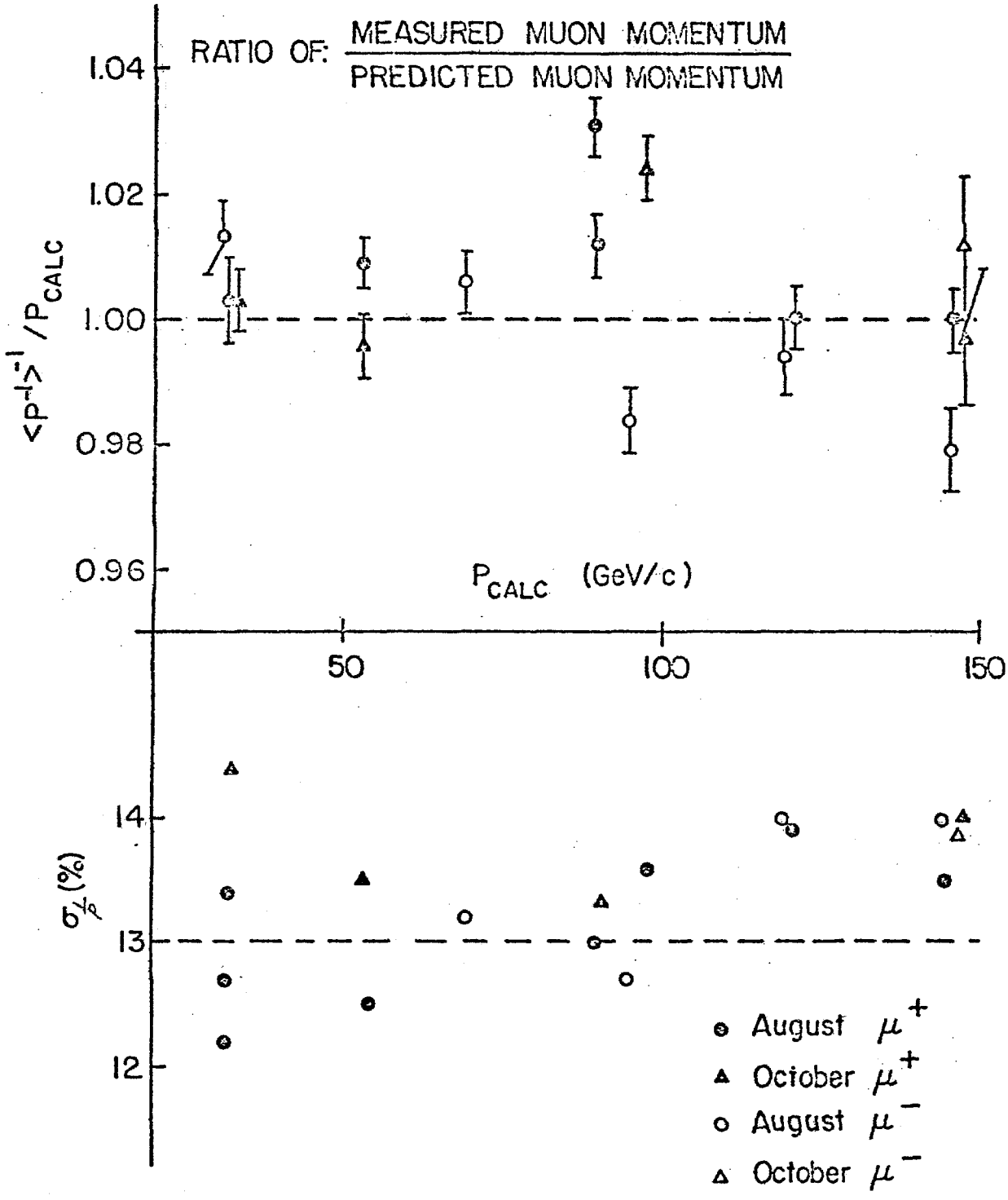

SPECTROMETER RESOLUTION vs. MUON ENERGY

SURVEY OF INFORMATION FROM THE SPARK CHAMBERS UPSTREAM OF THE SPECTROMETER

We consider the E26 apparatus to have two sections - a 'back' which has been shown to be almost completely shielded from the hadronic and electromagnetic showers produced in the target, and a 'front' which is not shielded. The back identifies muons and provides an 18% momentum measurement, but using the back information alone we have larger errors on the interaction vertex and the initial angle of the scattered muon. The front chambers determine the vertex and angle, permitting a 13% momentum measurement but in about 25% of the events the front muon track is obscured or lost because of high multiplicity cascades (see Figure /) from the target.

This problem need not scale between different configurations: At 56 and 150 GeV the number of interaction lengths in the target is changed from 3 to 8, while cascade lengths change ∝log E. The lost events are strongly biased toward high energy loss for the muon. A set of counters interspersed through the target provides somewhat complimentary information on the interaction vertex, i.e., providing more reliable information for large energy loss, but their performance has not been carefully studied yet. Preliminary studies indicate use of the pulse height information in these counters appears to significantly reduce the 25% loss.

At present we are trying to sort out the problems and biases attached to the available information, in particular:

- Can the 'back' information unambiguously separate halo tracks? The answer would appear to be yes.
- How well does the 'backfit' (fit using only 'back' information) separate events coming from different targets?

- How well does the 'backfit' reject wrong beam tracks when several are present?
- What are criteria for determining that the 'right' front track has been found and how does the quality of the found track affect the full momentum fit? Could hadrons masquerade as scattered muons in front?
- What biases are introduced by considering only events for which a track has been found in the front chambers?

Preliminary answers to many of these questions have been obtained within the context of RECON8.

BACKFIT INFORMATION

During the 'back' momentum fit ('backfit') the fitted track is extended upstream through the first magnet into the front chambers. A test of quality is to ask what minimum multiple scatter in the first magnet would attach this line to the measured beam track. The result is a most probable Z interaction and a χ^2_s for the scatter, = (multiple scatter)^2/(RMS multiple scatter)^2. Figures 2,3 show the backfit Z interaction for χ^2_s<15. <u>Moving upstream from the target, separation of halo from events is almost complete.</u> Moving downstream the three peaks are: Main target plus carbon target, auxiliary downstream target, and concrete absorber in the first magnet.

We have estimated the probability of picking an incorrect beam track, given that two are present and one picks the beam track giving the lowest χ^2_s for the spectrometer track to beam track match. We conclude that at the moment it is better to confine ourselves to the analysis of single beam track events (80-90% of all events).

26-36

This, however, has not been done in RECON7. We may estimate the number of events affected -

f_1 = fraction of events with more than one beam track = 10-20%

f_2 = fraction of events with inadequate front spark chamber information = 25-30%

f_3 = probability for picking wrong beam track, assume 50%

So $f_1 f_2 f_3$ = 1-3% is the fraction of events with wrong beam tracks. The net bias, if any, would be to increase the observed scattering angle, decrease the observed energy, and increase $q^2 \propto E'\theta^2$.

FRONT POINT FINDING

Two requirements can be used for limiting the sparks which may be considered for the front line. These do not constrain the target position.

(1) A multiple scattering cone is extended upstream from the first set of magnets. An effective source plane ZMSC is defined in the magnets and the accepted range ('window') has the form $R^2 = A^2+B^2(ZMSC-Z)^2$ where A is a 'circle of confusion' in the effective source plane for the multiple scatter. It is expected that the observed cone is wider than (P_T multiple scatter)/E' because of the 18% uncertainty of the back momentum measurement - a better window would be wider in the bend plane than transverse to it. The magnetic field P_T is 400 MeV/c so the bend uncertainty is .18 x 400 = 80 MeV/c, which is slightly smaller than the P_T from multiple scattering.

(2) The scattering plane is defined by the beam track plus the backfit prediction for the front line. The average |deviation| from this plane is 2.5-4 mm, independent of E' and E_0.

Figure 4 is a flowchart for the scheme used to find and test front tracks, and Figure 5 shows a plateau of the multiple scattering cone window for 56 and 150 GeV. We draw these general conclusions from the plateau:

- The effect of the windows is almost but not completely identical for 56 and 150 GeV.
- If three spark chambers are required, 80-85% is an upper limit on the fraction of events for which front tracks can be found.
- Our criteria for track quality (explained below) are justified to the extent that very few tracks result in a bad χ^2/DOF (somewhat arbitrarily set at 2.5) from the overall momentum fit. The level is $\leq$1%. This is greatly improved over the situation in RECON7, which had a tail on the χ^2 distribution.
- The present system for constructing front lines is somewhat sensitive to 'noise'; observe the decrease in the number of found tracks as the multiple scattering cone is opened beyond 3σ. Nonetheless, the system is picking up ≥90% of the events passing the scattering plane window cut.

TRACK QUALITY

The internal quality of the front line comes mostly from the number of contributing chambers and the straight line χ^2. A check showed that 3 point tracks, as found by our scheme, have a higher percentage of noise contamination than 4-6 point tracks, as shown in the table below.

No of Chambers Contributing to Line	No of Events with Found Track	No. of Events Passing All Cuts	% Passing	% of Total Passed
3	33	17	52%	5%
4	55	49	89%	13%
5	108	105	97%	29%
6	195	193	99%	53%

The other test of quality is the consistency of the front line with the backfit line. We are monitoring

DTH = (angle difference between backfit prediction and found front line) and

DR = (position difference between backfit prediction and found front line, evaluated at ZMSC)

Distributions of these quantities show good consistency between 56 and 150 GeV and fair agreement with theoretical distributions. Found tracks were cut at about 3σ on

DTH/(expected energy dependence) and

DR/(expected energy dependence)

and these cuts appear to result in only 1% level differences between 56 and 150 GeV in the number of events missed and in the 'noise' contamination. As shown in the flowchart in Figure 4, events passing these cuts and containing at least 4 points in the front line passed the overall momentum fit with X^2/DOF <2.5 at the 99% level.

DR and DTH can also be used to monitor alignment between the front and back of the apparatus, which is important - fixing a 3mm transverse misalignment between the front and back lowered the overall momentum fit average X^2/DOF from .63 to .54 (mean back X^2/DOF was .75).

The azimuthal symmetry of the apparatus greatly reduces the effects of residual misalignments in angle.

FRONT BIASES

Here, as for the scattering window plateau, we have cut the backfit Z interaction rather tightly around the main target (1 meter upstream of the Carbon target and 1 meter downstream of the downstream face of the main target at 150 GeV, scaled distance at 56 GeV).

We then monitor the fraction of events in each E' bin which successfully pass the overall momentum fit with X^2/DOF <2.5. Figure 6 shows that the fraction lost for 150 and 56 GeV is very similar for E' >50 GeV (at E_o = 150 GeV) and rather different for E' <50 GeV.

Fig 1

POSSIBLE EXPLANATION OF ORIGIN OF EVENT LOSSES

AV. # OF SPARKS IN "FRONT" SPARK CHAMBER

IF 2 WANDS HAVE N SPARKS, OTHERS <N, CLASSIFY AS N

CONCLUDE: LOST EVENTS CORRELATE WITH LARGE NUMBERS OF SECONDARY PARTICLES.

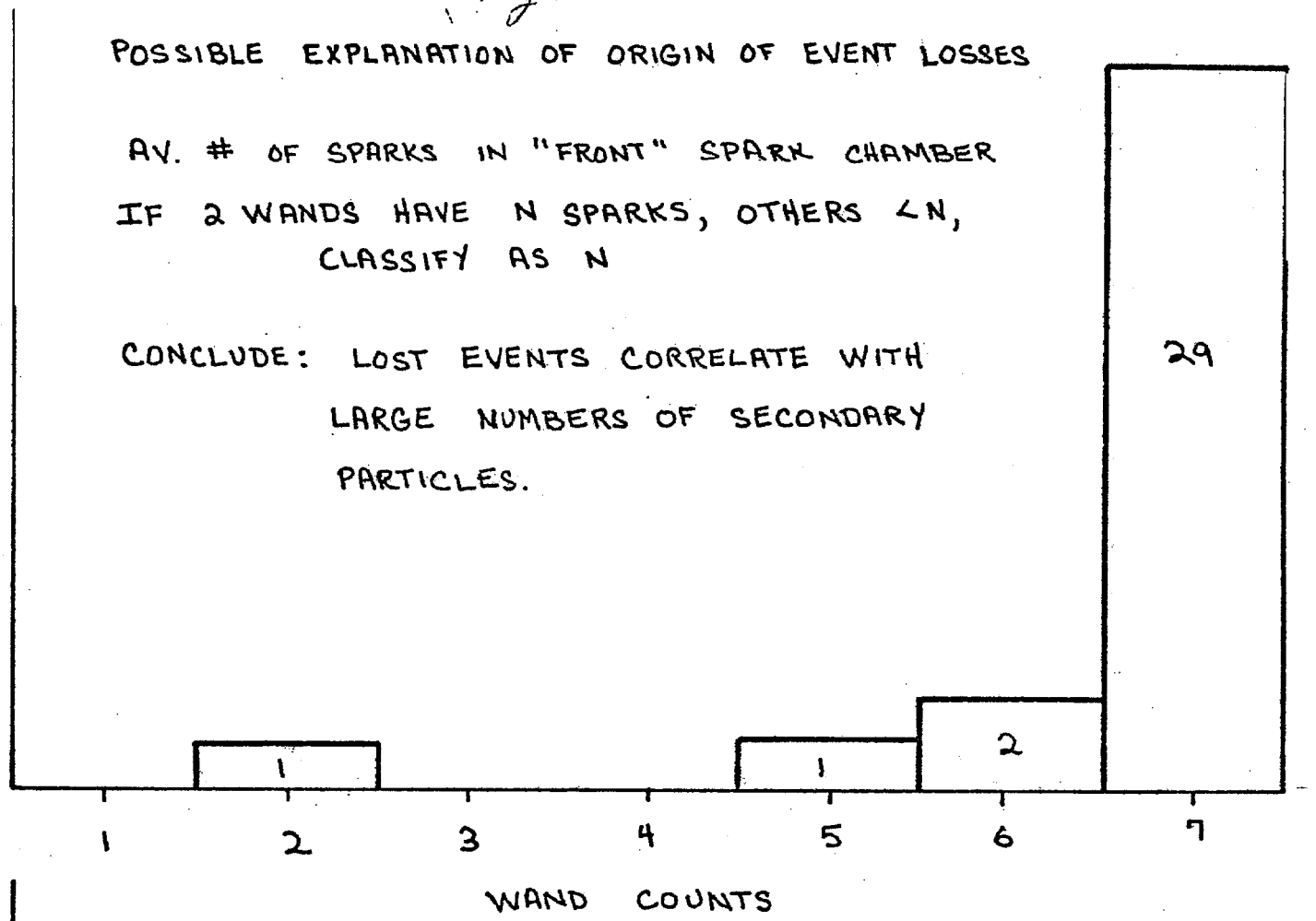

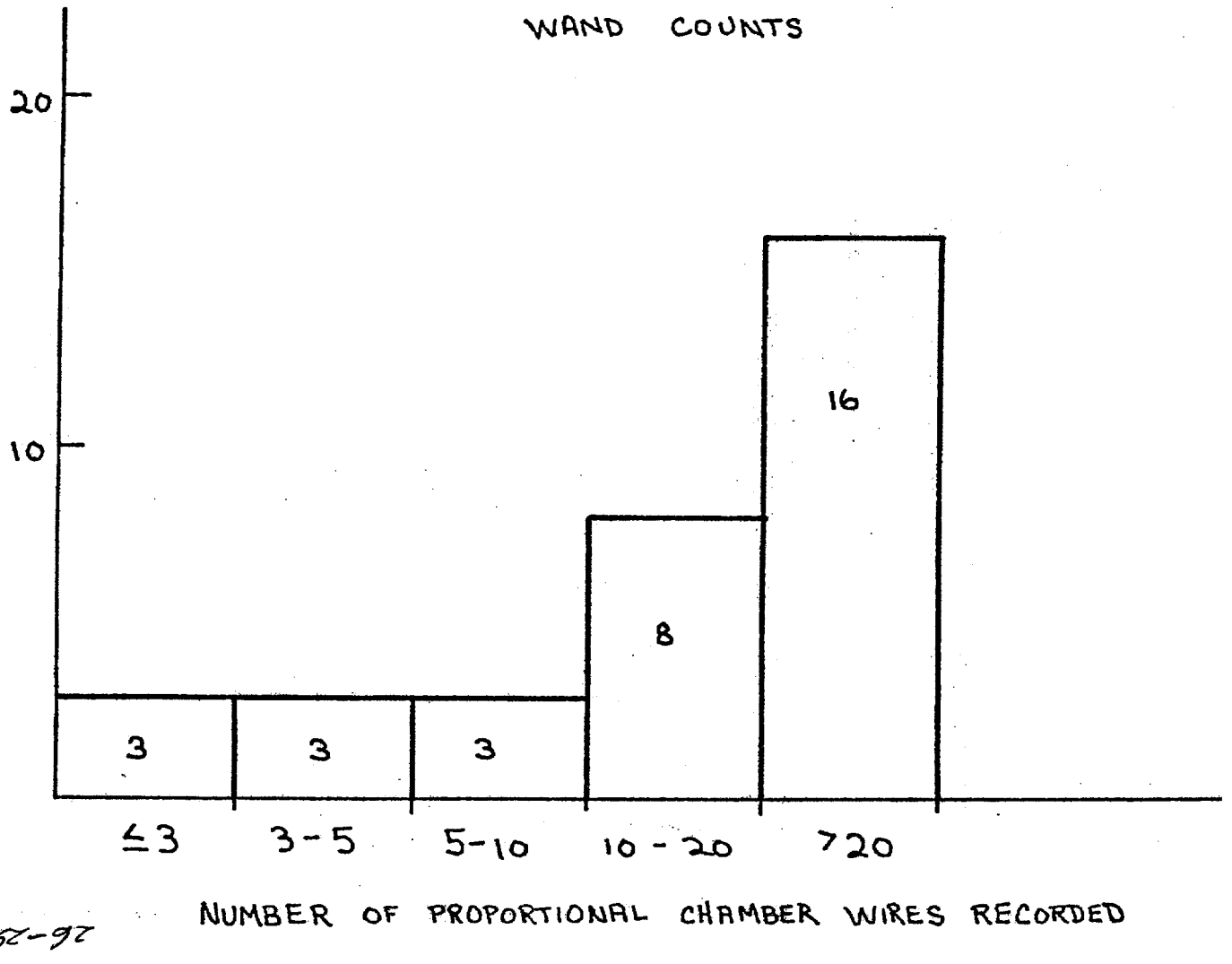

82-92

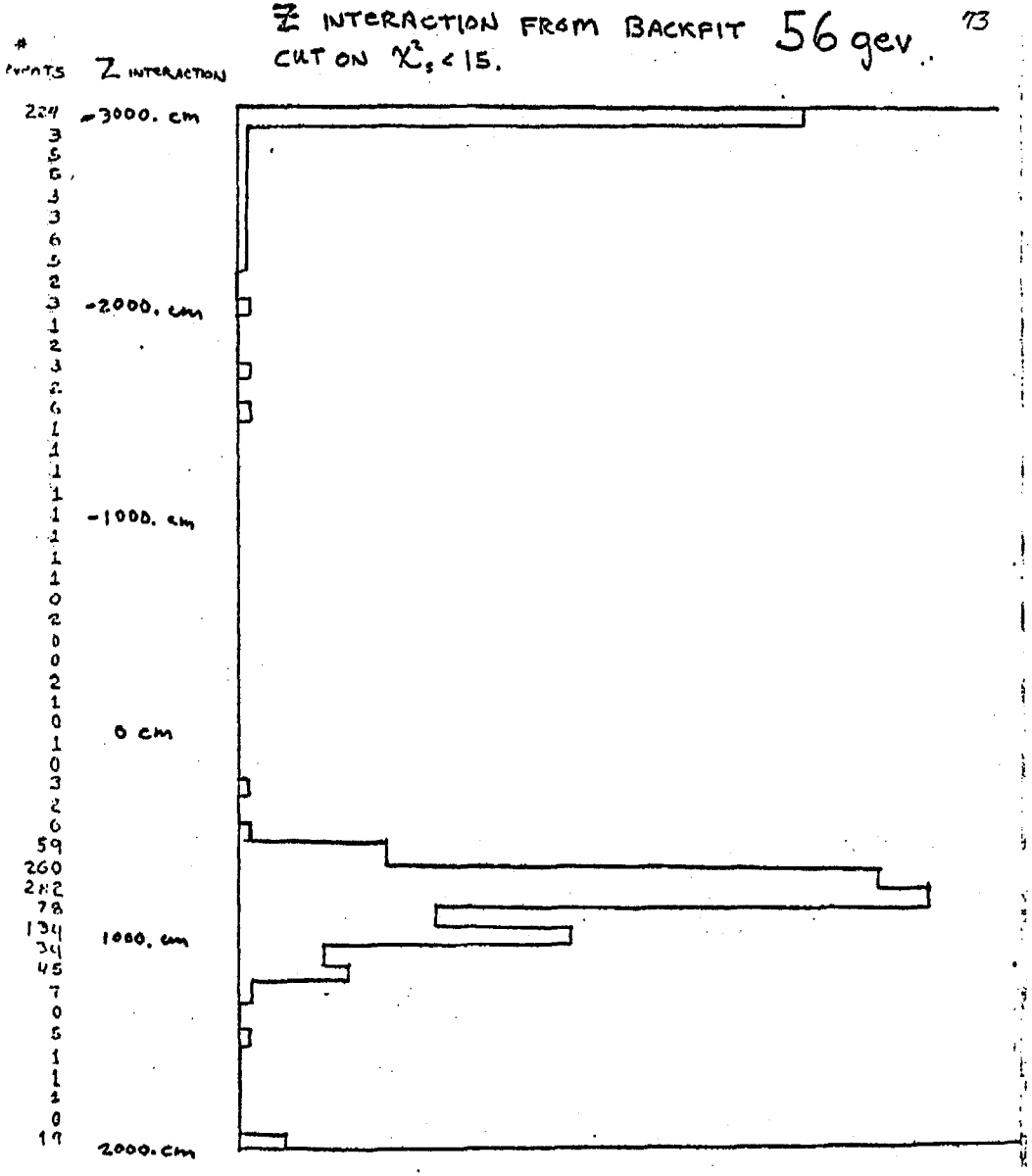
Z INTERACTION FROM BACKFIT 56 gev
CUT ON $\chi^2_s < 15$.
73
EVENTS
Z INTERACTION
-3000. cm
-2000. cm
-1000. cm
0 cm
1000. cm
2000. cm

Fig 3

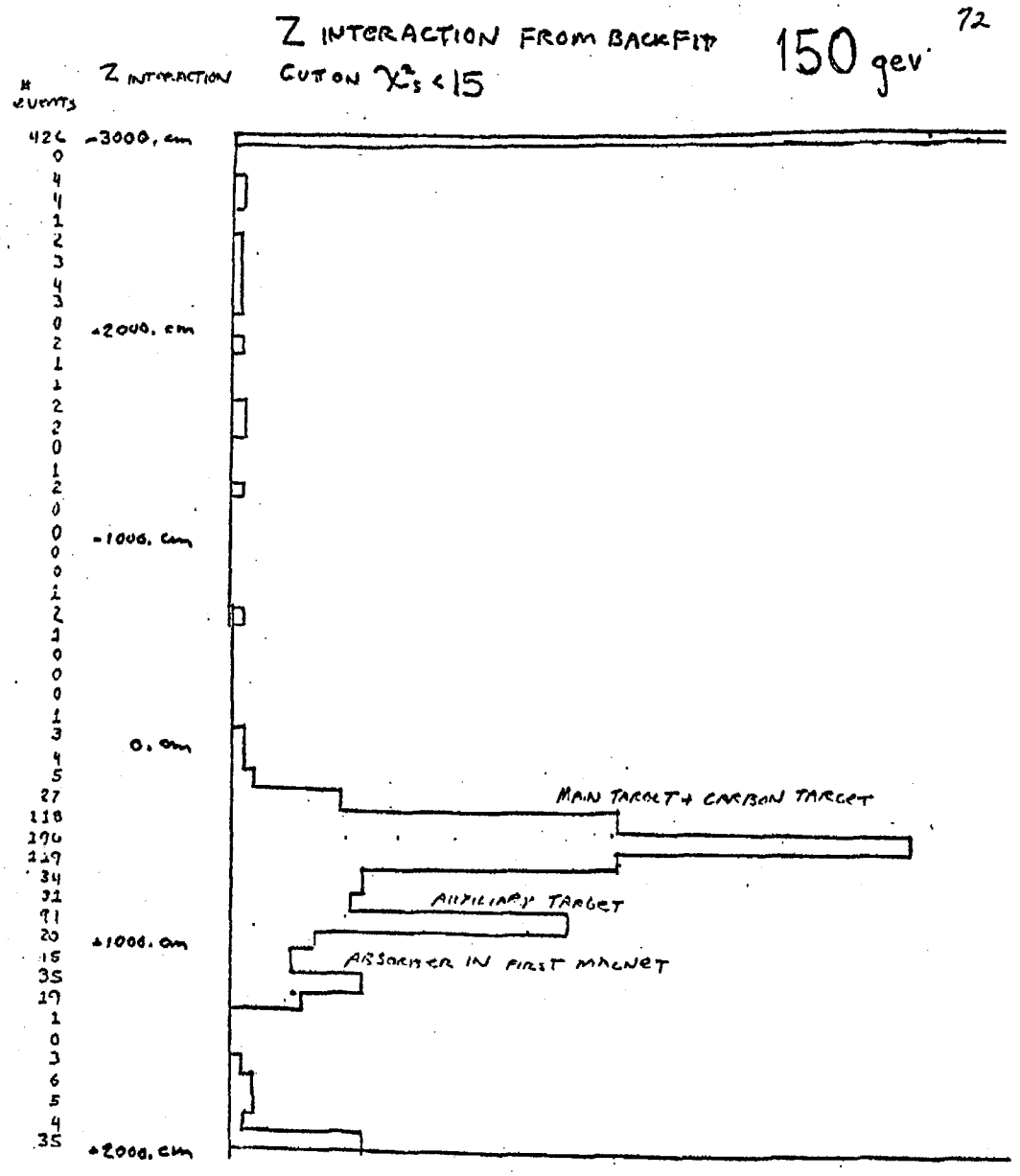
Z INTERACTION FROM BACKFIT 150 gev
CUT ON $\chi^2_s < 15$
72
EVENTS
Z INTERACTION
-3000. cm
-2000. cm
-1000. cm
0. cm
+1000. cm
+2000. cm
MAIN TARGET + CARBON TARGET
AUXILIARY TARGET
ABSORBER IN FIRST MAGNET

Fig 2

FLOWCHART FOR FRONT PROGRAM

	TRANSMISSION 56 GEV	TRANSMISSION 150 GEV
TRACK FROM BACKFIT (χ^2/DOF < 2.5) (1 beam track present)		
↓		
TEST FOR HYPOTHESIS OF SCATTER FROM BEAM (cut on χ^2_s) (cut on Zinteraction)	100%	100%
↓		
FIND ALL WIRES WITHIN MULTIPLE SCATTERING CONE (cut on ~ 3σ window) (require at least 3/6 chambers)	99%	98%
↓		
FIND (x,y) PAIRS WITHIN SCATTERING PLANE WINDOW (cut on 3-4σ window) (Require at least 3/4 spark chambers)	82%	83%
↓		
CONSTRUCT FRONT LINE WITH (x,y) CLOSEST TO SCATTERING PLANE IN EACH MODULE. THROW AWAY POINTS TO ACHIEVE (Deviation)^2/DOF < 0.05 cm^2		
↓		
PICK POINTS CLOSEST TO NEW LINE AND REPEAT (require at least 4/6 chambers) (cut on DR/(energy dependence)) (cut on DTH/(energy dependence))	73%	76%
↓		
PERFORM OVERALL MOMENTUM FIT (cut on χ^2/DOF < 2.5)	73%	75%

Fig 4

89-92

Fig 5

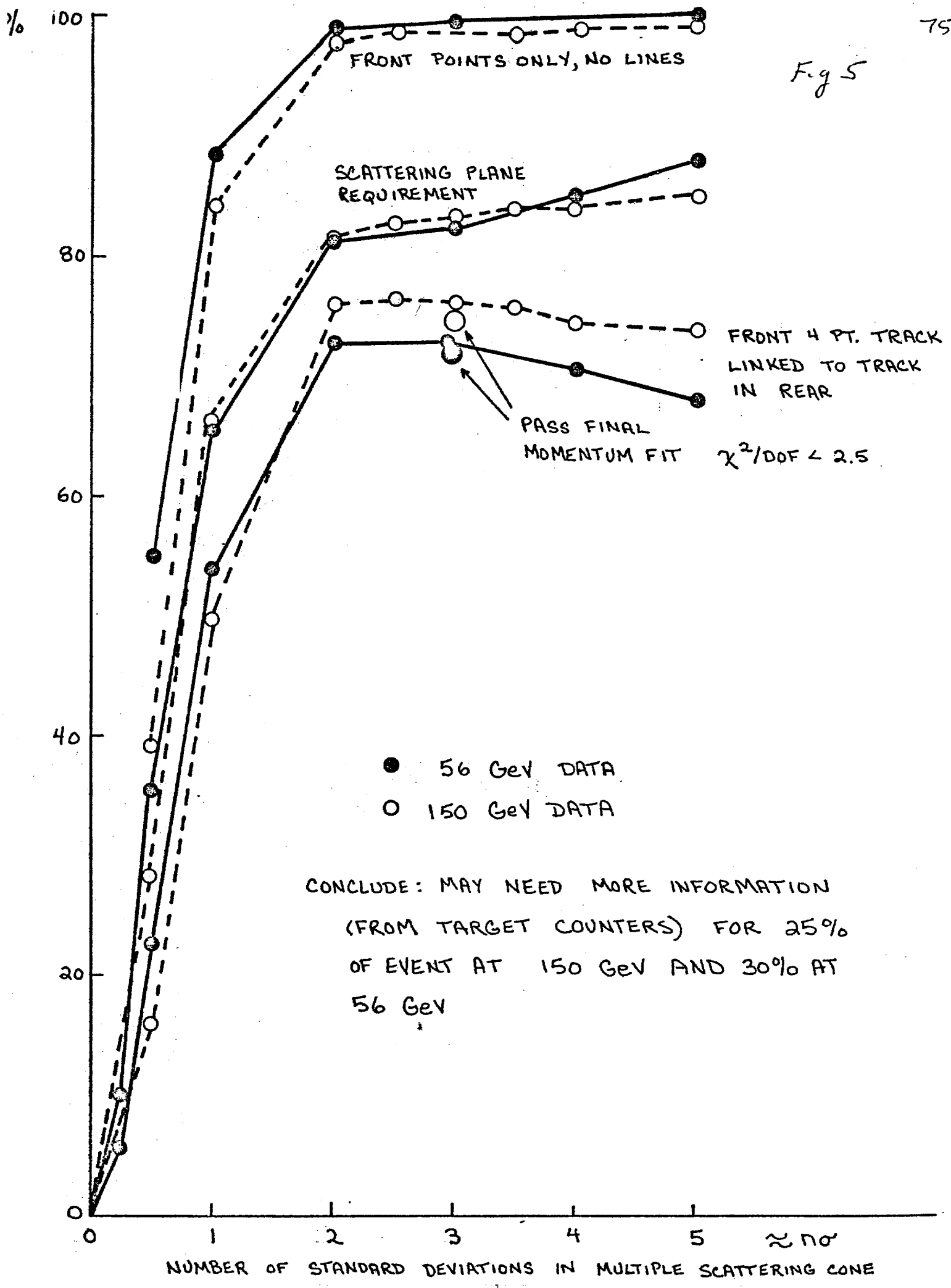
%
100
80
60
40
20
0
FRONT POINTS ONLY, NO LINES
SCATTERING PLANE REQUIREMENT
FRONT 4 PT. TRACK LINKED TO TRACK IN REAR
PASS FINAL MOMENTUM FIT
χ^2/DOF < 2.5
56 GeV DATA
150 GeV DATA
CONCLUDE: MAY NEED MORE INFORMATION (FROM TARGET COUNTERS) FOR 25% OF EVENT AT 150 GeV AND 30% AT 56 GeV
0
1
2
3
4
5
$\approx n\sigma$
NUMBER OF STANDARD DEVIATIONS IN MULTIPLE SCATTERING CONE

Fig 6

76

EVENTS LOST DUE TO RECONSTRUCTION INEFFICIENCY IN UNSHIELDED CHAMBERS IN FRONT OF SPECTROMETER VS. SECONDARY MUON MOMENTUM

RECON 8 ANALYSIS

○ INCIDENT MUON = 56 GeV

● INCIDENT MUON = 150 GeV

CONCLUDE:

≈ 25% NET LOSS AT 150

≈ 30% NET LOSS AT 56

ω BIAS MAY BE PRESENT IN RATIO COMPARISON AT VERY LARGE ω OR VERY LOW E'

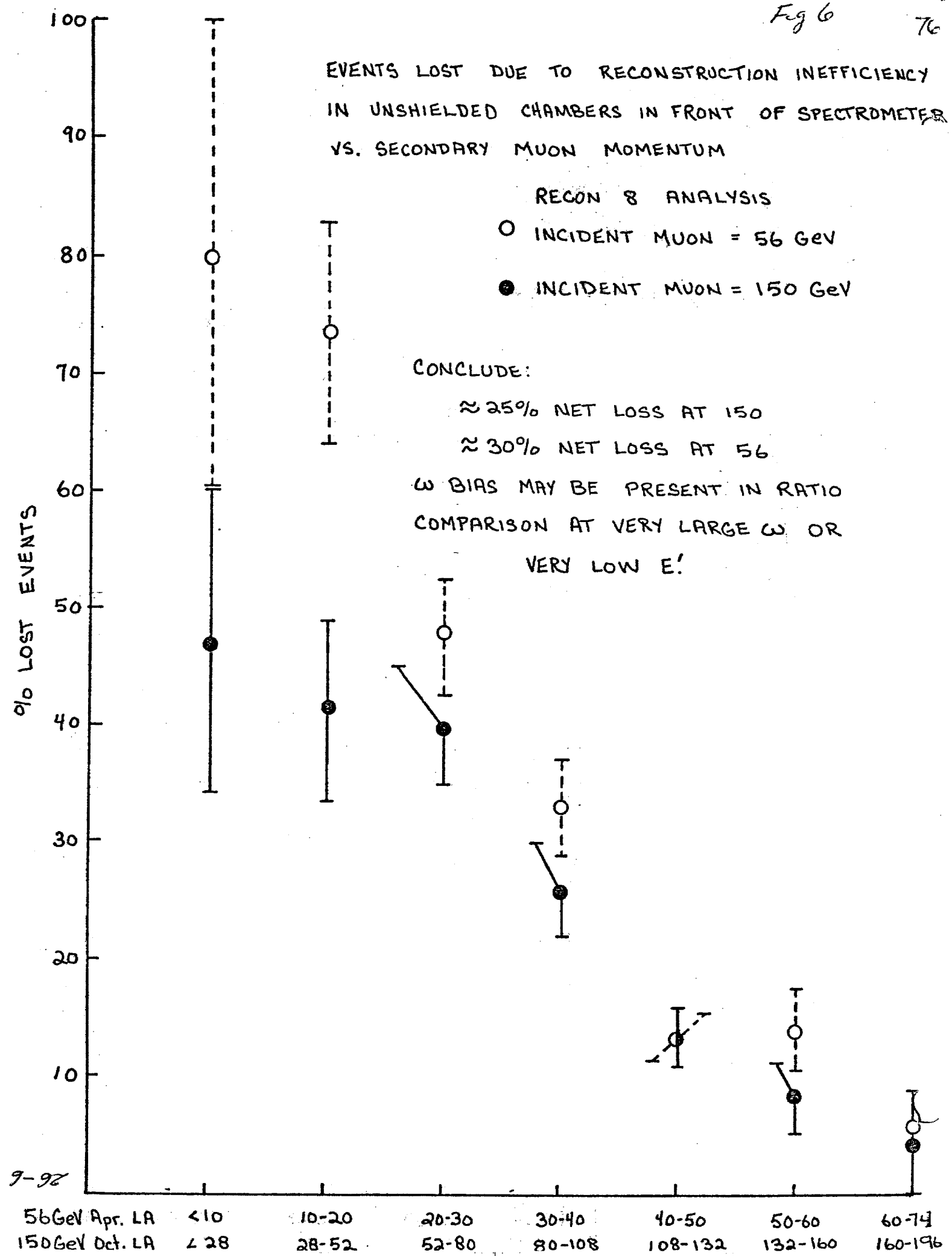

RECON8 SPECTROMETER PART: TRACK HUNTING

I. Introduction

The idea of establishing lines in the last three modules has been further extended. Given a line in the rear, it is possible to predict the complete trajectory through the spectrometer, once the momentum is known. The errors to this prediction come from several sources; among them, multiple scattering and extrapolation of lines. So the window to look for points in the spark chambers in the spectrometer has a funny shape (hourglass) as shown in Fig. 1, corresponding to $P^{-1} < P_{min}^{-1}$ (P is momentum). The obvious advantage of this window is that the size is statistically meaningful and the reconstruction efficiency vs. window discussed here is in principle predictable. Another good feature of establishing rear lines is that one can define a simple χ^2 to choose the best combination of points in the spectrometer modules (11 and 12). The χ^2 can include correlation effects, so that high and low energy are in principle treated equally. This new track hunting program has been debugged up to the level that the preliminary plateauing of the window was possible.

Further study of apparent losses and biases and detail comparison with other programs will be discussed separately.

II. Detail Description of the Method

1) Flow of analysis

1. Establish lines in the rear three modules (13,14,15).
   This has been studied in some detail.
2. Given an established line, prepare for the coefficients, using the backward ray tracing subroutine, to predict points in module 12 and 11.

$$x_m^{prediction} = x_m^{(0)} + x_m^{(1)} \cdot k + x_m^{(2)} \cdot k^2 \qquad (2.1)$$

$$k \propto \frac{1}{p}, \quad m = \text{module 12 or 11}$$

Looking for points about this prediction is helped by the following favorable observations.

a) The trajectory produced at module m by changing the momentum in Eq. (2.1) is very close to a straight line.

b) The distance d from the $k = \phi$ point ($p = \infty$) to the $k \neq \phi$ point is almost proportional to k within 10% as shown in Fig. 2.

c) The multiple scattering rms radius is proportional to k and thus to d.

d) The extrapolation error is independent of measurement most of the time. The realization of this funny shaped window ("hourglass window") is discussed in the next section.

3. Select wires in module 12 within the tangential boundary of the window in each coordinate (see figure 1). At this stage, apparent displacement due to finite angle and

finite separation between XY and UV chambers (2-7/8") can be corrected. These wires are matched and the program is general enough to include odd combinations (say X and U). But only matches of 3 and 4 coordinates are retained to guarantee good quality. The resulting counting histogram is fairly sharp as shown in Fig. 3.

4. These matched points are further checked if they are within the window, by the method discussed in the next section.

5. At present, the window is opened in module 11, for every point found in 12. The frequency of finding extra points is about 8% of the time and is summarized in Table I. This window in 11 uses the rough momentum guess obtained from measuring a point in 12. The same procedure follows to select points in 11.

6. For a given line in the roar, the best pair of points in 11 and 12 is chosen by selecting the minimum χ^2. χ^2 and its minimization is discussed in the next section.

7. These track candidates are checked against the labeled hodoscope counters (DCR), and ordered in favor of number of points, number of DCR confirmed points and less χ^2. Up to five tracks can come out.

2) Window and χ^2

1. Extrapolation error

Fit to the straight line is

$x_m^F = aZ_m + b$ at m^{th} module

Then from the error matrix for a and b,

$$\Delta r_m = \Delta x_m = \sqrt{Z_m^2(\Delta a)^2 + 2Z_m(\Delta a\Delta b) + (\Delta b)^2} \qquad (2.2)$$

where

$$\begin{pmatrix} (\Delta a)^2 & \Delta a\Delta b \\ \Delta a\Delta b & (\Delta b)^2 \end{pmatrix} = \sigma^2 \begin{pmatrix} \Sigma Z_i^2 & -\Sigma Z_i \\ -\Sigma Z_i & \Sigma 1 \end{pmatrix} \Big/ \text{det.}$$

σ = measurement error

i = module 13, 14, 15

2. Multiple scattering

$$\Delta r_m = \sqrt{\left\langle \sum_i (Z_{i+1} - Z_i)\theta_i^{\,2} \right\rangle}$$

$$= \sqrt{\sum_i (Z_{i+1} - Z_i)^2 \langle\theta\rangle} \qquad (2.3)$$

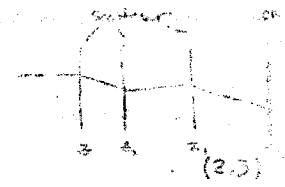

where θ_i is the projected multiple scattering angle at i^{th} module at Z_i, and $\theta_i \cdot \theta_j = \delta_{ij}\langle\theta\rangle^2$ because of statistical independence.

3. Realization of window

Let r_m = multiple scattering rms radius at $p = p_{min}$.

r_e = extrapolation error

Move the origin to the $p = \infty$ point and rotate such that the $p = p_{min}$ point lies on the x axis.

Given an observed point in (x_o, y_o) in this coordinate, solve for x (and thus p) that satisfies

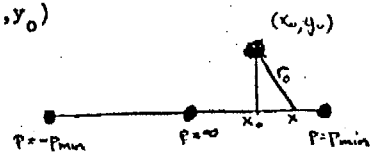

$$r_o^2 = r_e^2 + \left(r_m \cdot \frac{x}{x_{max}}\right)^2 = y_o^2 + (x_o - x)^2$$

or

$$(1 - (r_m/x_{max})^2)x^2 - 2x_o x + x_o^2 + y_o^2 - r_e^2 = 0 \qquad (2.4)$$

If there is no solution or it lies outside of $x < x_{max} + R_{max}$, the point is outside of the window.

4. Definition of a one parameter $\chi^2(p)$

It is useful to have a simple χ^2 that is close to the physics. Given a line, it is possible to predict points in module 12 and 11 as a function of momentum as given in Eq. (2.1); so

$$\chi^2(p) = \sum_{i,j} \delta x_i (d(p)^{-1})_{ij} \delta x_j + y \text{ term} \qquad (2.5)$$

where

$$\delta x_i = x_i^{meas} - x_i^{pred}(p); \; x_i^{pred} \text{ as given in (2.1)}$$

$$(d(p))_{ij} = \sum_{magnet} z_{im} z_{jm} \langle\theta^2\rangle + \delta_{ij} \sigma^2$$

This χ^2 is not a simple function of p, but can be minimized easily by approximating the shape around the minimum by a 2nd order polynomial. The shape of χ^2 vs. 1/p is shown in Fig. 4 . This one parameter χ^2 is well correlated with the 5 parameter χ^2 of the full momentum fit using only the information inside and to the rear of the spectrometer.

5. Correction of finite separation between XY and UV chambers (with a module).

The correction can be done, once the angle is known. The coordinates are evaluated at the center of XY and UV chamber. In the case of the last three modules, the angle is known and a correction easily obtained. Given a line, one can also predict the angle in each coordinate once the momentum is known. As an observation of a wire corresponds to an observation of momentum, this can be corrected at wire finding stage.

3) Advantages and Disadvantages

Advantages:

1. It is the first time that we complain about a too sharp χ^2 distribution! σ_{meas} = 0.5 mm is not small enough to degrade to the right χ^2 shape. This does not imply the alignment is good, but good lines in the back and finite angle correction ensures the good quality.
2. The windows correspond to physical ones and one can in principle estimate losses statistically.

3. χ^2 in selecting tracks includes correlation effects and treats high and low energy tracks on the same footing.

Disadvantages

1. It is much more restrictive to the present geometry and its change requires the change of the program.
2. It is more subject to particular inefficiencies, especially of misfiring a spark gap in the rear modules.
3. It is probably inefficient to reconstruct low energy wrong sign tracks. The lines in the rear shoot into the field free region and the expansion of (2.1) breaks down.
4. Right now finding points in module 11 is heavily dependent on points in module 12. Also, point finding is done for every point in 12, which is possibly inefficient.

III. Preliminary Study of Track Reconstruction Efficiency

The "hourglass" window and matching window were plateaued, and the results were shown in the upper and lower graphs in Fig. 5. The efficiency of reconstructing calibration data is fairly well understood, and the lost events are easily accounted for. The apparent loss of 4% is due to a χ^2 cut and most of them are slightly worse than $\chi^2/\text{dof} = 5$. But event reconstruction efficiency is apparently worse, and at this stage, we cannot deny that this difference is real until we make a more careful study of those lost events.

1) Requirement of good tracks

1. Last three modules give good lines. At the minimum two coordinates of (X,Y,U,V) have straight lines and one confirming matching coordinate linking X,Y to give spatial information.
2. Both of module 11 and 12 contribute. Only matches of 4 and 3 coordinates (say U,V,X) are considered. A match of 4 eliminates one of 3 if one of the wires is common.
3. χ^2/dof of a 5 parameter fit is less than 5.

2) Runs studied:

Run		
564	Small magnet	$E_0 = 53$ GeV
569	"	$E_0 = 18.5$
535	APR 56 LA	($\mu_\mu \sim 120$ K/pulse)
542	"	($\mu_\mu \sim 200$ K/pulse)
457	OCT 150 LA	

(LA = "large angle" target configuration)

3) Discussions

1. Line finding

The curves shown in Fig. 5 are for the case when there is one and only one line in the rear. So the efficiency is to be multiplied by the line finding efficiency. For calibration runs the efficiency of finding lines was

measured to be better than 99.8%, but that for event triggers is apparently about 90%. Of those lost events, at least 20% and probably 50% are lost because of geometrical reasons, but the rest of them look messy and are not easily accounted for. So at worst the efficiency is down by another 8%. In studying data, the events with non-scattered muons were taken out to reduce events from absorber.

2. Energy dependence

The apparent difference for low energy and high energy in the start of the plateau and its height for $\chi^2 < 2.5$ is because the measurement error assumed (0.5 mm) is still large, as seen from Fig. 6 . Large χ^2 events are definitely there and have probably something to do with muon interactions in iron magnets.

3. Data

If we insist that both 11 and 12 contribute, the apparent efficiency is about 85%. Those events with 11 or 12 missing were studied closely and it turned out that 3.8% is due to small angle scattering going through the patch of module 11, 1.2% is definitely hadron punch through and the rest is difficult to judge. The losses that occur even allowing 11 or 12 to miss are mostly because of bad χ^2 resulting from bad lines, but we have

to remember those are the only lines found in those triggers.

So at this stage, the tight requirement gives the efficiency in the range of 80 to 90%, and our next objective is to pin this number down to more solid one and to prove the lost events are not badly biased.

A slight difference between the 56 GeV and the 150 GeV configurations might be due to alignment and needs more investigation.

IV. Comments, etc.

1) Bugs and refinements:

There are several things not understood yet:

1. The efficiency of picking up points in 12 is much more efficient at small σ. Shouldn't the window look the same apart from the scale? (Fig. 1)
2. Without using the information from module 12, the window in 11 could partly fall into outside of fiducial volume, and reducing its size with this constraint will help reduce picking up noise.
3. The drop observed at $\sigma = 7$ in Run 542 is due to a large loss of points in 12, and is most suspicious. It might be a breakdown of the approximation or something simpler such as noise pickup.

26-64

4. Run 569 (18.6 GeV) was studied with p_{min} = 18 GeV, and we lost about 10%. This is because the momentum derived from the one parameter $\chi^2_{(p)}$ is required to be larger than p_{min} to ensure not choosing a strange track with smaller χ^2. $p_{min} = 0.1\ E_0$ usually. We need more study here.

2) Speeding up the analysis:

We now use the symmetric matrix inversion routine for 5x5 error and slope matrix inversion and a new tape decoding routine in reading tape.

The CPU time on the 6600:

Tape read and decoding	14 msec/event
Beam finding	27 msec/event
Wand and line decoding	27 msec/event
Track hunting	27 msec/event
Momentum fit	56 msec/track

3) Matching vs. radius

If XY and UV chambers are not exactly 45°, the matching error grows with radius, thus creating radial bias. Run 569 is convenient to study the effect because tracks go to large radius.

Matching peak (cm)

Module	Radius	$\langle X - \frac{U-V}{2} \rangle$ East	West	$\langle Y - \frac{U+V}{2} \rangle$ Up	Down
11	33-76	0.01±0.09	-0.00±0.07	0.00±0.07	0.09±0.07
12	33-80	-0.03±0.04	-0.07±0.06	-0.13±0.06	-0.03±0.06
13	30-80	0.03±0.06	-0.07±0.06	-0.05±0.06	-0.02±0.07
14	25-80	0.01±0.06	-0.09±0.06	-0.09±0.04	-0.04±0.05
15	20-70	0.01±0.06	-0.01±0.06	-0.06±0.05	0.05±0.06

So there could be at worst a / mrad rotation but not more. This is also dependent on wands and discriminator performance on this level.

TABLE I NUMBER OF POINTS IN THE 'HOURGLASS' WINDOW

		MODULE 11					MODULE 12				
RUN	DESCRIP.	0	1	2	3	>3	0	1	2	3	>3
564	53 GeV	0.7%	90.2	6.2	1.3	1.4	0.4	91.2	5.9	1.3	1.3
569	18 GeV	0.8	93.1	3.8	1.0	1.2	0.2	91.0	6.2	1.7	1.3
542	56 DATA	8.6	81.7	6.0	2.2	1.5	3.9	86.8	5.8	2.5	1.0

TABLE II MATCHES IN MODULES 11 AND 12 (ONE LINE IN REAR)

RUN 564

12 \ 11	0	3	4
0	0.1%	0.2	0.6
3	0.1	1.2	10.9
4	1.0	3.4	82.4

RUN 569

12 \ 11	0	3	4
0	0.1%	0.0	0.5
3	0.2	0.8	17.6
4	1.2	3.4	76.1

RUN 542

12 \ 11	0	3	4
0	2.8%	0.8	0.6
3	0.9	0.5	6.7
4	5.6	3.5	78.5

3.8% geometry (very small angles)
1.4% punch through
1.3% ?

Fig 1

90

WINDOW FOR POINT FINDING IN MIDDLE OF SPECTROMETER

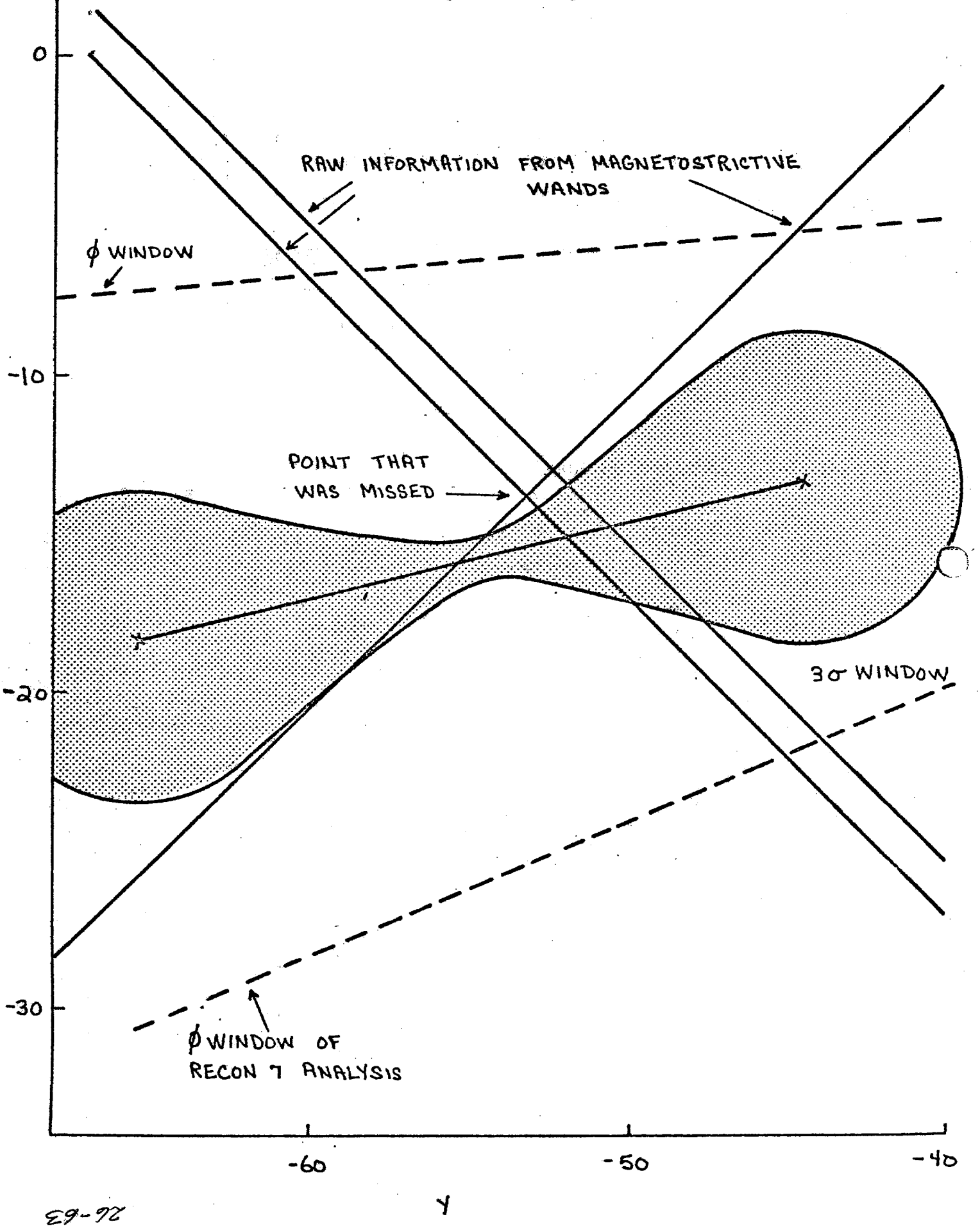

E9-92

Fig 2

91

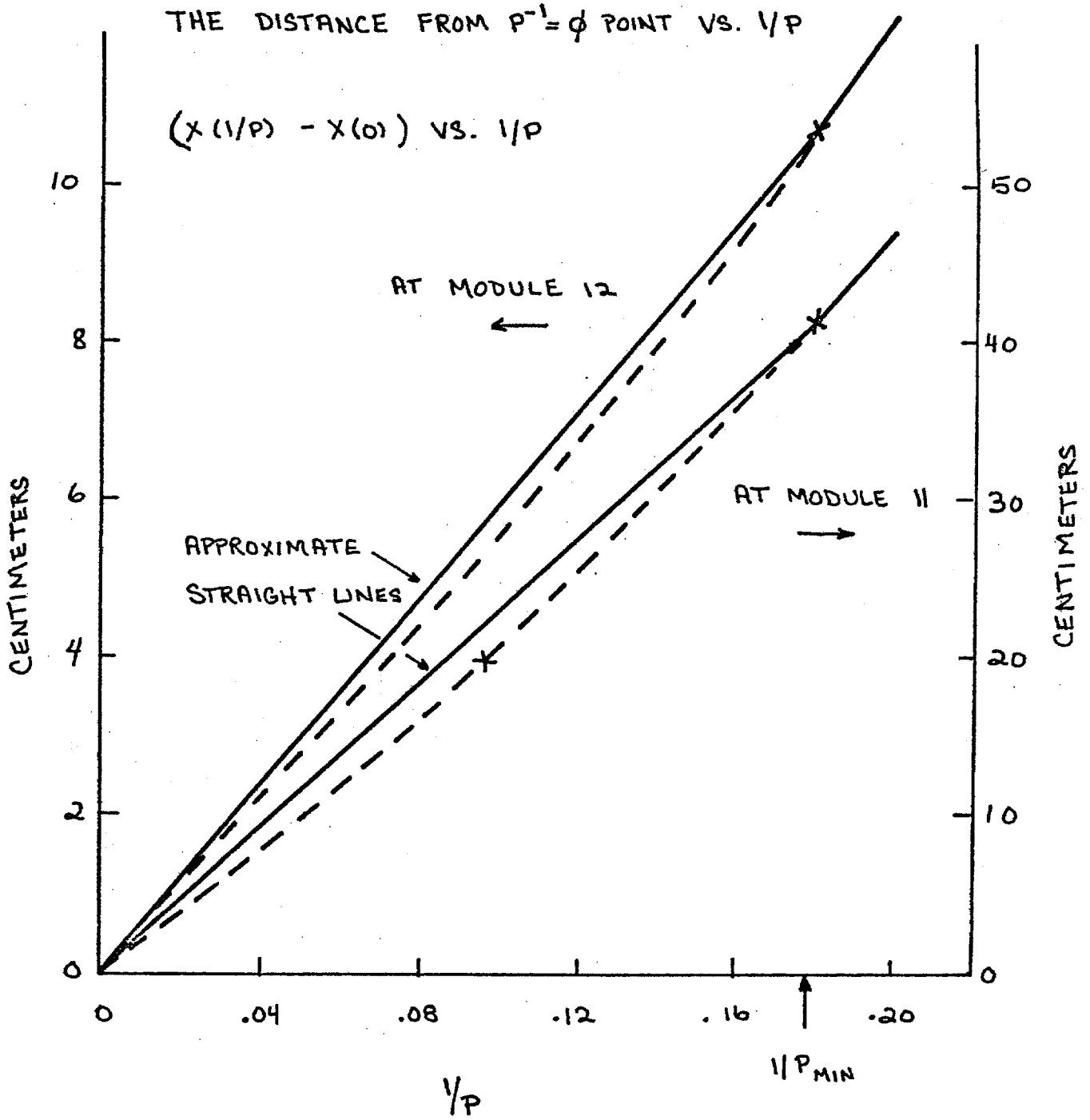
THE DISTANCE FROM $P^{-1} = \phi$ POINT VS. 1/P
(X (1/P) - X (0)) VS. 1/P
AT MODULE 12
AT MODULE 11
APPROXIMATE
STRAIGHT LINES
CENTIMETERS
CENTIMETERS
0
2
4
6
8
10
0
10
20
30
40
50
0
.04
.08
.12
.16
.20
1/P
$1/P_{MIN}$

Fig 3

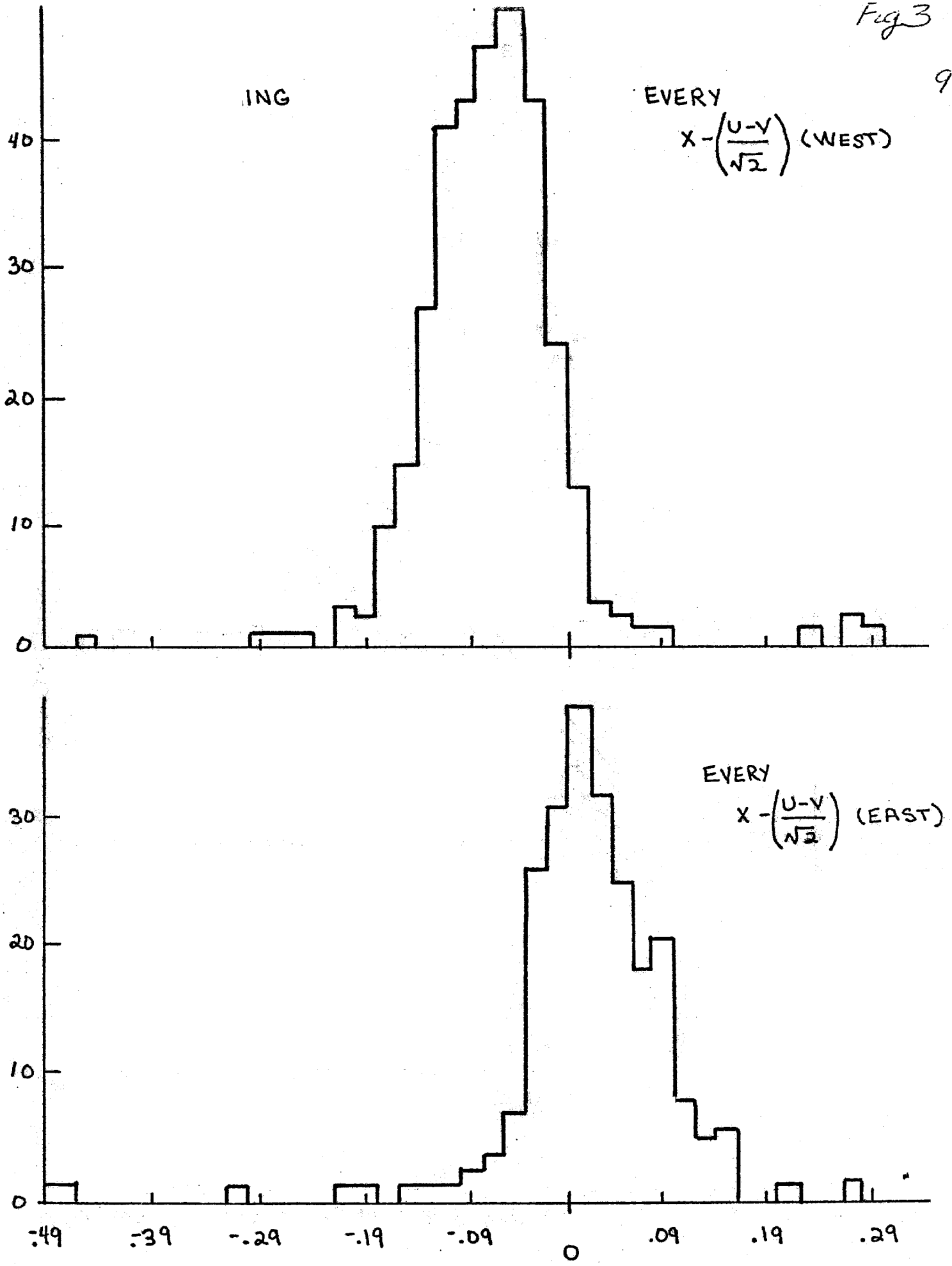
ING
EVERY
$X - \left(\frac{U-V}{\sqrt{2}}\right)$ (WEST)
40
30
20
10
0
EVERY
$X - \left(\frac{U-V}{\sqrt{2}}\right)$ (EAST)
30
20
10
0
-.49
-.39
-.29
-.19
-.09
0
.09
.19
.29
Scale in centimeters

Fig 4

$\chi^2(P)$ vs. $1/P$

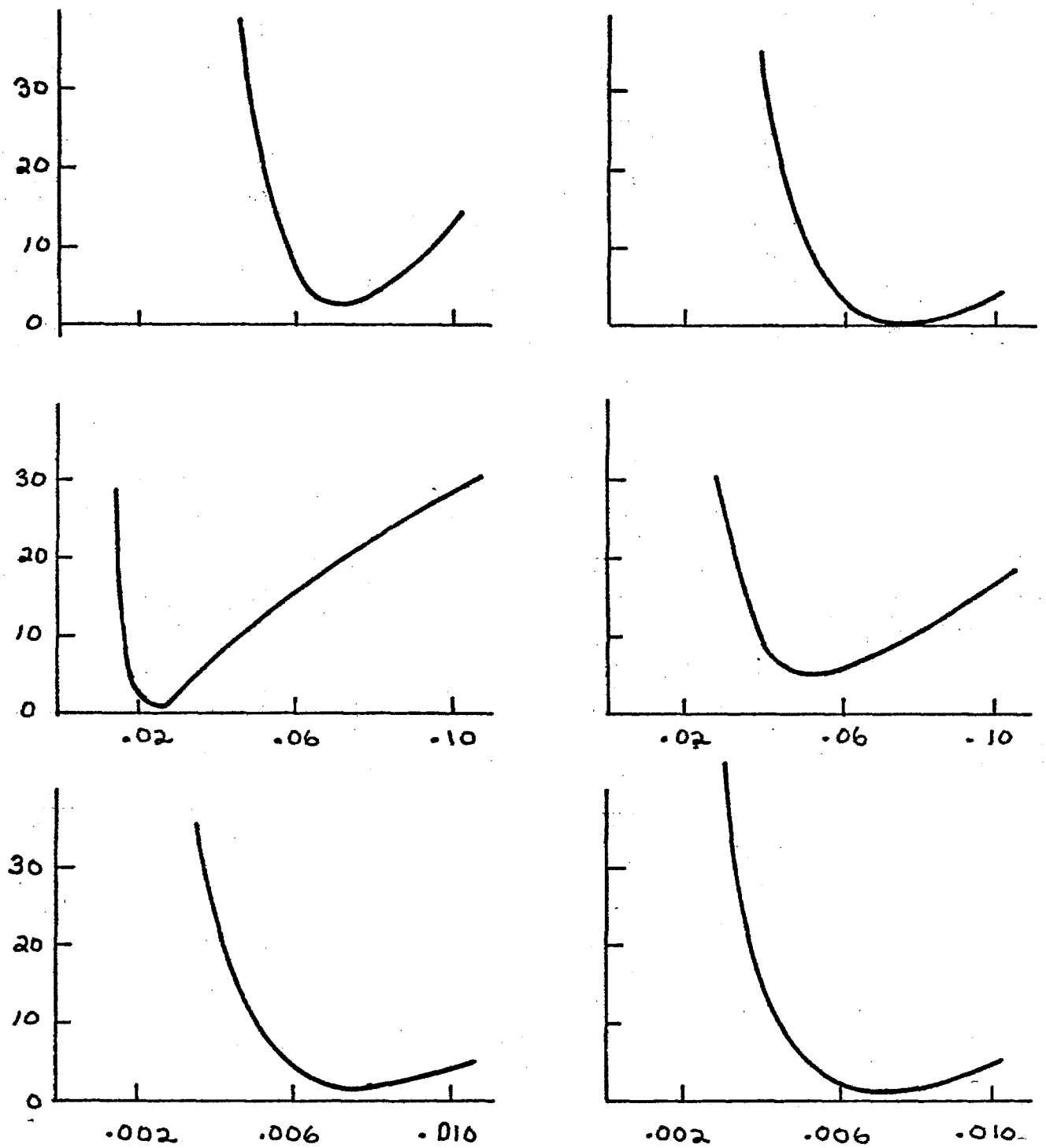

SAMPLE MINIMIZATION OF ONE-DIMENSIONAL χ^2 vs. $1/P$

TRACK REC'N EFFICIENCY VS. WINDOWS (ONE AND ONLY ONE LINE IN THE REAR)

HOUR GLASS WINDOW : $n\sigma$ MEANS n STD. DEVIATION

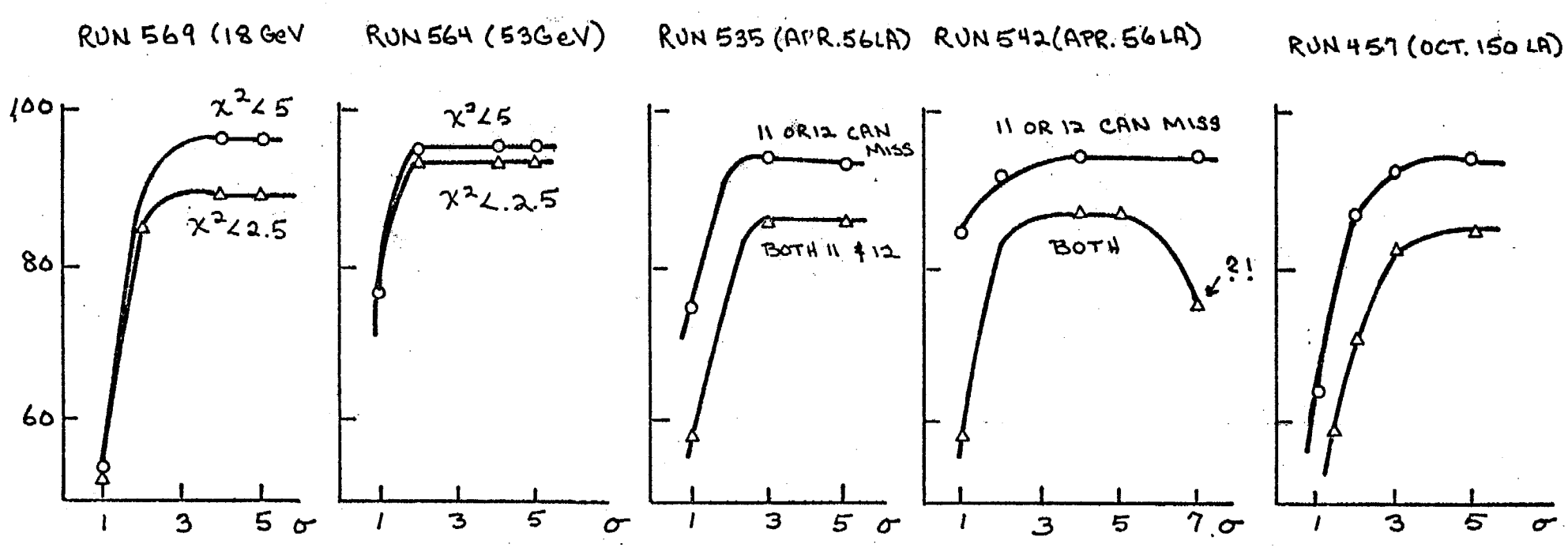

MATCHING WINDOW ($|X - \frac{U-V}{\sqrt{2}}| < WM$ etc.)

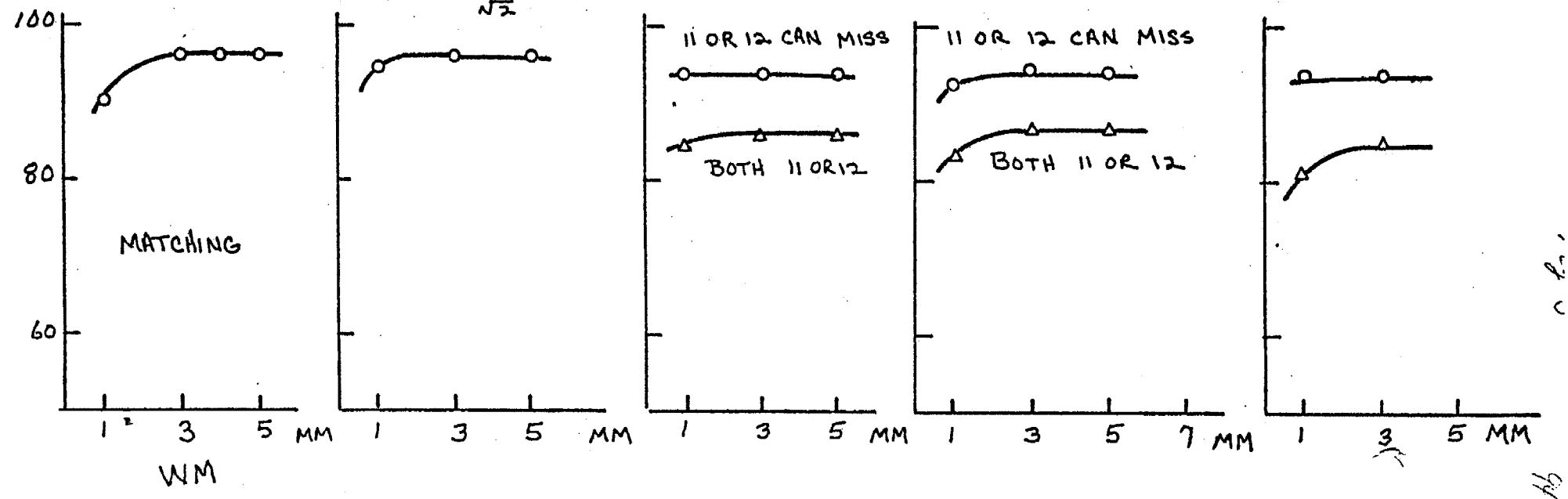

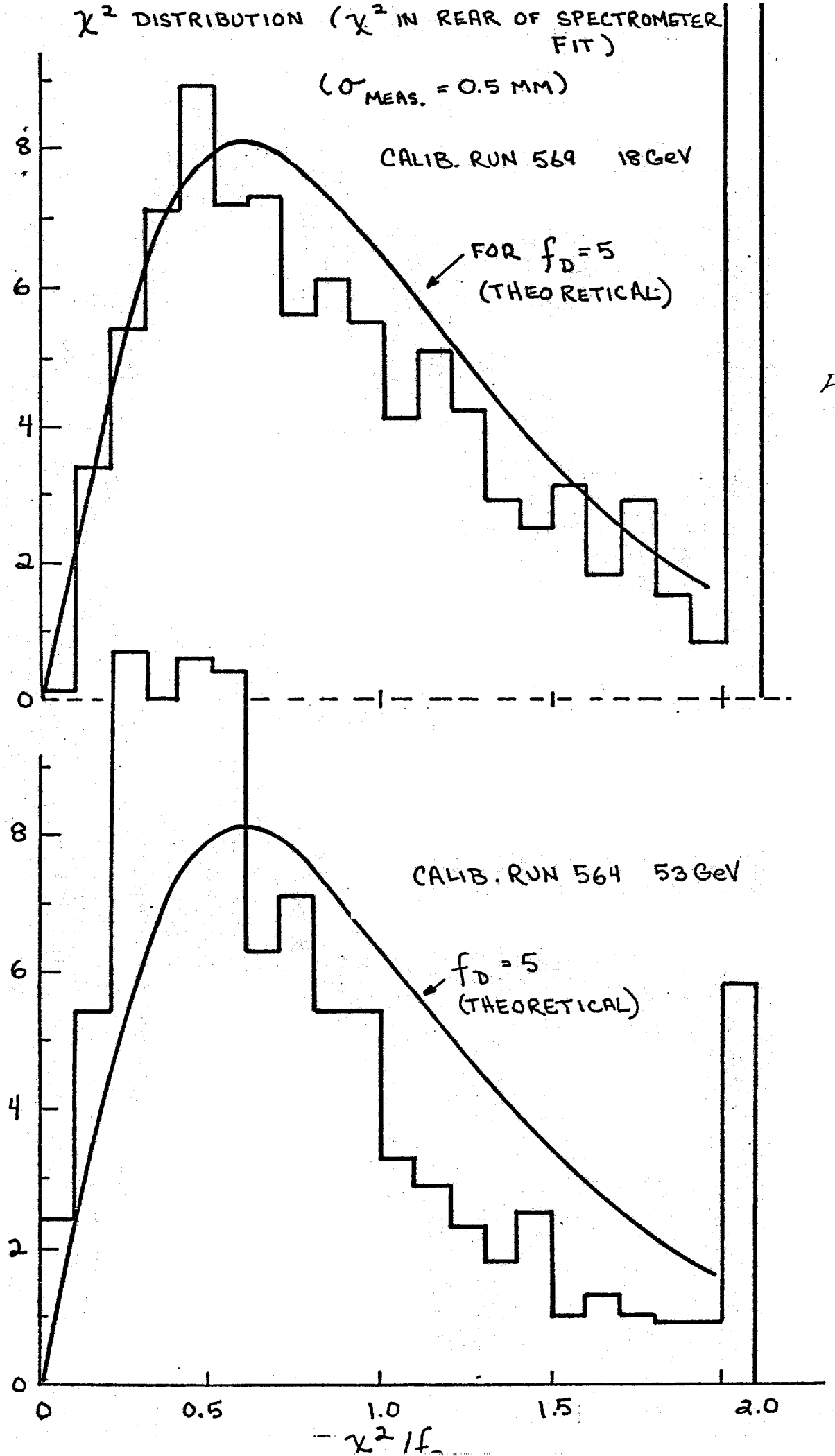
χ^2 DISTRIBUTION (χ^2 IN REAR OF SPECTROMETER FIT)
($\sigma_{MEAS.}$ = 0.5 MM)
CALIB. RUN 569 18 GeV
FOR $f_D = 5$ (THEORETICAL)
CALIB. RUN 564 53 GeV
$f_D = 5$ (THEORETICAL)
0
2
4
6
8
0.5
1.0
1.5
2.0
χ^2/f_D

Fig 6

APPENDIX IX

STUDIES OF TRACK RECONSTRUCTION...BACKFIT ONLY

The track hunting part of analysis programs has been studied in detail by comparing three different programs on an event by event basis. These programs are all searching for muon tracks within the spectrometer and are ignoring the "front". Some specific problem areas such as halo properties have been investigated with RECON8 only. A general conclusion from this study is that both RECON8 and VOREP(backfit only) programs are free from track finding bias. It also appears that these two programs are 95% efficient with respect to the composite set of found events. RECON8 is significantly better than RECON7 in both efficiency and quality of fit. Characteristics of the runs used are given in Table 3 .

A. RECON8-VOREP Comparison

Following Table 1 step by step, starting with a), note that every variable is scaled to the λ=1.6 (E_0=150 GeV) configuration even though this is 56.25 GeV data. Differences in χ^2distributions between RECON8 and VOREP are mostly due to assigning 1/2 mm measurement errors by RECON8 and 1 mm errors by VOREP. The "magnet face" cut is 6.5" at the front face of the first magnet. "Geometry" refers to the fiducial volume cuts. In list c) and d) "lost" refers to events not in "common" and approximately half of these are not true losses because bookkeeping is done differently by the two programs. The χ^2cut reveals events which usually have spark chamber modules with less than four ordinates. This is most likely a result of muon induced showers from the iron magnet faces causing confusion and leading to incorrect linking of coordinates. In part e) the spark chamber performance is tabulated. A module consists of four wire planes at four different angles, and the only weak part appears to be slight losses in module 12. Finally, in f) the spectrometer hodoscopes are compared to scattered muons and to clearly labeled halo muons. The halo is usually out of time coincidence as shown by the poor hodoscope correlation(see also section C, Bias Studies).

B. RECON8-RECON7 Comparison

This comparison is of interest because RECON7 has been used for total fitting of most available data, and RECON8 is considerably better but has yet to be applied to very much data. The events labeled "lost" in Table 1 are presumably true losses. This comparison is for Run 550 only with measurement errors of 1 mm assigned by RECON7 and 1/2 mm by RECON8.

C. Studies of Halo and Miscellaneous Biases

Halo muons are labeled by the vertex location being far from the target: z<-300 cm or z>500 cm. Comparison of x-y illumination plots for scattered muon(sans halo) in Figure 1 and halo only in Figure 2 reveal the asymmetric nature and large radial extent of the halo. In table 4 the ordinate matching in the spark chamber modules is tabulated (compare to non-halo in Table 1,e). The spark chambers behave poorly because of the time dispersion of the halo seen also in Table 1,f If halo is treated as events, the Q^2 vs radius plot of Figure 3b results. The handful of events at higher Q^2 are probably the result of incorrect linking due to poor quality of the halo track. There seems to be no problem separating halo from real events in the downstream target runs such as those considered in this section. The separation may be reduced to a level which causes trouble with upstream target, low Q^2 runs, but tests of this are incomplete.

In Table 5 there are several bias tests listed. Part a) shows the effects of hadron "punch through" and muon induced showers on the behavior of the downstream beam veto. The trigger requires $\overline{BV}\cdot AND\cdot \overline{BV'}$ so that the last line being non-zero is a measure of some latch-veto dead-time. Track multiplicity is investigated in part b), and shows no significant correlations. Variations of distributions with the number of latched counters in the first trigger bank of the spectrometer can be seen in part c). We conclude that showers and δ-rays giving extra latched counters are not biased in Q^2, but may have some E' dependence. The final check is the X^2 dependence shown in part d). Once again, no strong bias is seen.

Table 1. RECON8-VOREP Comparison

a) Progressive Cuts (# surviving after cut)

	Total #	Magnet Face	Geom.	|z| <300 cm	E'> 35 GeV	Beam	χ^2 <5	All 5 Modules
RECON8	4539	3214	2504	1070	1001	968	940	927
VOREP	3721	2598	1672	1076	980	980	945	937

b) Common Events (1 for RECON8, 2 for VOREP)

	$E_1'-E_2'$ GeV	$E_1'/E_2'-1$	$\theta_1-\theta_2$ mrad	θ_1/θ_2-1	Q_1^2/Q_1^2-1 $(GeV/c)^2$	z_1-z_2 cm	$\chi_1^2-\chi_2^2$
Mean	0.62	0.78%	-0.08	-0.22%	-0.03%	-2.35	0.16
Sigma	6.46	5.94	1.40	4.60	4.90	22.90	0.51

c) Distributions of Common and Lost Events (1 for RECON8, 2 for VOREP)

		Events #	<E'> GeV	σ	<θ> mrad	σ	$<Q^2>$ $(GeV/c)^2$	σ	$<\chi^2>$	σ	<z> cm	σ
1	common	816	98.9	35.5	29.0	10.4	12.1	7.3	0.92	0.70	-19.4	95.8
	"lost"	121	105.9	43.2	26.6	11.6	10.5	7.0	1.08	0.97	-28.1	120.1
2	common	816	98.5	35.1	29.1	10.4	12.1	7.2	0.80	0.72	-15.3	98.2
	"lost"	111	100.2	41.1	27.5	11.5	10.9	7.9	1.20	0.93	-23.4	107.2

d) Accounting for "lost" Events

Category	RECON8	VOREP	
Geometry	32	28	
|z|<300 cm	20	20	
E'<35 GeV	2	4	
No beam	16	6+α	α<6
Two beam	4	--	↑recoverable losses
χ^2>5	15	19	↓ true losses
lost cham. 11	7	0	
lost cham. 12	5	2	
Halo only	12	3	
Not on tape	8	29-α	
Total	121	111	

e) Matching in Each Module (4 ordinates, max, per module)

#Ord/Mod#→	RECON8 11	12	13	14	15	VOREP 11	12	13	14	15
↓ 0	0.9%	0.8	0	0	0	0.3%	0.4	0.0	0.0	0.1
2	0.5	0.9	0.5	0.1	1.0	0.3	0.6	0.4	0.4	0.5
3	3.6	12.2	3.2	2.6	6.2	2.6	11.0	1.8	1.5	6.3
4	95.0	86.1	96.4	97.4	92.8	96.8	88.0	98.8	99.1	93.1

f) Latched Spectrometer Hodoscope Counters (DCR) which Agree with Track Location

# of latched./agree →	0	1	2	3
RECON8 ("events")	0.0%	0.3	4.4	95.1
VOREP ("events")	0.3	0.3	3.4	96.0
Halo only	40.9	24.0	17.0	18.1

26-59

Table 2. RECON8-RECON7 Comparison

a) Progressive Cuts

	Total #	Magnet Face	Geom.	$\lvert z\rvert<$ 300 cm	$E'>35$ GeV	Beam	$\chi^2<5$	All 5 Modules
RECON8	4200	2825	2210	1058	986	986	964	964
RECON7	5067	3547	2583	1076	973	973	889	873

b) Common Events (1 for RECON8, 2 for RECON7)

	$E_1'-E_2'$ GeV	$\lvert E_1'/E_2'-1\rvert$	$\lvert\theta_1-\theta_2$ mrad	$\lvert\theta_1/\theta_2-1\rvert$	$\lvert Q_1^2/Q_2^2-1\rvert$ $(GeV/c)^2$	$\lvert z_1-z_2\rvert$ cm	$\lvert\chi_1^2-\chi_2^2$
Mean	0.21	0.13%	-.18	-.53%	0.01%	-0.86	-.008
Sigma	2.93	3.23	1.43	4.56	5.23	15.8	.743

c) Distributions of Common and Lost Events

	Events	$\langle E'\rangle$ GeV	σ	$\langle\theta\rangle$ mrad	σ	$\langle Q^2\rangle$ $(GeV/c)^2$	σ	$\langle\chi^2\rangle$	σ	$\langle z\rangle$ cm	σ
RECON8											
Common	824	100.6	36.6	29.1	10.8	12.5	7.6	.89	.64	-19.9	94.6
Lost	49	100.7	51.6	30.2	12.2	11.6	6.2	1.81	1.40	-21.5	134.3
RECON7											
Common	824	99.2	36.7	29.4	10.9	12.4	7.5	1.10	1.06	-15.6	104.1
Lost	140	99.6	39.9	27.7	11.0	11.2	8.6	1.20	0.88	-25.3	116.4

TABLE 3

Characteristics of Runs 550 and 554 (April'74, 56.3 GeV)

Event Trigger	$(B.S.\overline{BV}_{evg})$	4104	4005
Pulser	$(B.PULSER_{evg})$	722	781
Useful muons	$(B.\overline{BV}_d)$	$189*10^6$	$192*10^6$
Intensity	(B_{spg}/spills)	$290*10^3$	$230*10^3$
Probability of two mu/RF bucket	$(B104.B104_d/B104)$	2%	2%
Halo/Beam	(S_{evg}/B_{evg})	70%	70%
Dead time	$(1-B.\overline{BV}_d/B_{spg})$	20%	20%

TABLE 4

Spark Chamber Matching for Halo Tracks

# of matches	Module# 11	12	13	14	15
0	9.1%	3.4	0	0	0
2	8.4	6.5	5.5	4.9	5.2
3	17.4	19.3	9.3	6.1	10.9
4	65.2	70.8	85.2	89.0	83.9

Table 5. Bias Tests

	Events	%	$\langle E'/E_0 \rangle$	σ	$\langle Q^2 \rangle$ $(GeV/c)^2$	σ	interaction $\langle z \rangle$ cm	σ	$\langle \chi^2 \rangle$	σ
a) Beam Veto										
BV BV'										
off off	1874	89.2	0.66	0.24	12.4	7.6	-8.4	80.2	0.95	0.73
off on	144	6.9	0.72	0.23	9.4	4.6	-7.2	83.8	0.96	0.74
on off	74	3.4	0.68	0.25	11.1	7.1	-22.7	84.4	0.89	0.67
on on	10	0.5	0.56	0.23	9.4	4.2	-57.7	74.0	0.83	0.45
b) Spark Chambers										
# of Tracks										
1	1604	76.3	0.67	0.24	12.1	7.3	-8.7	79.6	0.94	0.73
2	411	25.6	0.66	0.24	12.2	8.0	-9.7	84.0	0.95	0.70
3	62	3.0	0.69	0.23	11.8	7.5	-13.0	86.6	0.97	0.76
4	16	0.8	0.61	0.23	10.3	6.8	-9.0	85.0	1.10	1.10
5	8	0.4	0.73	0.22	11.0	5.6	-15.8	83.4	1.11	0.76
c) Counter Latching										
# of SA Latched										
1	826	78.3	0.69	0.24	11.7	6.9	-10.5	81.2		
2	197	18.7	0.58	0.22	12.8	8.1	-7.1	83.4		
3	29	2.7	0.46	0.14	12.7	7.5	-9.1	77.9		
4	3	0.3								
5	0									
d) Dependence on χ^2										
χ^2										
0-2.5	2000	93.7	0.66	0.24	12.0	7.4	-8.5	80.1		
2.5-5.0	102	4.8	0.63	0.27	13.5	8.5	-21.5	92.1		
5.0-7.5	13	0.6	0.69	0.21	15.5	10.5	-39.3	70.7		
7.5-10.0	15	0.7	0.61	0.27	14.6	6.9	4.6	80.9		
10.0-12.5	5	0.2								

26-58

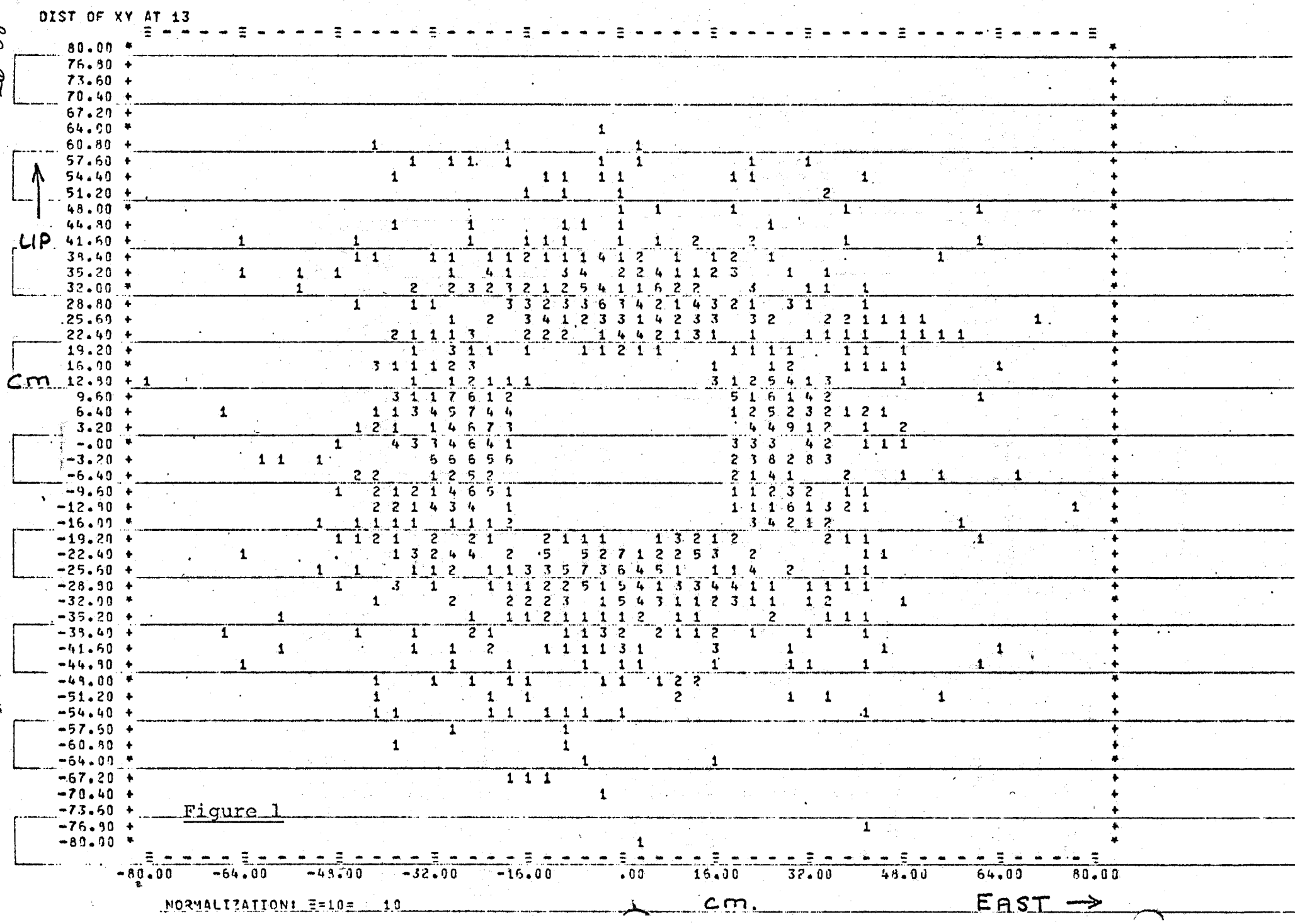

Figure 1

SPATIAL DISTRIBUTION - "GOOD DATA"

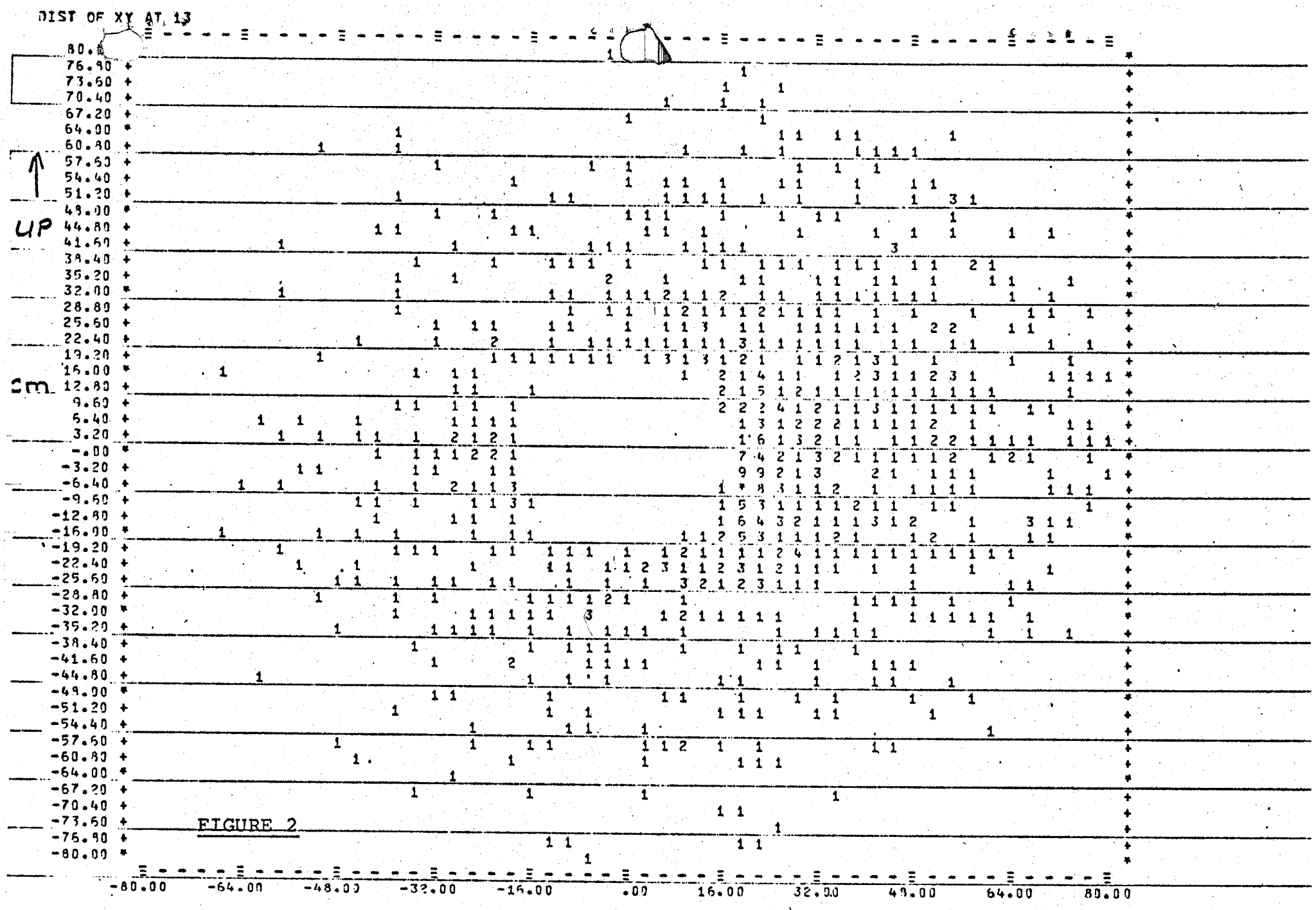

FIGURE 2

SPATIAL DISTRIBUTION - "HALO TRACKS"

Fig 2

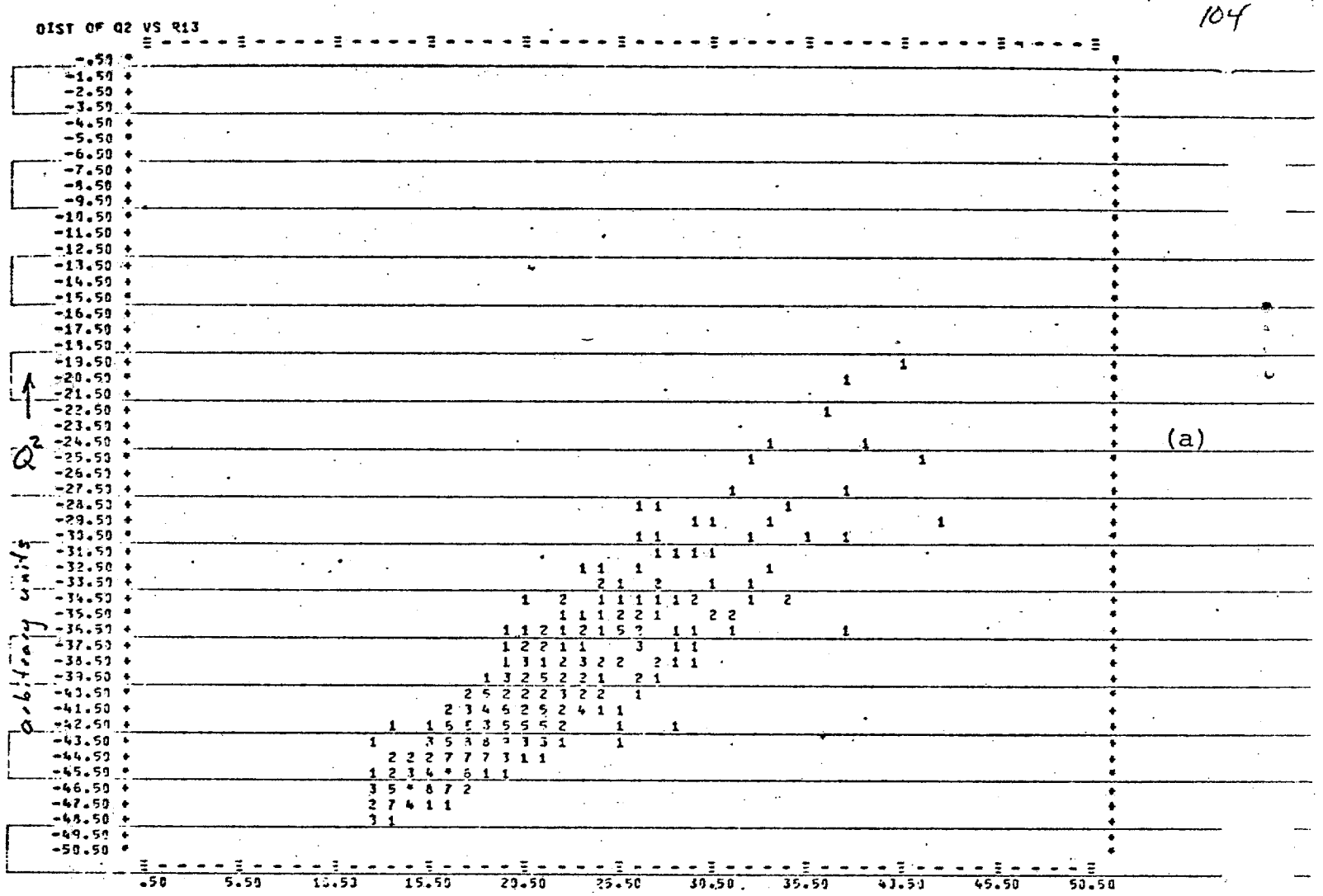

Q^2 VS RADIUS AT CHAMBER 13 - "DATA"

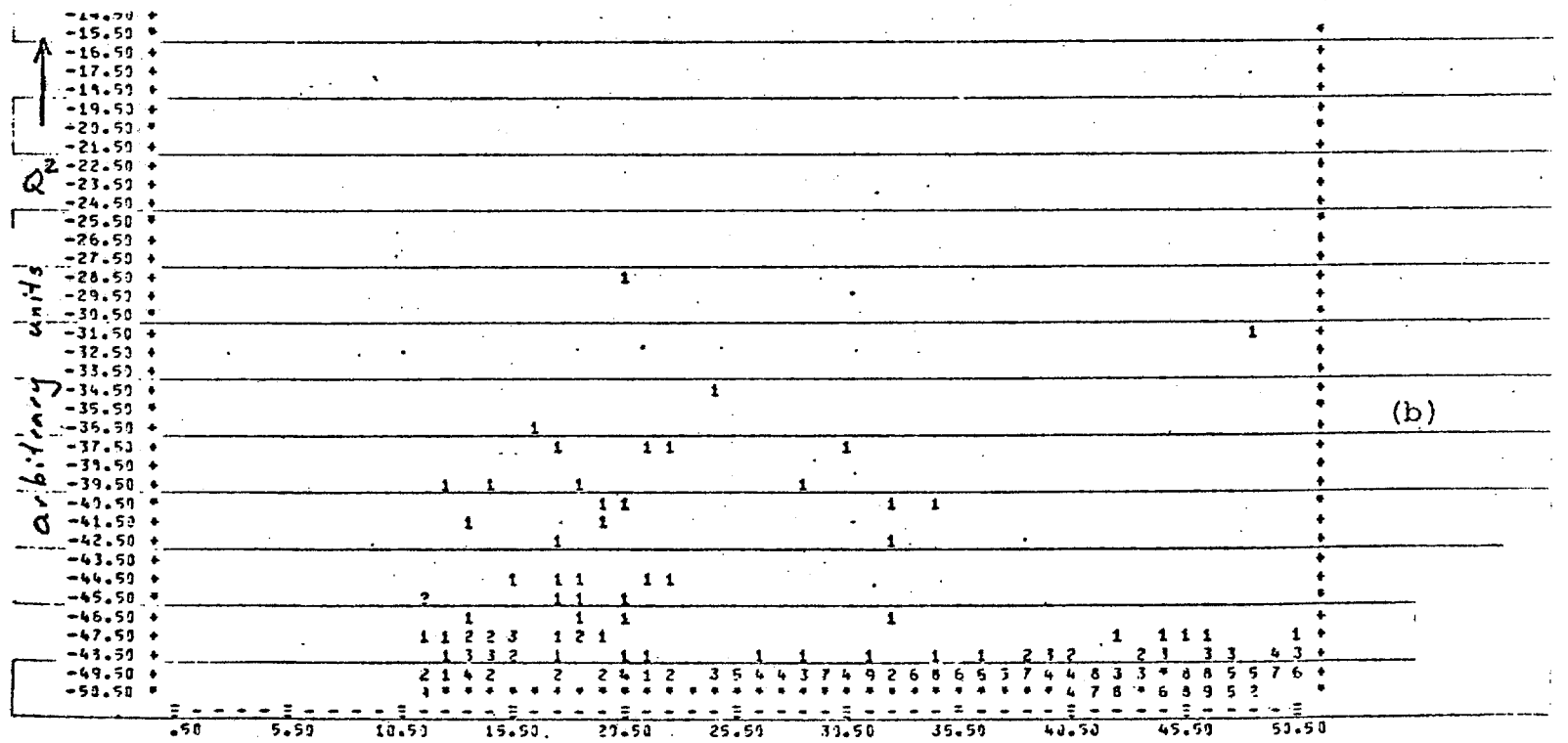

FIGURE 3

Q^2 VS RADIUS AT CHAMBER 13 - "HALO"

69-96

Fig. 3